University of South-Eastern Norway

www.usn.no

FMH606 Master's Thesis 2023

Process Technology

Electrified calcination in a fluidized bed calciner – Experiments with Scaled Binary particles

Nitish Kumar Jha

Faculty of Technology, Natural sciences, and Maritime Sciences

Campus Porsgrunn

University of South-Eastern Norway

www.usn.no

Course: FMH606 Master's Thesis, 2023

Title: Electrified calcination in a fluidized bed calciner Experiments with Scaled Binary particles

Number of pages: 91

Keywords: Fluidized bed calcination, Bubbling Fluidized Bed Reactor, binary mixture, raw meal particles, particle characteristics, fluidization behavior, segregation, chemical composition.

Student: Nitish Kumar Jha

Supervisor: Lars-André Tokheim & Ron M. Jacob

External partner: Norcem and Heidelberg Cement Northern Europe (Christoffer Moen)

University of South-Eastern Norway

www.usn.no

Summary:

Fluidized bed calcination is a process that is used in various industries to heat a bed of particles to high temperatures for chemical reactions and calcination. However, traditional methods can be energy intensive and result in uneven heating. Electrified calcination is a promising alternative to improve efficiency and performance, especially in the cement industry, which is a significant emitter of CO_2. The ELSE project explores the feasibility of electrified calcination using a Bubbling Fluidized Bed Reactor with immersed heating elements. Studies have shown that a binary mixture of smaller raw meal particles and coarser particles can enhance fluidization properties. The work aims to investigate the behavior of particles in a fluidized bed reactor under cold-flow conditions that simulate hot-flow conditions. Binary particles are used to study the dynamics and feasibility of fluidizing raw meal with coarser particles while separating them from the system. Tests in cold-bed reactors will be conducted to understand the effects of particle characteristics on fluidization processes and optimize industrial processes. Experiments were conducted on fluidized bed particles in a narrow rectangular column under scaled cold-flow conditions. The study found that pure coarse particles have good fluidization behavior, while pure fine particles have poor fluidization behavior. Mixing fine particles with coarse particles is feasible, but may result in entrapment, poor mixing, and reduced fluidization performance. Segregation can occur due to differences in particle size or density, and increasing the particle size difference increases the possibility of segregation. Understanding particle characteristics is crucial for optimizing reactor performance. There may be a small change in the chemical composition of segregated particles due to erosion or breakdown during fluidization, but the segregation process used in the experiment is effective.

Preface

The thesis was written as part of the Master of Science degree program at the University of South-East Norway, Porsgrunn. The thesis is focused on calcination in an electrically heated bubbling fluidized bed with scaled binary particles for a research project on "combined calcination and CO2 capture in cement clinker production using CO2-neutral electrical energy." It was completed in collaboration with USN, SINTEF Tel-Tek, and Norcem.

The preface acknowledges the purpose of the report, which was to assess whether coarser particles could be mixed with fine raw meal to achieve good mixing and segregation in a bubbling fluidized bed for electrically calcining raw meal in cement production.

Writing my thesis has been a great learning experience, forcing me to think critically and creatively about the challenges. I have been privileged to have the supervision and support of my thesis supervisor, Prof. Lars-André Tokheim, who has provided me with vital insights and comments throughout the process. I am also thankful to my co- supervisor Ron M. Jacob for providing me with the resources and assistance. The author is also grateful to Christoffer Moen for support and encouragement throughout this process.

Porsgrunn, May 2023

Nitish Kumar Jha

Contents

Nomenclature

Symbol	Description	Unit
Ar	Archimedes number	[-]
D	The diameter of the reactor	[m]
H	The height of the reactor	[m]
M_{CO2}	The molecular masses of CO_2	[kg/mol]
M_{CaCO3}	The molecular masses of $CaCO_3$	[kg/mol]
ΔP	The pressure drops	[Pa]
Re_{mf}	Reynolds number	[-]
T_{ref}	Reference temperature (T_{ref}=25 °C and p_{ref}= 1atm)	[K]
Wt. %	Mass fraction of particles	[-]
d_p	Particle diameter	[m]
u_{mf}	Minimum fluidization velocity	[m/s]
μ	The dynamic viscosity	[Pa. s]
u_t	Terminal settling velocity	[m/s]
ρ_{bulk}	Bulk density	[kg/m^3]
ρ_p	Particle density	[kg/m^3]
ρ	Density	[kg/m3]
φ	Sphericity	[-]
ϵ_{mf}	minimum fluidization voidage	[-]

List of Figures

List of Tables

1 Introduction

1.1 Background

Fluidized bed calcination is a widely used process in industries such as ceramics, metallurgy, and chemical production. The process involves heating a bed of particles to high temperatures to cause chemical reactions and calcination. However, traditional fluidized bed calcination can be energy-intensive and can lead to uneven heating of the particles. Electrified calcination is a promising alternative that can potentially improve the efficiency and performance of fluidized bed calcination [1]. The ELSE project (electrification of cement production) explores the technical feasibility and requirements for the introduction of electrified calcination in cement production, with the aim of reducing CO2 emissions. The calciner is the most energy-intensive part of the cement manufacturing process and the main sources of CO2 emissions are decarbonization of limestone and combustion [2]. Electrification of the calciner is suggested as a solution, with a Bubbling Fluidized Bed (BFBR) reactor with immersed heating elements as a viable option. BFBR reactors have a high heat transfer coefficient and uniform temperature distribution, making them suitable for the process [3]. However, regular raw meal is hard to properly fluidize, so studies have been conducted using a binary mixture of smaller raw meal particles and coarser particles to enhance fluidization properties [2].

1.2 Process Description

This section presents modifications to the traditional coal-based combustion calcination system along with a CO_2 heat exchanger and proposes a new calcination system, using a fluidized bed with electrical heating.

In the traditional cement production process, as in Figure 1.1, the raw meal is heated to approximately 700 ° C on preheaters using hot gases from the calciner. The meal is then calcined in the calciner at 900 ° C by direct contact with hot gases produced by combustion of the fuel. The pre-calcined meal is calcined in the rotary kiln, then heated to 1400-1450°C by fuel combustion to generate the partial melt phase and the clinker materials [1]. Finally, in the clinker cooler, the clinker is cooled by ambient air.

In Figure 1.2, the calciner fuel is replaced with electrical energy and the tertiary air is used to preheat rather than being released into the calciner. The hot rotary kiln exit gas skips the calciner and is directed to the preheater, where its sensible heat is used. The only significant gas component in the calciner's exit gas stream is CO2 from decarbonation. When fuel combustion with electrical energy as the calciner's energy source, the generation of CO2 from fuel combustion is decreased, and the calciner's exhaust gas becomes practically pure CO2, which can be sent straight to a CO2 processing unit. This is attractive because it can achieve a high CO2 reduction rate (about 70%), requires only adjustment to one primary equipment element (the calciner) and does not require consideration of very high temperatures in the rotary kiln [1].

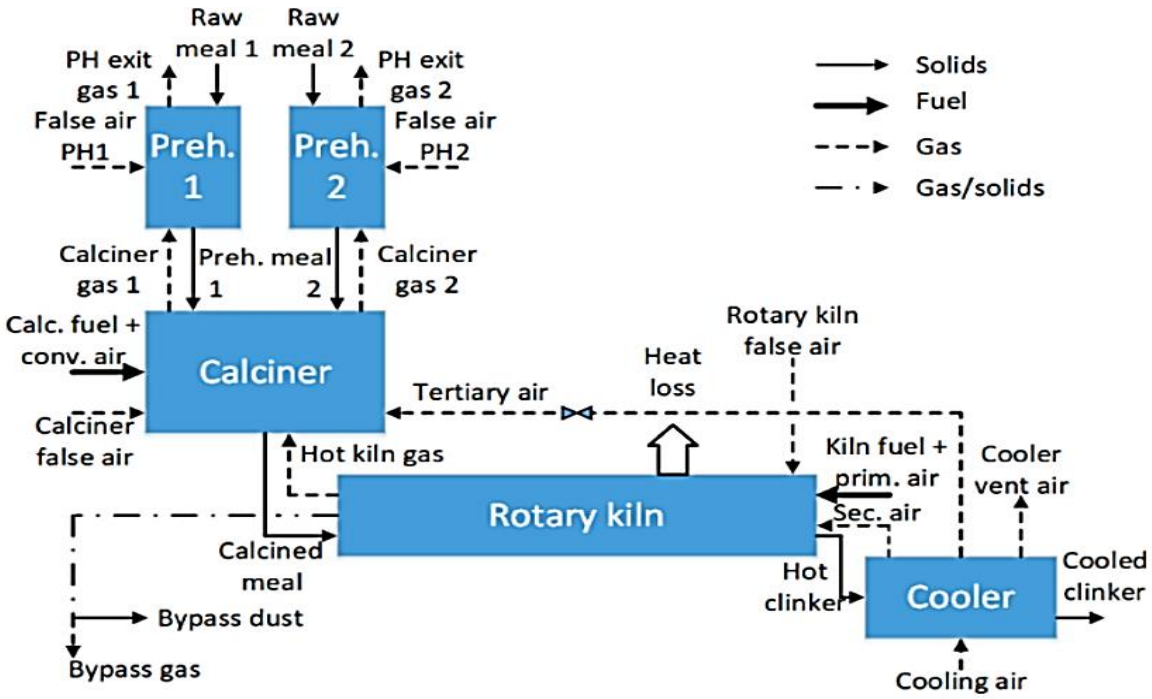

Figure 1.1: Existing cement production process [1]

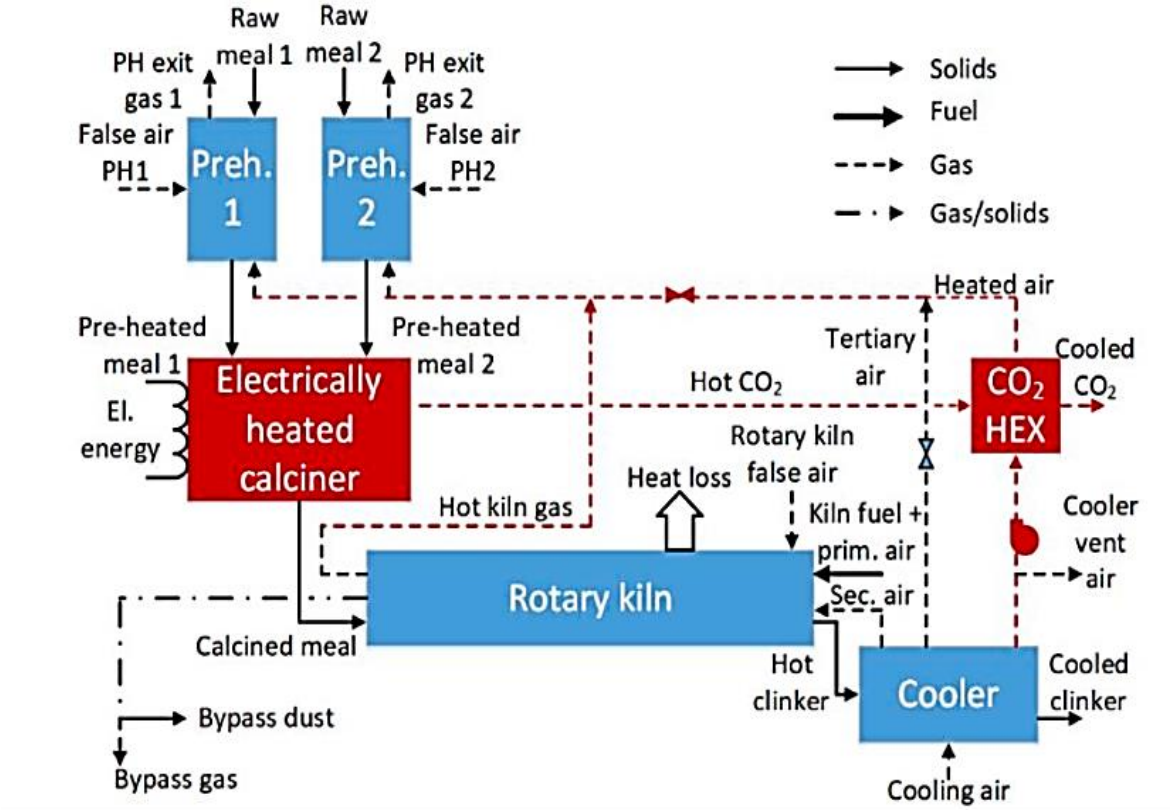

Figure 1.2: Proposed cement production process [1]

The main challenge in the reactor is fluidizing the raw meal, which contains fine or ultra-fine particles that are difficult to fluidize due to interparticle forces and cohesiveness. Improved fluidization has been observed at a mixing ratio of 1:3 raw meal and coarse sand, and at velocities higher than 0.25 m/s [2].

1.3 Objective

The main objectives of this work are to investigate and describe the behavior of the particles in a fluidized bed reactor under cold-flow (scaled) conditions that have similar behavior under hot-flow conditions.

In the scope of this thesis binary particles are used in fluidization to study the behavior and dynamics of a mixture of two distinct types of particles in a fluidized bed and learn if it is feasible to fluidize raw meal with coarser particles while keeping the coarse particles in the system and separating the raw meal out. This will be accomplished by conducting a series of tests in cold-bed reactors and watching how they interact. This helps to understand the effects of particle size, shape, chemical composition and density on fluidization quality, mixing, segregation, and other processes. The information gained from the fluidization of binary particles can be used to optimize industrial processes. The design basis with hot and cold process conditions is attached in Appendix G.

1.4 Key Questions

1. How to investigate the hot-flow process under cold flow conditions?
2. How to calculate the purity of the entrained particles?
3. How does the superficial gas velocity affect the segregation efficiency?
4. What is the optimal condition for mixing and segregating binary particles?
5. How are the results comparable with the previous group project?

2 Fluidization Theory

2.1 Fluidization Principle

Fluidization is the operation by which solid particles are transformed into a fluid-like state through suspension in a gas or liquid [3]. Since Fritz Winkler noticed particle fluidization in a crucible containing coke particles in 1921, many forms of fluidized beds have been produced [4]. Solid particles in a fluidized bed are fluidized (lifted and mixed) by a liquid or a gas as in Figure 2.1. The focus of this study is on gas fluidization. The gas, which is delivered from the bottom of the reactor through a porous or perforated distributor plate, lifts particles in a column and causes fluidization. Increasing the gas flow results in varied fluidization regimes, depending on the fluid and particles utilized.

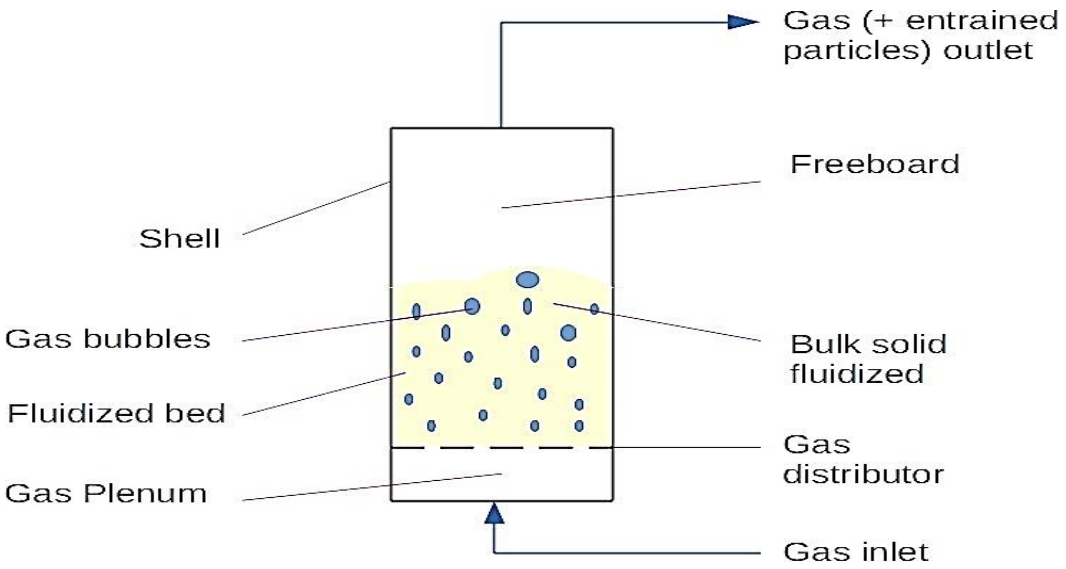

Figure 2.1: Typical fluidized bed

'Fluidization' means an operation or a phenomenon in which static stresses in the bed are canceled out by the other forces, typically by drag force of the interstitial fluid as shown in Figure 2.2 [5]. When an upward-flowing gas exerts a strong enough drag force to counteract gravity's downward pull, particles become fluidized. The drag force is the friction force exerted on the particle by the gas; the particle exerts an equal and opposite drag force on the gas [3]. As a particle becomes increasingly fluidized, the superficial gas velocity surrounding it changes due to drag forces. This effect is minimal for spherical particles, but the drag force has a greater impact on irregularly shaped particles.

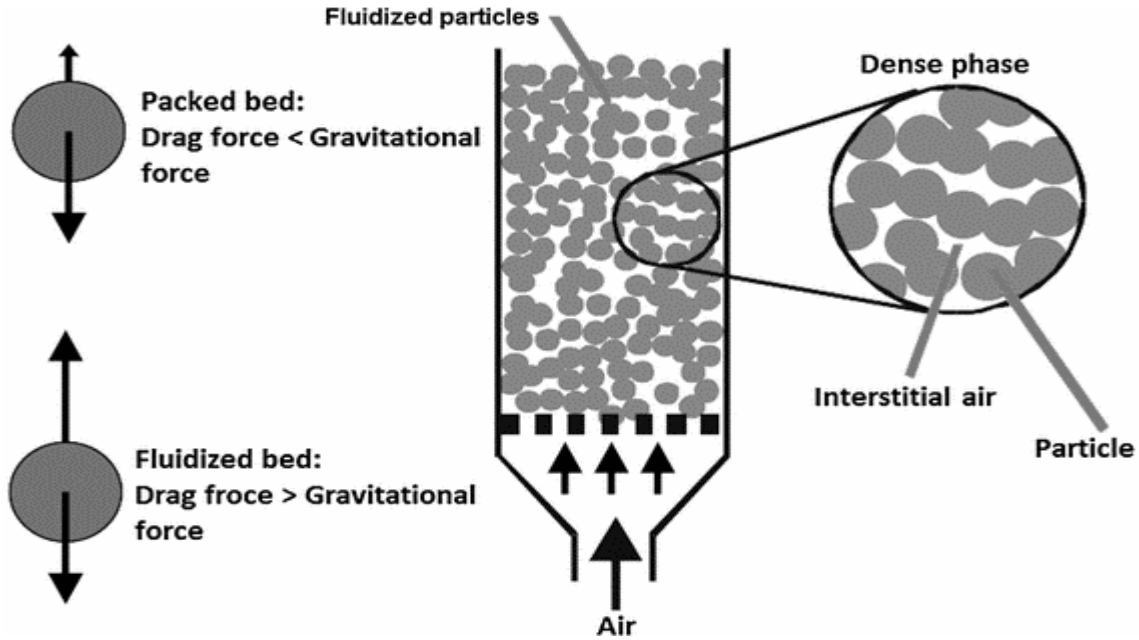

Figure 2.2: Fluidized bed principle.

Another vital component of the fluidization process is the pressure drop through a fixed bed. Changes in pressure drop with varying gas velocity are seen in Figure 2.3. Initially, increasing pressure drop can be observed, up to a point where it stays constant, despite increased gas velocity. This change in the trend of pressure drops can be linked to the formation of a dense phase of a fluidized bed, which occurs when fluidization happens [6].

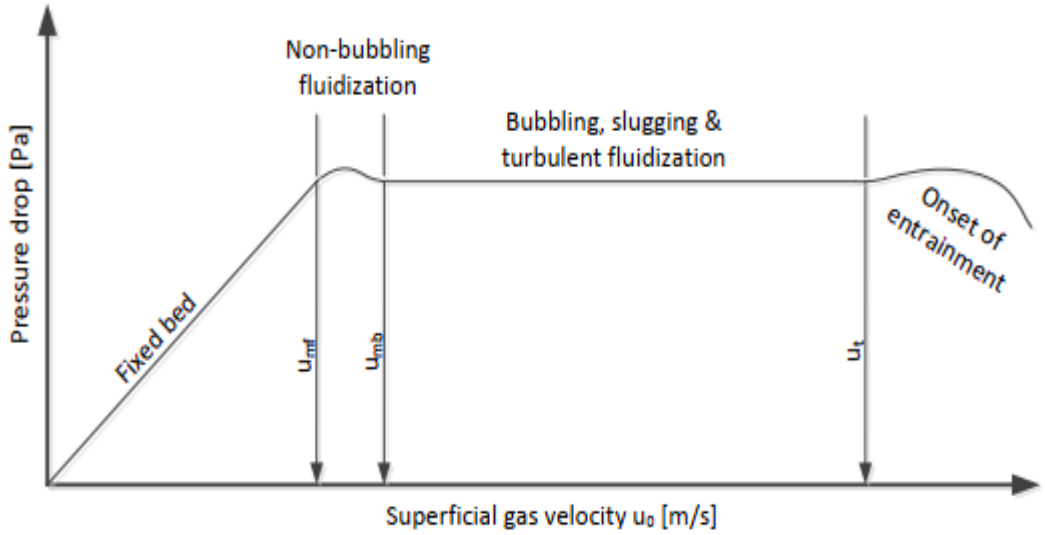

Figure 2.3: Pressure drop in a column filled with particles as a function of superficial gas flow.[4]

2.1.1 Fluidization Regimes

In fluidized bed systems, there are several fluidization regimes depending on the velocity of the gas, that describe the behavior of the bed and the fluid-particle interactions. These regimes are shown in Figure 2.4.

a) **Fixed bed**: In this regime the flow of a gas is passed through a bed of particles and is increased continually, a few vibrate, but still within the same height as the bed at rest.

b) **Minimum fluidization**: This is the fluidization regime that occurs when the fluid velocity is just enough to support the particles and prevent them from settling. In this regime, the bed is well mixed, but the fluid-particle interaction is limited. It is also called homogeneous fluidization.
c) **Bubbling fluidization**: In this regime, the fluid velocity is higher than the minimum fluidization velocity, leading to the formation of small bubbles in the bed. The bubbles rise to the surface and burst, causing the particles to be lifted and mixed. This regime is characterized by a high degree of fluid-particle interaction and improved mixing.
d) **Slugging fluidization:** In this regime, large slugs of gas and particles are formed and move through the bed. This regime is characterized by high fluid-particle interaction, but poor mixing.
e) **Turbulent fluidization:** In this regime, the fluid velocity is even higher than in the bubbling fluidization regime, leading to the formation of large bubbles that mix and entrain the particles. This regime is characterized by high fluid-particle interaction and improved heat- and mass-transfer rates.

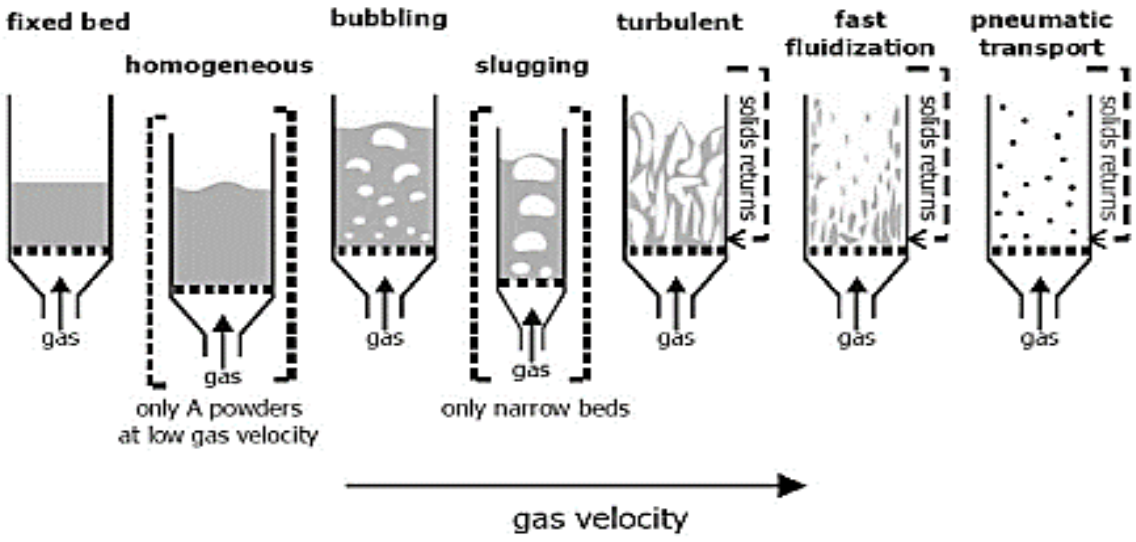

Figure 2.4: Fluidization type depending on the gas velocity. [7]

f) **Fast fluidization**: In this regime, the fluid velocity is extremely high, leading to the formation of high-velocity jets and the breakup of the bed into individual particles. This regime is characterized by high fluid-particle interaction, but poor mixing and bed stability.
g) **Pneumatic transport:** This is the fluidization in which the further increases of gas velocity, eventually the fluidized bed becomes an entrained bed in which we have disperse, dilute, or lean phase fluidized bed, which amounts to pneumatic transport of solids.

In conclusion, fluidization regimes describe the different behaviors of fluidized beds and the fluid-particle interactions that occur at different fluid velocities. Each regime offers unique benefits and challenges, and the proper fluidization regime for a specific application is determined by the desired process outcomes and operating conditions.

2.1.2 Particle Size Distribution

In fluidization technology, particle characterization is of major importance because the different particle properties directly influence the fluidization behavior. The particle size is usually stated as one of the most important particle properties when used in fluidized bed systems. The variety of particle forms and sizes makes it difficult to accurately describe or characterize the bed.

For this description, we can define two functions of the size distribution p and P. If we have a solid bed with diameters dpi, for i (1, 2, …, N), then p gives the fraction (mass, volume, number) of particles that are of diameter d (dp_1, dp_{i+1}). The cumulative distribution is represented by the function P, which is the fraction of solids that are less than the given value d_p [3]. Particle size distribution (PSD) can be obtained by sieve analysis, microscopy combined with an image analysis tool, or laser diffraction measurements [4]. Obtaining information about the particle size forms the first step towards the definition of the so-called Geldart classification.

2.1.3 Geldart's Classification

Geldart classified particles into four categories or classes, namely Geldart A, B, C, and D particles as in figure 2.5. The basic hydrodynamic properties and particle behavior are quite similar among various Geldart groupings. The groups are determined by the difference in particle density and fluid density, as well as the mean particle size [8]. Outside of the Geldart groups, particle behavior deviates significantly from the norm. From smallest to largest particle, they are as follows:

1) Group C
    - Cohesive
    - Difficult to fluidize, and channeling occurs.
    - The forces greatly affect the fluidization behavior of these powders.
    - Particle Diameter (d_p)~ 0-30µm
    - Example: flour, cement
2) Group A
    - Aeratable and small
    - Bubbling velocity (u_{mb}) is significantly higher than fluidization velocity (u_{mf}).
    - Large bed expansion before bubbling starts.
    - Gross circulation of powder even if only a few bubbles are present.
    - Large gas back mixing in the emulsion phase
    - The rate at which gas is exchanged between the bubbles and the emulsion is high.
    - The bubble size is reduced by either using a wider particle size distribution or reducing the average particle diameter.
    - There is a maximum bubble size.
    - Particle Diameter (d_p)~ 30-100µm
    - Examples: FCC, milk flour
3) Group B
    - Bubbling
    - The bubbling velocity, Umb, and the fluidization velocity, Umf, are almost identical.
    - The solids recirculation rates are lower.
    - The rate at which gas is exchanged between bubbles and emulsion is smaller.
    - The size is almost independent of the mean particle diameter and the width of the particle size distribution.
    - No observable maximum bubble size

- Particle Diameter (d_p)~ 100-1000µm
- Example: sand

4) Group D
   - Spoutable
   - Either very large or very dense particles.
   - Bubbles coalesce rapidly and flow to large sizes.
   - Bubbles rise more slowly than the rest of the gas percolating through the emulsion.
   - The dense phase has a low voidage.
   - Particle Diameter (d_p)> 1000µm
   - Examples: Coffee beans, wheat, lead shot

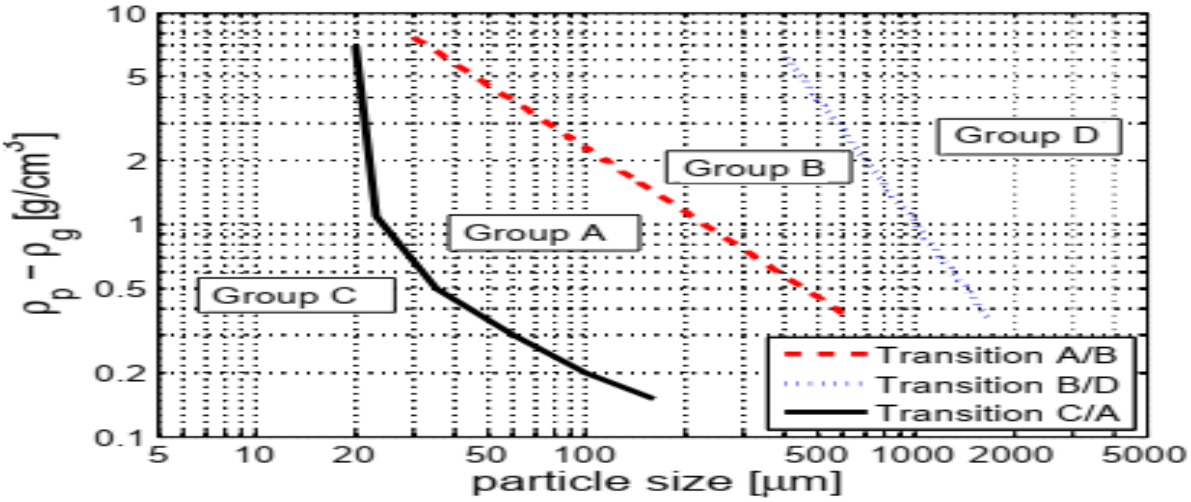

Figure 2.5: Geldart classification of particles in fluidized beds[4]

2.1.4 Minimum Fluidization Velocity, u_{mf}

One of the key characteristics to know to operate a fluidized bed is the minimum fluidization velocity, the air velocity above which the bed of particles starts to fluidize. There is a change in the pressure drop with varying gas velocity, but higher gas velocities do not create a higher pressure drop. [9] This is because at this point the pressure drop is due solely to the weight of the suspended bed. Figure 2.6 shows the graphical representation of the above phenomenon.

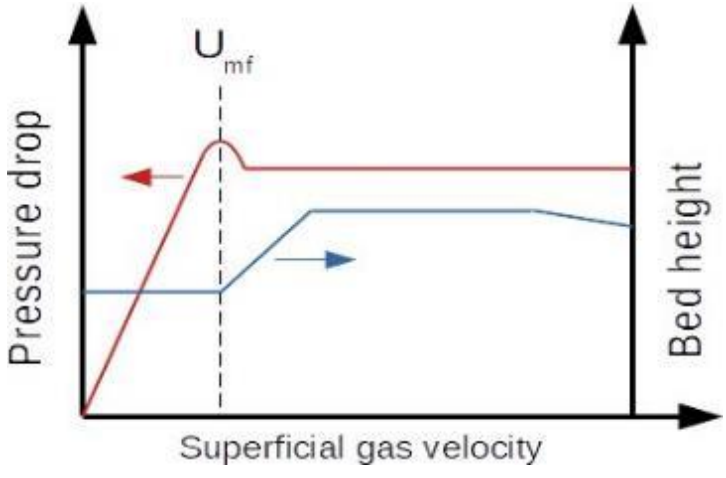

Figure 2.6: Minimum fluidization velocity [9]

Pressure drops through fixed bed of solids of uniform size (d_p) of the bed height (L) is given by Ergun correlation:

$$\frac{\Delta P}{L} = 150\frac{\left(1-\epsilon_{mf}\right)^2}{{\epsilon_{mf}}^3}\frac{\mu.u_0}{(\phi_s d_p)^2} + 1.75\frac{\left(1-\epsilon_{mf}\right)\rho_g {u_0}^2}{{\epsilon_{mf}}^3(\phi_s d_p)} \quad (2.1)$$

where,

ΔP = pressure drop across bed — d_p = particle diameter

L = bed height — ρ_g = gas density

μ = gas viscosity — ϕ_s = particle sphericity

ϵ_{mf} = minimum fluidization voidage — u_0, = superficial gas velocity

Since fluidization phenomena occur when the drag force caused by the upward flow of gas is at least equal to the weight of particles in the bed, it can be expressed mathematically as follows:

$$\Delta P A_t = A_t L_{mf}(1 - \epsilon_{mf})[(\rho_s - \rho_g)g] \quad (2.2)$$

where

A_t = cross sectional area of tube — ρ_s= density of the particle

L_{mf} = Bed height at fluidization — g = acceleration due to gravity

Rearranging equation (2.2) and combining with equation (2.1) gives a quadratic in u_{mf} which can be presented in dimensionless form of the equation (2.3).

$$Ar = 150\frac{\left(1-\epsilon_{mf}\right)}{{\epsilon_{mf}}^3{\phi_s}^2}Re_{p,mf} + 1.75\frac{1}{{\epsilon_{mf}}^3\phi_s}{Re_{p,mf}}^2 \quad (2.3)$$

As ϵ_{mf} is itself a function of velocity, in fluidization studies it is usual to simplify Eq. 2.3 using the experimentally determined "voidage functions" [10]

$$\frac{\left(1-\epsilon_{mf}\right)}{{\epsilon_{mf}}^3{\phi_s}^2} \approx 11 \quad (2.4)$$

Here Re and Ar are the two dimensionless numbers: Reynolds and Archimedes respectively.

$$Re = \frac{d_p u_{mf}\rho_g}{\mu} \quad (2.5)$$

$$Ar = \frac{{d_p}^3\rho_{g(\rho_s-\rho_g)g}}{\mu^2} \quad (2.6)$$

If sphericity and voidage are known, solving Equation (2.3) yields a reliable estimate of u_{mf}.

For fine particles, Equation (2.6) proposed by Wen and Yu can be used to obtain Reynolds number in minimum fluidization conditions.

$$Re_{p,mf} < 20$$

And

$$Re_{\mathrm{p,mf}} = \sqrt{[(33.7)^2 + 0.0408\mathrm{Ar})]} - 33.7 \tag{2.7}$$

The minimum fluidization velocity can be calculated by simplifying equation 2.3,

$$u_{mf} = \frac{{d_p}^2 \cdot (\rho_s - \rho_g)g}{150\mu} \frac{{\epsilon_{mf}}^3 {\phi_s}^2}{(1 - \epsilon_{mf})} \tag{2.8}$$

Substituting the value from equation 2.4

$$u_{mf} = \frac{{d_p}^2 \cdot (\rho_s - \rho_g)g}{1650\mu} \tag{2.9}$$

2.2 Bubbling Fluidized Bed

2.2.1 Bubble Formation

Bubbling bed must be treated as a two-phase system, with solids in dense phase and gas bubbles in lean phase. Increasing the velocity of a gas passing through a bed of solids affects the fluidization mode. At relatively low gas velocities, we can see a thick bubbling fluidized bed, which is distinguished by the presence of low solid concentration areas known as bubbles [11] [6].The dense phase, with higher solid concentration is called emulsion. Bubbles moving upward change their size (grow with height over the distributor). Bubbles are not always spherical and include relatively small amounts of particles. Figure 2.7 depicts a schematic diagram of such a system's element [11].

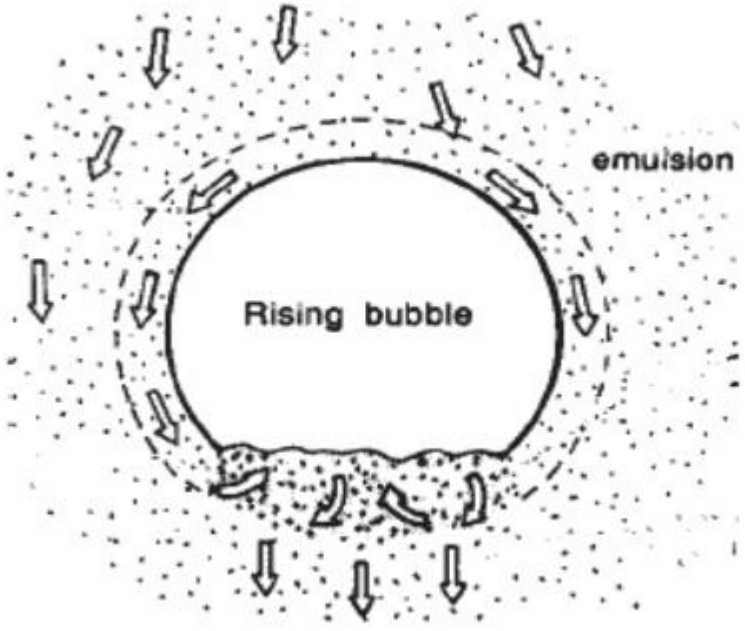

Figure 2.7: Schematic bubble in bubbling bed [11].

As observed, the bubbles are roughly hemispherical, with a pushed-in bottom. A wake is an area right underneath the bubble that contains a substantial amount of solids. Furthermore, each bubble is surrounded by a cloud, which is a component of the emulsion that was pierced by rising bubble gas [6]. The concentration of solid in the cloud is greater than that in the bubble but less than that in the emulsion.

2.2.2 Entrainment and Elutriation

A fluidized reactor can be divided into two parts, the bottom one called the dense phase and the dispersed phase, where the concentration of particles decreases. The flux of particles suspended in gas over the dense phase is called entrainment. The zone of fluidization vessel above the border between the dense phase and the dispersed phase is called a freeboard. The entrainment of particles lowers with increasing freeboard height until it reaches a constant level, and that height is called TDH - transport disengaging height.

Finally, elutriation refers to removal of fine particles from a mixture of solids with different sizes. Larger particles fall back to bed, because they are too heavy to be carried up, but smaller ones are flowing upward with the gas.

2.3 Terminal Settling Velocity, u_t

It is also vital to understand the fluid velocity at which the bed is about to be entrained. This velocity is known as the maximum fluidizing velocity or terminal velocity (u_t,) and for a bed of uniform spheres, it is equivalent to the free-falling velocity of one of these spherical particles in a large diameter tube [12].

When a particle of size d_p falls through a fluid, its terminal free-fall velocity can be estimated from fluid mechanics by equation 2.10 [3].

$$u_t = \sqrt{\frac{4d_p(\rho_s - \rho_g)g}{3\rho_g C_D}} \tag{2.10}$$

where C_D is an experimentally determined drag coefficient.

When numerous particles are present, such as in a fluidized bed or a particle separation system, the terminal velocity of the particles is determined by the dimensionless particle size d* and the dimensionless gas velocity u*[13].

$$u_t = u^* \left[\sqrt[3]{\frac{\mu(\rho_s - \rho_g)g}{{\rho_g}^2}} \right] \tag{2.11}$$

Where

$$u^* = \left[\frac{18}{({d^*}_p)^2} + \frac{2.335 - 1.744\phi_s}{({d^*}_p)^{0.5}} \right]^{-1}, for\ 0.5 < \phi_s < 1 \tag{2.12}$$

For spherical particles this expression reduces to

$$u^* = \left[\frac{18}{({d^*}_p)^2} + \frac{0.591}{({d^*}_p)^{0.5}} \right]^{-1}, for\ \phi_s = 1 \tag{2.13}$$

Dimensionless particle size d* is measured by

$${d^*}_p = d_p \left[\sqrt[3]{\frac{\rho_g(\rho_s - \rho_g)g}{\mu^2}} \right] \tag{2.14}$$

2.4 Particle Behavior in Binary Mixture

Since the fundamentals of fluidized beds have been established and equations to explain the behavior of single-particle type systems have been proposed, it would be relevant to examine how these systems alter in the binary mixtures. We study the effects of the superficial gas velocity and the particle size distribution on mixing and segregation. The behavior of particle-mixing dynamic is of profound significance for heat transfer and reaction efficiencies in energy engineering [14].

2.4.1 Particle Mixing and Segregation

We have previously assumed that the bed particles are homogenous. However, if the physical parameters of the bed particles differ, most notably size and density, segregation can occur. Segregation results in non-uniform mixing and reduces operating efficiency. In recent years, many researchers have experimentally studied the fluidization behavior for some binary particle systems and have found that the difference in the physical properties and mass fraction of the binary particles of fluidized bed is found to strongly influence the minimum fluidization velocity(u_{mf}) and the bed void fraction [15].

The mixing index measures the degree of homogeneity between the two particles based on their percentage composition. An equilibrium particle distribution that fluctuates with height in the bed results from simultaneous mixing and segregation by rising bubble motion. The fluidization process of binary particles identifies three distinct regimes: the bottom of the column, where particles of large size or heavy density make fluidization difficult, the mixing region, which contains binary mixtures of particles of different density and size, and the top region, which contains small particle and light particles [15], [16]. The particle in the top region is called flotsam and that at the bottom is jetsam. As the flow velocity increases, the segregation pattern shifts from a pure jetsam layer at the bottom to a uniform mixture through a change in jetsam concentration. Radial distribution is essentially uniform, and axial distribution varies with height [6].

2.4.2 Fluidization of Binary Particles

Particle fluidization is a process that has been widely used in industry because of its efficient mixing between particles and fluid. Binary particle fluidization is defined as a method in which a relatively compact bed of particles is fluidized by an upward bulk flow of fluid [16]. Density, size, and superficial velocity are significant factors for mixing and segregation in the fluidization of binary particles.

There are several other factors that influence fluidization, and several studies have been done on the behavior of different particle attributes in a fluidized bed reactor. A list of desirable and undesirable particle perks is given in Table 2.1. If one or more of the properties in Table 2.1 fall into the "undesirable" category, the system may display poor fluidization and non-ideal behavior. Such particles are called non ideal particles [17].

Interparticle interactions, particularly van der Waal's and electrostatic forces, are one of the key issues with fluidizing very small particles. The particles demonstrate significant cohesion when these interparticle forces reach extreme magnitudes in relation to particle weight. When exposed to a flowing gas, this cohesiveness results in the formation of "rat holes" or air vents.

Table 2.1: Desirable particle qualities when fluidization is performed [17].

Property	Desirable	Undesirable
Shape	Rounded, sphericity ≥ 0.7	Extreme
Mean diameter	Between 50 µm and 1.6 mm	≤ 40 µm or ≥ 3 mm
Size distribution	Unimodal	Bi-or tri-modal, uniform
Surface roughness	Smooth surface	Asperities higher than $\frac{d_p}{20}$
Rigidity/flexibility	Rigid	Flexible
Attrition resistance	Robust	Friable
Gas relative humidity (RH)	$10 \leq RH \leq 60$	$2 \geq RH \geq 80$

Combining non-ideal particles with coarser particles, an inert fraction of perfectly behaved particles is believed to resolve the issues that occur with fluidizing non-ideal particles. According to [2], adding raw meal with coarser particles enhances fluidization and causes the process to behave more steadily than a raw meal alone.

3 Scaling of Particles

Scale-up transfers data gathered on smaller fluidized bed units to larger beds so that they may be operated satisfactorily at a greater scale. Scaling up fluidized beds is problematic since it is well known that the hydrodynamics of small, fluidized beds can differ dramatically from those of bigger beds. The fact that different particle sizes scale differently contributes to this challenge [11]. Therefore, it is a good idea to construct a physical model to get an idea, observe and confirm the hydrodynamic behavior of the commercial unit.

The scaling of particles in a fluidized bed is a critical aspect of achieving optimal performance in fluidized bed processes. The particle size distribution, bed height, fluid flow rate, particle density, and particle shape and surface characteristics are all important factors that must be considered when scaling a fluidized bed [18]. By adjusting these factors to match the properties of the particles being used, it is possible to achieve efficient heat and mass transfer between the fluid and solid, which can lead to improved overall performance of the system.

Scaling laws for bubbling fluidized beds were first proposed some two decades ago. Although the scaling laws for bubbling beds are for the most part successful, experimental verification has generally been limited to small-scale equipment [19]. Scaling laws in fluidized beds refer to the relationships between various properties of the fluidized bed and the particles used in it, and how they change with changes in the size of the bed or the scale of the system. These relationships are used to predict how the behavior of a fluidized bed will change when it is scaled up or down, and they can be used to design and optimize fluidized beds for different applications.

3.1 Horio Scaling Law

Horio stated that a similarity between a large bed and its model or small bed is achieved if one matched the scaling parameters.

$$u_2 - u_{mf,2} = \sqrt{m}\left(u_1 - u_{mf,1}\right) \tag{3.1}$$

$$u_{mf,2} = \sqrt{m}\left(u_{mf,1}\right) \tag{3.2}$$

The first statement is the condition necessary for equivalent bubble coalescence. The second is the condition necessary for equivalent bubble splitting and similar interstitial flow pattern. This set of conditions is termed the similarity rule [20]

3.2 Glicksman Scaling Law

Glicksman (1984) obtained a full set of scaling parameters by non-dimensionalizing the mass and momentum balances, as well as their boundary conditions. The following assumptions are critical in determining the parameters:

- The fluid is incompressible.
- Inter-particle forces other than mechanical forces due to collisions are excluded.
- The influence of the particle coefficient of restitution and the friction coefficient on interparticle collisions is not included.

With these assumptions, the following set is derived.
Froude numbers, density ratios, Reynolds numbers bed-to-particle size ratios, bed geometry ratios, particle sphericity, and particle size distributions should be matched in the complete set to yield following dimensionless numbers: This is known as full set [3].

$$\frac{u^2}{gL}, \frac{\rho_s}{\rho_g}, \frac{d_p \mu \rho_g}{\mu}, \frac{L}{d_p}, \frac{L_1}{L_2}, \varphi, particle\ size\ distribution \tag{3.3}$$

In practice, it is found to be difficult to match all the parameters expressed in the full set of scaling parameters. Very unusual particles and gases will be required to meet these requirements[21], [22] Therefore, the simplified set, which has fewer parameters than the full set, was developed to solve this problem.

$$\frac{u^2}{gL}, \frac{\rho_s}{\rho_g}, \frac{u}{u_{mf}}, \frac{L_1}{L_2}, \varphi, particle\ size\ distribution \tag{3.4}$$

There are two flow conditions in the simplified set.

a) Inertial forces > Viscous forces
   i.e., Re_p >1000 and for High velocities

$$\frac{u^2}{gL}, \frac{\rho_s}{\rho_g}, \frac{L_1}{L_2}, \varphi, particle\ size\ distribution \tag{3.5}$$

b) Viscous forces > Inertial forces
   i.e., Re_p < 4 and for low velocities

$$\frac{u^2}{gL}, \frac{u}{u_{mf}}, \frac{L_1}{L_2}, \varphi, particle\ size\ distribution \tag{3.6}$$

3.3 Fitzergald and Crane Scaling Law

The Fitzgerald and Crane scaling rule is a scaling law that was proposed in 1957 by Fitzgerald and Crane to predict the minimum fluidization velocity of a fluidized bed. The rule states that the minimum fluidization velocity is directly proportional to the square root of the particle diameter and inversely proportional to the square root of the bed height. The Fitzgerald and Crane scaling rule is often expressed mathematically as follows.

$$\frac{\boldsymbol{u_2}}{\boldsymbol{u_1}} = \frac{\boldsymbol{t_2}}{\boldsymbol{t_1}} = (\boldsymbol{m})^{\mathbf{0.5}} \tag{3.7}$$

The Fitzgerald and Crane scaling rule assumes that the fluidization characteristics of a fluidized bed are primarily determined by the balance between the upward force on the particles due to the fluid flow and the downward force on the particles due to gravity. According to the rule, as the diameter or the bed height increases, the minimum fluidization velocity required to keep the particles suspended in the bed will also increase [19].

Therefore, it's important to validate the predictions of the rule with experimental data.

Hence, Fitzgerald and Crane proposed using the more restrictive set of scaling parameters: -

$\frac{d_p \mu \rho_g}{\mu}$ Reynolds Number

.

$\frac{\rho_s}{\rho_g}$ Density Ratio

.

$\frac{\mu}{(g d_p)^{0.5}}$ Froude Number

$\frac{L}{d_p}$ Geometric Similarity of distributor bed and particle (3.8)

The suggested calculation procedure when using Fitzgerald's criteria of Eq. (3.8) is as follows:[3] [23]

1) Calculate density ratio for system to be modeled. (Here: Hot Fluidized Bed)
2) Choose a gas for the model $(\rho_g)_2$. Usually, ambient air is used. Then calculate the $(\rho_s)_2$.

$$\left(\frac{\rho_s}{\rho_g}\right)_1 = \left(\frac{\rho_s}{\rho_g}\right)_2 \tag{3.9}$$

3) Combining the Reynolds and Froude numbers gives the scale factor for the two beds, or:

$$\text{Scale factor}(\mathbf{m}) = \frac{\boldsymbol{L2}}{\boldsymbol{L1}} = \left(\frac{\boldsymbol{\rho_{g1}\mu_2}}{\boldsymbol{\rho_{g2}\mu_1}}\right)^{\frac{2}{3}} \tag{3.10}$$

Note that one cannot arbitrarily choose the size of the model; this is necessarily fixed by the choice of ρ_{g2}.

4) Calculate the time factor and gas velocity, from Reynolds and Froude number which determines the similarity in bed behavior.

$$\frac{\boldsymbol{u_2}}{\boldsymbol{u_1}} = \frac{\boldsymbol{t_2}}{\boldsymbol{t_1}} = (\boldsymbol{m})^{0.5} \tag{3.11}$$

4 Experimental Method

The following chapter contains the experimental preparations, setup and procedure for sieving, fluidization, and segregation experiments. Theoretical calculations were done to determine the particles that would best match the scaled characteristics, and those particles were examined throughout the project. Sieving and PSD analysis was performed in the SINTEF lab while mixing and segregation experiments were performed in A-102 Maskinhall/A105 Sentralverksted, campus Porsgrunn. Materials used are listed in Table 4.1.

4.1 Analysis equipment

4.1.1 Particle Size Analyzer

Figure 4.1 shows the Sympatec Helos Magic KFS laser diffraction tester particle size analyzer. A particle size analyzer is an instrument that is used to determine the size distribution of particles in a sample. The machine uses laser diffraction to measure particle size. In this technique, a laser beam is directed at the sample, and the scattered light is collected by the detectors. The size of the particles is determined by analyzing the pattern of the scattered light.

Figure 4.1: Sympatec Helos Magic KFS Laser Diffraction Tester Particle Size Analyzer

4.1.2 Vibratory sieve shaker

The alumina was sieved using a vibrating shaker, as seen in Figure 4.2a. The apparatus was operated for 10 minutes with an amplitude of 1.5. After each sieving, a precise weighing scale was used as that in Figure 4.2b was used to weigh the collected particles.

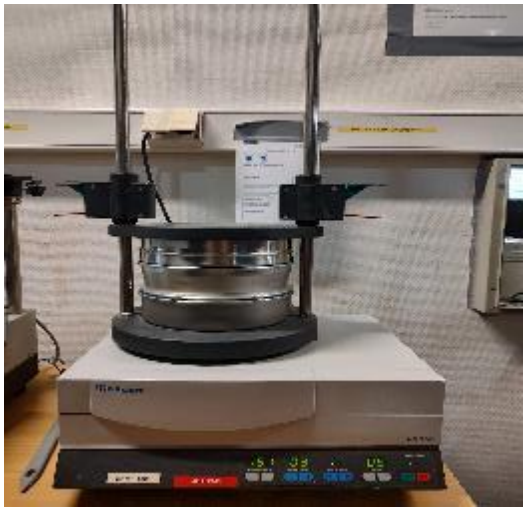

Figure 4.2a: Vibrator sieve shaker

Figure 4.2b: Weighing scale.

The white alumina was sieved with lowest available sieve of 20µm after the segregation to determine the required scaled size as shown in the Figure 4.3. As the segregation were in batches of different flow rates the sieving were done multiple times. Also, the white alumina made a thin layer over the sieve constantly, which stops the sieving process, so cleaning was required frequently.

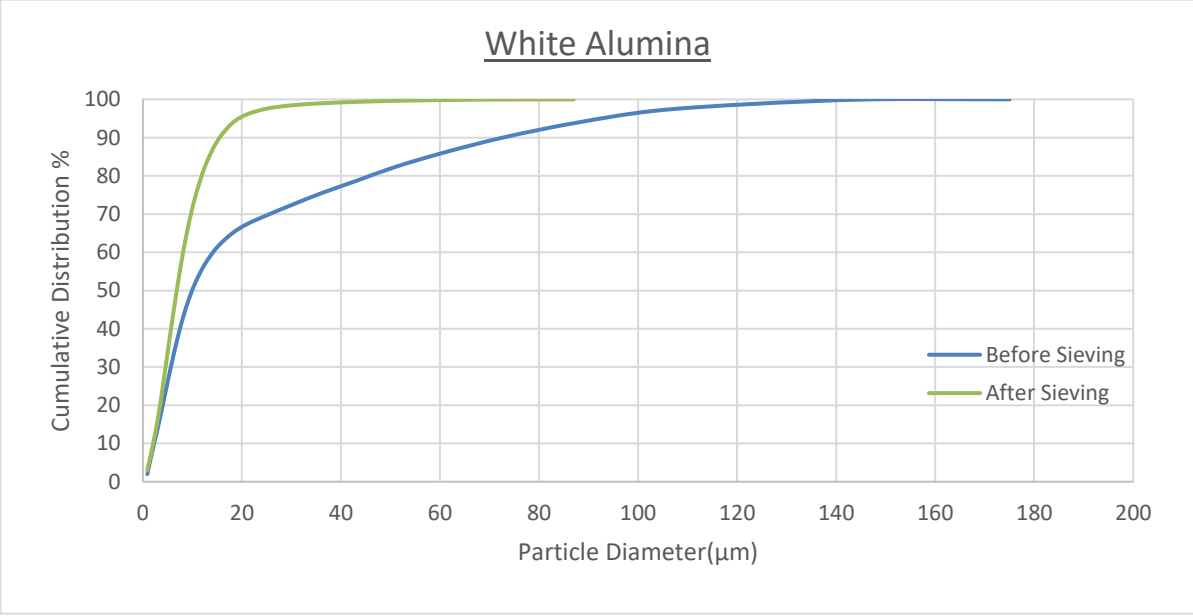

Figure 4.3: Particle Size distribution of white alumina

The brown alumina was sieved with 250µm sieve on top and 150µm sieve at the bottom to get the desired scaled size as shown in Figure 4.4. The sieving was performed multiple times for the different batches of segregated coarse particles and the weight was measured.

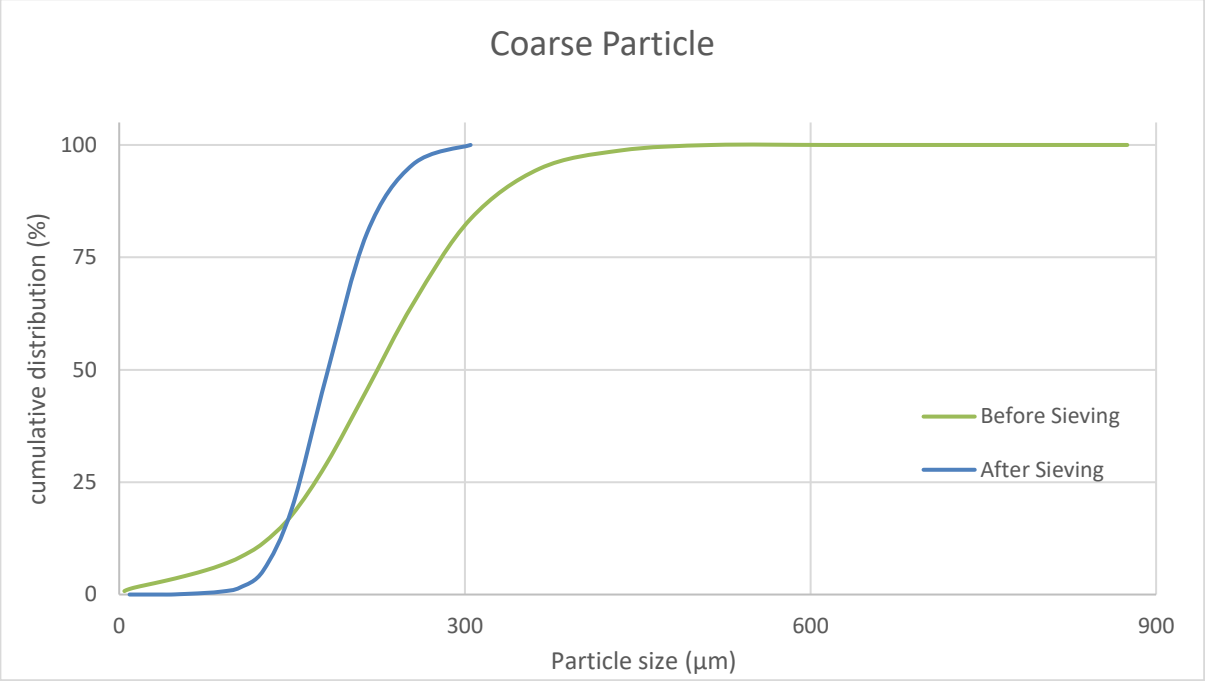

Figure 4.4: Particle Size distribution of Brown alumina

4.2 Fluidized Bed Rig

All experiments were conducted in a cylinder-shaped cold flow fluidized bed as shown in Figure 4.5. The fluidized bed is made of transparent plastic cylinder and is 1.4m in height with a diameter of 0.084 m. The air distributor at the bottom of the cylindrical tube is connected to an air supply. A mass flow rate controller that is linked to a PC is used to regulate the air supply. There are nine pressure transmitters separated by 10 cm each, installed and a LabVIEW® program is used to record the pressure measurements.

The fluidization and segregation part of the experiments is carried on this cold bed unit. The cold bed required a separate capture system on top of the bed. This particle capture system was built and tested to improve capturing efficiency. The capture system was flexible cylindrical tube with smooth inner walls attached at both ends by a transparent plastic bag. One end is connected to a Y shaped pipe, which is placed on top of the bed unit. The cylindrical tube was large enough to cope with the various flow velocities and maintain the efficient capturing of the particles. Being transparent, the plastic bag helped in the visibility of the particle movement from the cold bed unit to the other end into the collection bucket, which is wrapped with a filter bag to prevent the particle from getting out. The entire system is shown in Figure 4.6.

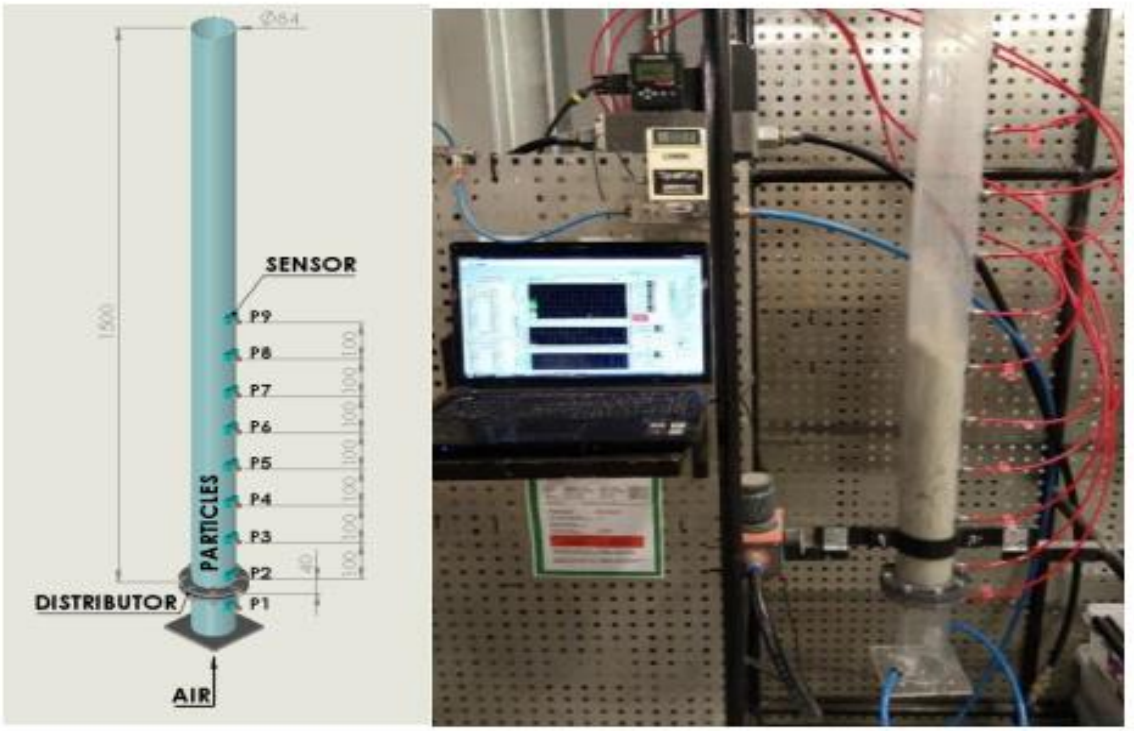

Figure 4.5: Cold flow lab-scaled fluidized bed unit [24]

Figure 4.6: Fluidized bed unit with capturing system

4.3 The Materials

4.3.1 Brown Alumina

TITGGI #80 grit Aluminium Oxide (212-180 μm) coated brown was used as a coarse particle.

Figure 4.7: Pure Brown Alumina

4.3.2 White Alumina

AztroGrit ~5μm white Alumina was used as a fine particle. The material is available in

Figure 4.8: Pure White Alumina

various purities depending on the specific application. The percentage of alumina typically lies between 92-99,7% Al_2O_3, the remaining percentage consists of SiO2, CaO, Na2O and Fe_2O_3.

4.4 Experimental Procedure

The experimental rig and equipment were cleaned to prevent contamination. The pressure sensors and air supply tubes were checked for leaks, and the required weight of the particles was measured and added to the rig. Bed height was recorded to calculate the void fraction and the minimum fluidization velocity was determined from the pressure drop vs. gas superficial velocity graph. Ron et al. (2002) observed that the system reached a pseudo-steady state in 160 seconds. So, the flow rate was increased only after 180 seconds of each velocity setting.

A capture system was added to the top of the apparatus for segregation studies, as illustrated in Figure 4.6, to capture entraining particles for further study. Throughout the procedure, the filter cloth and tube were shaken at regular intervals to remove any particles that may have become stuck to the capture system during the entrainment process. A constant measurement of the segregated weight was taken at the interval of 3 minutes (180 sec) for a given set of flow rates. This was done for both pure particles and binary mixture. A graph of segregated weight against time was plotted. In each experiment, pressure drop profiles were obtained from the data. Gas velocities (m/s) were estimated by dividing the airflow rates (L/min) by the rig's cross-sectional area (m^2). ΔP (mbar) denotes pressure drop and is the difference between PT2 and PT3 pressure readings. Table 4.1 shows that two types of studies were planned: pure particles and binary mixtures.

Table 4.1: Experimental parameters

Material	Experiment type	Sample weight (Kg)	Gas flow rate(L/min)	Run time(min)
Brown Alumina	Fluidization	4	0-28	10
	Mixing	4	Based on Observation	Based on Observation
	Segregation	4	300-750	108
White Alumina	Fluidization	2	0-10	10
	Mixing	2	Based on Observation	Based on Observation
	Segregation	2	100-450	75
Binary Mixture (25%White Alumina+75% Brown Alumina)	Fluidization	2	0-20	10
	Mixing	2	Based on Observation	Based on Observation
	Segregation	0.5	300-750	30

For each fluidized bed (FB) experiment with brown alumina, 4 kg of mass was poured in the rig at first. Following the same procedure as mentioned above, the fluidization velocity was determined and extended to segregation. Bed height was recorded to determine the void fraction. FB was run for a total of 108 minutes during segregation and collecting the entrained particles and recording the mass. The segregated mass was recorded at the interval of 3 minutes (180 seconds) after pseudo steady state for each segregated velocity until the segregation becomes stable. Similarly, for white alumina, 2 kg of mass was poured in the rig at first and the FB was run for total of 75 minutes.

After sieving, the mass ratio of 25% fine and 75% coarse was used to form a bed of 2kg for binary mixture. Because the colors of fine and coarse particles differ, this allows for good visual observations. The segregation experiment was maintained until the FB contained exclusively brown particles. The mass of the entrained particles was measured at the interval of 3 minutes at every segregated velocity. All FB tests for white Alumina, brown Alumina, and binary combination videos may be viewed at the following link. https://1drv.ms/f/s!Autbj7Y-uN1VjS3nb4JCKiR91DFA?e=qvcvDc.

5 Calculations

In this chapter we will scale particles from hot-flow to cold-flow situations using the Fitzergald and Crane scaling method as explained in sub-chapter 3.3. We will calculate the diameter and density of the particles, both fine and coarse, from this. The minimum fluidization and terminal settling velocities of the scaled particle will also be determined.

The Fitzgerald and Crane rule has been designed to predict the minimum fluidization velocity for fluidized beds, but it's important to note that it's based on idealized conditions and assumptions, and the actual behavior of a fluidized bed can be affected by many other factors such as the shape, size, and density of the particles, the properties of the fluid, and the presence of any chemical reactions.

5.1 Calculation of density ratio

With reference to the sub-chapter 1.2, the general calcination process can be presented by the following reaction:

Given,

$$CaCO_3(s) \rightarrow CaO(s) + CO_2(g). \quad \text{(R1)}$$

Table 5.1: Hot and Cold Flow Condition data

Parameters	**Hot Flow Conditions**	**Cold Flow Conditions**
Material	(Limestone) $CaCO_3$	-
Density of Material (Kg/m^3)	2700	-
Reactor temperature (°C)	920	25
Reactor pressure (Pa)	100000	100000
Density of fluidization gas (Kg/m^3)	0.4436 (CO_2)	1.184 (AIR)
Viscosity of the gas (Kg/ms)	0.0000475(CO_2)	0.00001846(AIR)
Density of fine particles (Kg/m^3)	1583	4226
Density of coarse particles (Kg/m^3)	1512	4036

The Hot flow Condition and the Cold flow condition are presented in Table 5.1 and is represented by 1 and 2, respectively.

a. Calculate $\left(\frac{\rho_s}{\rho_g}\right)_1$ for Hot flow conditions.

The density of calcined raw meal, **fine particle (ρ_s)** is derived from the following equation.

$$m_{CaCO3} - m_{CO2} = m_{CaCO3} - \frac{M_{CO_2}}{M_{CaCO_3}} \cdot m_{CaCO3}. X_c \quad (5.1)$$

-m_{CaCO3} is mass of raw meal (or limestone)

- m_{CO2} is mass of CO_2.

-molar weight ratio is $\left(\frac{M_{CO_2}}{M_{CaCO_3}}\right) = \frac{44gm/mol}{100gm/mol}$ =0.44

Considering 94% of the fine particles are calcined.

-Fraction of calcination (Xc) = 0.94

From Equation 5.1 and considering the volume of raw meal to be $1m^3$.

$(m_{CaCO3} - m_{CO2}) = (\rho_{CaCO3} - \rho_{CO2}) = m_{CaCO3} - \left(\frac{M_{CO2}}{M_{CaCO3}}\right) \cdot m_{CaCO3}. X_c$

$(\rho_{CaCO3} - \rho_{CO2}) = 2700 - 0.44*2700*0.94$

$= 1583.28$ Kg / m3

Similarly, considering that all the coarse material is completely calcined, the fraction of calcination (X_c) is 1.

Then the density of **coarse particles (ρ_s)** (Limestone) is given by equation (5.1)

$(\rho_{CaCO3} - \rho_{CO2}) = 2700 - 0.44*2700*1$

$= 1512$ Kg / m3

The density the gas **(CO_2) (ρ_g)** at given temperature (920°C) is 0.4436 kg/m^3.

Hence calculating the density ratio,

Fine Particle: - $\left(\frac{\rho_s}{\rho_g}\right)_1 = \left(\frac{1583.28}{0.4436}\right)_1 = 3570.2$ (5.2)

Coarse Particle: - $\left(\frac{\rho_s}{\rho_g}\right)_1 = \left(\frac{1512}{0.4436}\right)_1 = 3408.5$ (5.3)

b. Calculate $\left(\frac{\rho_s}{\rho_g}\right)_2$ for Cold flow conditions.

As per Fitzgerald's calculating procedure, using equation (3.9)

$$\left(\frac{\rho_s}{\rho_g}\right)_1 = \left(\frac{\rho_s}{\rho_g}\right)_2 \quad (5.4)$$

Equating (5.2) and (5.3),

Fine Particle: - $\left(\frac{\rho_s}{\rho_g}\right)_2 = 3570.2$

$\rho_{s2} = 3570.2*1.184 = 4225$ Kg/m^3

Coarse Particle: - $\left(\frac{\rho_s}{\rho_g}\right)_2 = 3408.5$

$\rho_{s2} = 3408.5*1.184 = 4036$ Kg/m^3

5.2 Calculation of Particle Diameter

Combining Reynolds and Froude numbers gives the scale factor for two beds. Using equation (3.10)

Scale factor(m) = $\frac{L2}{L1} = \left(\frac{\rho_{g1}\mu_2}{\rho_{g2}\mu_1}\right)^{\frac{2}{3}} = \left(\frac{0.4436*0.00001846}{1.184*0.0000475}\right)^{\frac{2}{3}} = 0.277$

Fine particle

(Hot)Mean Diameter (dp_1) =0.000002096m = 20.93 μm [Appendix D]

(Cold) Mean diameter (dp_2) = dp_1 * m = 0.000002093*0.277 = 0.000005805 m = 5.79 μm

Coarse Particle

(Hot) Mean Diameter (dp_1) = 0.000604m = 604µm [Appendix E]

(Cold)Avg. Diameter (dp_2) = dp * m = 0.000604*0.277 = 0.000167m = 167 µm

The mean diameter of both fine and coarse particles is calculated on the PSD given in Appendix F.

5.3 Calculation of Minimum fluidization Velocity

From Equation. (2.9), Minimum fluidization velocity (u_{mf})

$$u_{mf} = \frac{{d_p}^2 \cdot (\rho_s - \rho_g) g}{1650\mu} \quad (5.5)$$

Fine Particles

From Equation. (2.7)

When, Reynolds number (Re_{mf}) = $\left[\sqrt{33.7^2 + 0.0408 \frac{d_p^3 \rho_g (\rho_s - \rho_g) g}{\mu^2}} - 33.7\right] < 20$

$$= \sqrt{33.7^2 + 0.0408 \frac{0.00002093^3 * (1583 - 0.4436) * 0.4436 * 9.81}{0.0000475^2}} - 33.7$$

= 1.70E-05 < 20

Now, From Equation (5.5)

(Hot) MVF (u_{mf}) = $\frac{0.00002093^2 * (1583 - 0.4436) * 9.81}{1650 * 0.0000475}$ = 8.677 E-05 m/s

(Cold/Scaled) MVF (u_{mf})= $\frac{0.000000579^2 * (4226 - 1.184) * 9.81}{1650 * 0.0000185}$= 4.55 E-05 m/s

The minimum fluidization velocity of the fine particle is shown in Figure 5.1 as a function of particle diameter. For fine particles, the average minimum fluidization velocity in hot and cold flow conditions is very small.

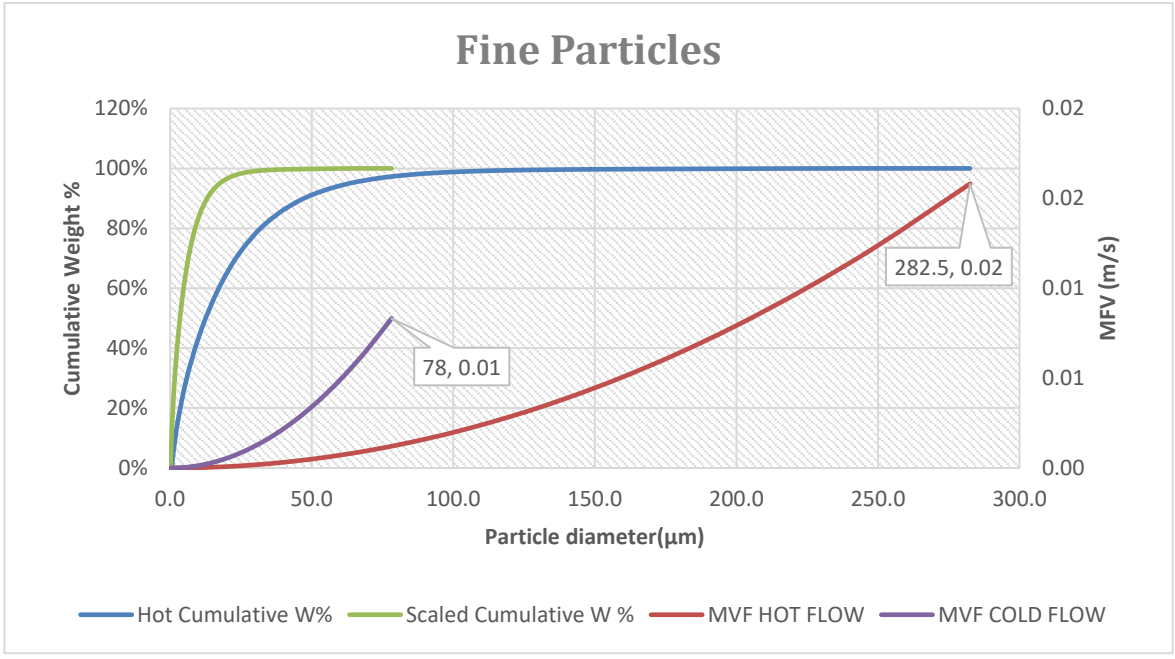

Figure 5.1: MFV of Fine Particles in Hot and Cold Flow Condition

Coarse Particles

From Equation (2.7)

When, Reynolds number (Re_{mf}) = $\left[\sqrt{33.7^2 + 0.0408\frac{d_p^3 \rho_g(\rho_s-\rho_g)g}{\mu^2}} - 33.7\right] < 20$

$$= \sqrt{33.7^2 + 0.0408\frac{0.000604^3*(1512-0.4436)*0.4436*9.81}{0.0000475^2}} - 33.7$$

$$= 0.387 < 20$$

From Equation (5.5)

(Hot) MVF (u_{mf}) = $\frac{0.000604^2*(1512-0.4436)*9.81}{1650*0.0000475}$ = 0.06854 m/s

(Cold/Scaled) MVF (u_{mf})= $\frac{0.000167^2*(4036-1.184)*9.81}{1650*0.0000185}$= 0.0363 m/s

The minimum fluidization velocity of the coarse particle is shown in Figure 5.2 as a function of particle diameter. For coarse particles, the average minimum fluidization velocity was determined to be 0.0695m/s in hot flow and 0.036m/s in cold flow conditions.

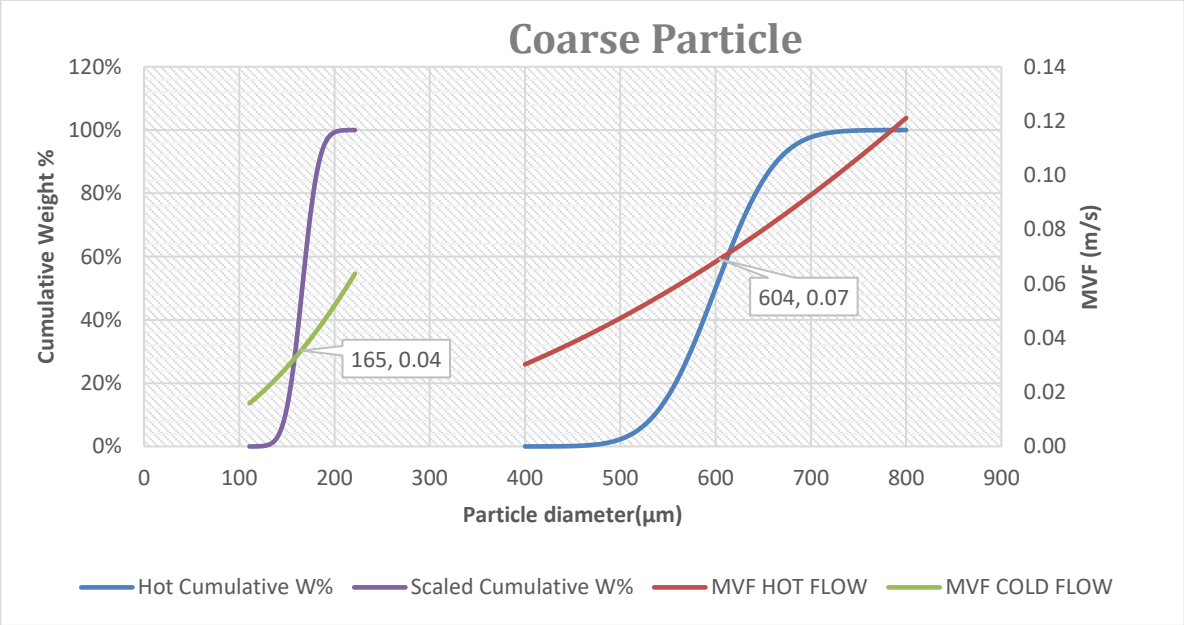

Figure 5.2: MFV of Coarse Particles in Hot flow and Cold Flow conditions

Figure 5.3 and 5.4 shows comparison of minimum fluidization velocity of fine and coarse particles as function of particle diameter in hot and flow condition respectively. Also, it shows the operating diameter of both fine and coarse particles for the binary mixture.

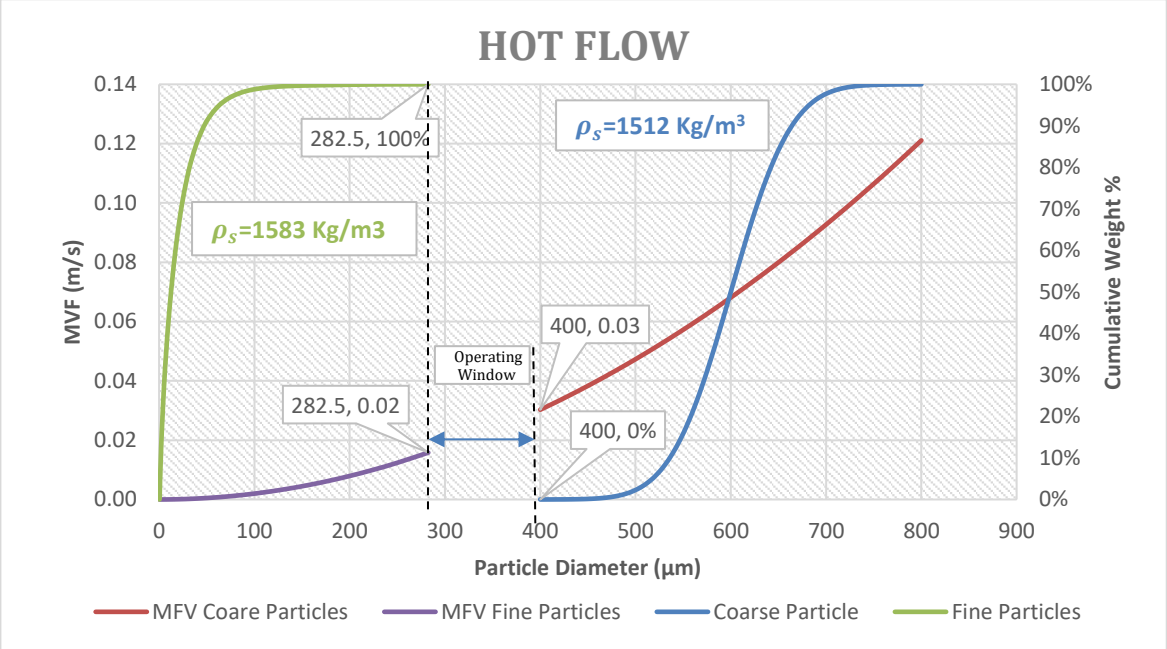

Figure 5.3: Comparison of MFV of Fine and Coarse Particles in Hot Flow Condition

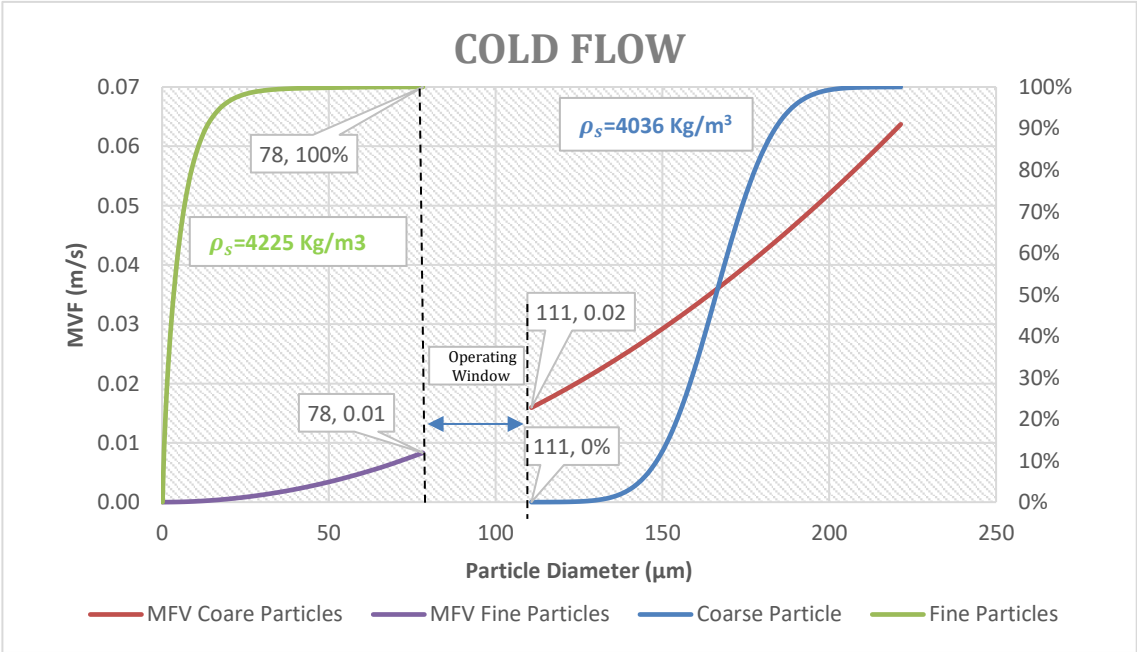

Figure 5.4:Comparison of MVF of fine and Coarse Particles in Cold Flow Condition

The Minimum fluidization velocity of each particle diameter in a hot and cold flow condition for coarse particles is shown in Appendix E and the same for the fine particles is shown in Appendix D.

5.4 Calculation of Terminal Settling Velocity

From Equation (2.14), The dimensionless particle size d* is measured by,

$$d^*_p = d_p \left[\sqrt[3]{\frac{\rho_g(\rho_s - \rho_g)g}{\mu^2}} \right]$$

$$=0.00002096 \left[\sqrt[3]{\frac{0.4436(1583-0.4436)*9.81}{0.0000475^2}} \right]$$

$$=0.30$$

From Equation (2.13), The dimensionless gas velocity u*

$$u^* = \left[\frac{18}{(d^*_p)^2} + \frac{2.335 - 1.744\phi_s}{(d^*_p)^{0.5}} \right]^{-1}, for\ 0.5 < \phi_s < 1$$

$\{Assuming\ Sphericity\ of\ particle(\phi_s) = 0.84\}$

$$= \left[\frac{18}{(0.30)^2} + \frac{2.335 - 1.744 * 0.84}{(0.30)^{0.5}} \right]^{-1}$$

$$=0.0049$$

From Equation (2.11)

Fine particle

(Hot) Terminal settling velocity $(u_t) = u^* \left[\sqrt[3]{\frac{\mu(\rho_s-\rho_g)g}{{\rho_g}^2}} \right]$

$$= 0.0049 * \left[\sqrt[3]{\frac{0.0000475*(1583-0.4436)*9.81}{0.4436^2}} \right]$$

$$= 0.00761 \text{m/s}$$

(Cold/Scaled) Terminal settling velocity(u_t) =0.00401m/s

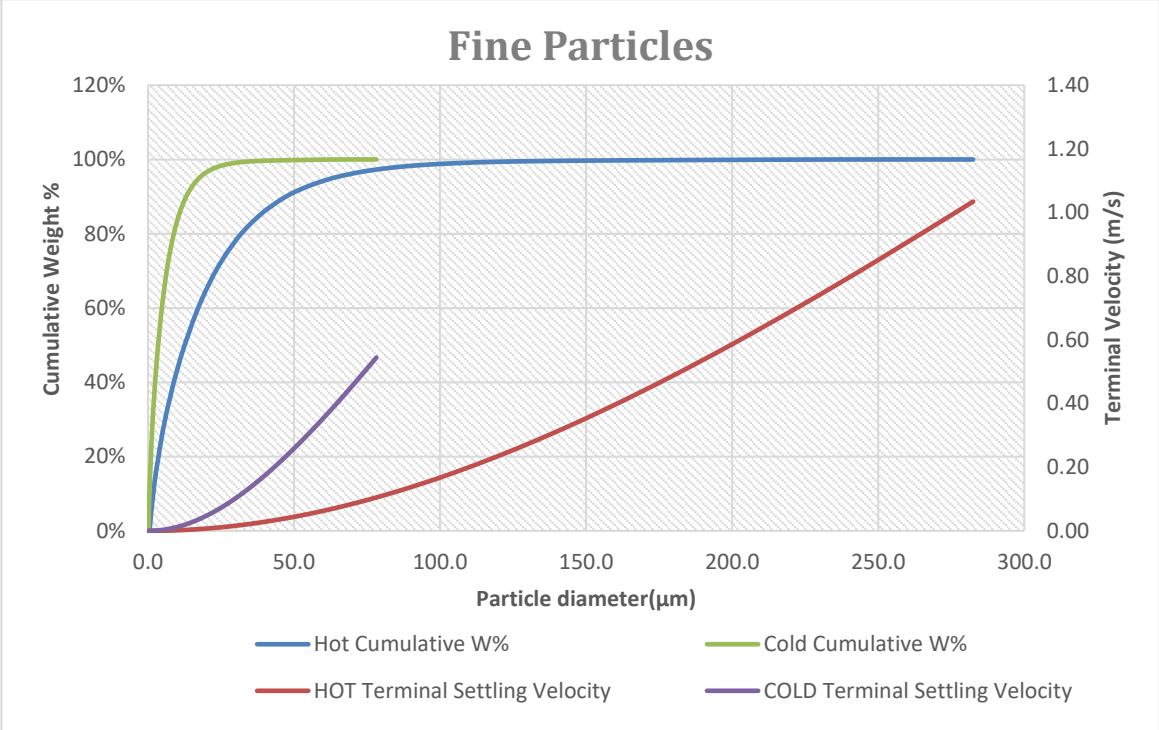

Figure 5.5: Terminal setting velocity of Fine Particles in Hot and cold flow

The terminal settling velocity of fine particles is shown in Figure 5.5 as a function of particle diameter. For fine particles, the average terminal settling velocity in hot and cold flow conditions is very small.

Coarse Particle

Similarly,

(Hot) Terminal settling velocity (u_t) = 2.84m/s

(Cold/Scaled) Terminal settling velocity (u_t) = 1.5m/s

The terminal settling velocity of coarse particle is shown in Figure 5.6 as a function of particle diameter. For coarse particles, the average terminal settling velocity was determined to be 2.84m/s n hot flow and 1.5m/s in cold flow conditions.

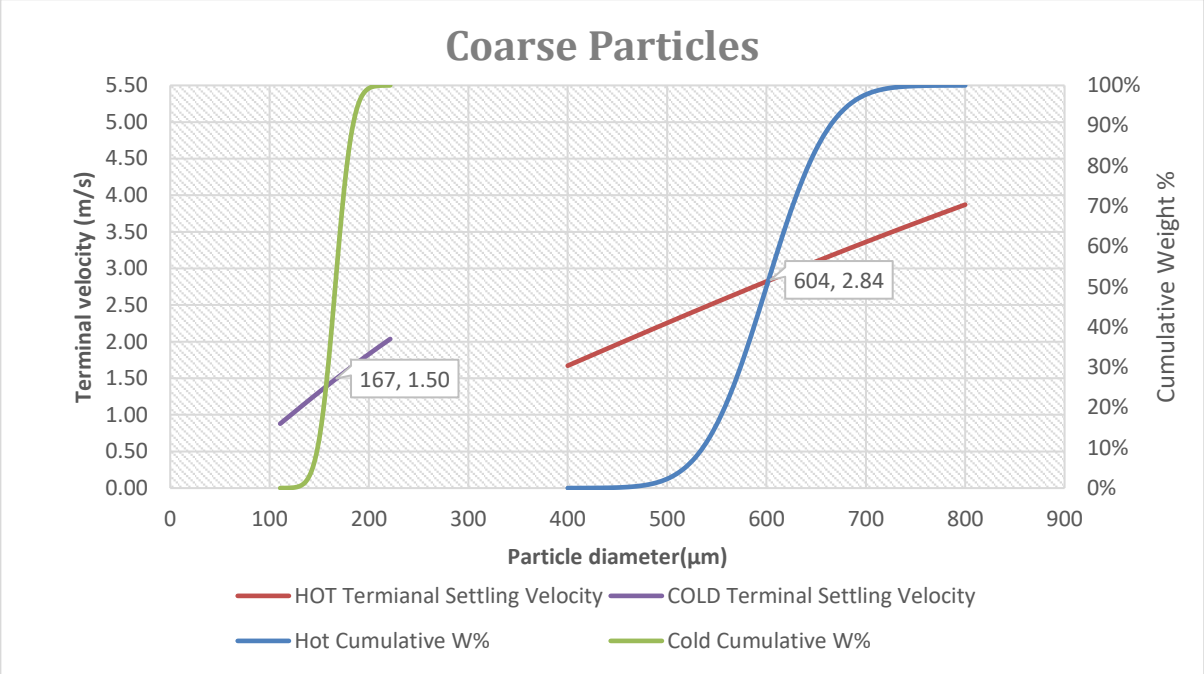

Figure 5.6 :Terminal settling Velocity of Coarse Particles in Hot and Cold Flow

The Terminal Settling velocity of each particle diameter in a hot and cold flow condition for coarse particles is shown in Appendix E and the same for the fine particles is shown in Appendix D.

5.5 Mass Balance Calculations

A total of 500 g of segregated fine particles and 1500 g of coarse particles were mixed in a 1: 3 ratio of 1:3 to prepare the binary mixture. The chemical composition of both fine and coarse particles at different segregated velocities was obtained from NORCEM (Appendix C). The change in the chemical composition of samples in the pre and post binary experiment can be calculated using the mass balance principle.

Here, we find the amount of Al_2O_3 in 500 gm of the pre binary experiment for fine particles.

Mass of fine particles at 200L/min (M_{200}) = 143gm (Table 6.3)

% Al_2O_3 in M_{200} = 98.61%

Mass of fine particles at 250L/min (M_{250}) = 357gm (Table 6.3)

% Al_2O_3 in M_{200} = 99.54%

Using Mass balance principle,

M_{200} *% Al_2O_3 in M_{200} + M_{250} * % of Al_2O_3 in M_{200} = M_{500} * Y (% Al_2O_3 in 500gm)

143*98.61+357*99.54 = 500 * Y

Y = 99.27 %

i.e., Amount of Al_2O_3 = 500* 99.27% = 496.37 gm

Similarly, the amount of other chemicals can be calculated for pre- and post-binary experiments. The calculations results are in sub-Chapter 6.4.

5.6 Purity Calculations

The purity calculation is done to analyze the amount of respective chemical compounds present in the entrained mass. After binary experiments fine particles (white alumina) were collected. The mass of white alumina segregated from the brown alumina after the binary experiment was less so, we can say that there are changes in the composition of chemical compounds. Because we intend to collect only fine particles, which means 100% purity, but the presence of coarse particles in entrained mass along with fine particles cannot be avoided in this case. Since Al_2O_3 is a major chemical compound, we are interested in calculating its purity.

From the mass balance calculations, we already have the chemical compositions of pre- and post-binary experiments. (Appendix C).

Here we calculate the amount of (Alumina) Al_2O_3 in 480 gm of particles in the post binary experiment.

Let, Mass of fine particles in segregated mass = X_F gm

Mass of coarse particles in segregated mass = X_C gm

Segregated mass after Binary Experiment = 480 gm (Figure 6.11)

Then,

[X_F] * % of Al_2O_3 in pre binary fine + [X_C] * % of Al_2O_3 in pre binary coarse = segregated mass * % % of Al_2O_3 in post binary fine

X_F * 99.27% + X_C * 40.28% = 480 * 98.87% ……I

Also,

$X_F + X_C = 480$..... II

Solving I and II gives.

X_F = 479.97 gm

X_C = 0.0325gm

% purity in terms of Al_2O_3 = $\frac{479.97}{480} * 100\% = 99.99\%$

This signifies that 479.97g of (Alumina) Al_2O_3 is present in the 480g of segregated mass. Similarly, masses for other chemical compounds can be calculated but are negligible.

6 Results

6.1 Pure Particles

The Particles which were purchased as per the scaled characteristics were tested with PSD Analyzer to determine the particle size. The mean diameter of the white alumina claimed by the manufacturer was 5µm, but on testing in the lab it was found to be 7.63 µm. This was slightly on the higher side than the required size. The mean diameter after sieving was 6.38 µm. The PSD of fine particles before and after is given in Appendix K and L respectively.

Similarly, the average diameter of Brown Alumina claimed by manufacturer was between 180 to 212µm but was found to be 224.34µm. Hence, constant sieving and testing of the particles were done to get the required size of the brown alumina of 181.38µm. The materials used in the experiments can be viewed in table 6.1. The PSD of coarse particles before and after is given in Appendix H and I respectively.

Table 6.1: Overview of materials used for experiments.

Material	**Particle Type**	**Average Diameter[μm]**		**Density[$kg/m3$]**
		After Sieving	**PSD Analyzer (Before Sieving)**	
Brown Alumina	Coarse	181.38	224.34	3950
White Alumina	Fine	6.38	7.63	3950

6.1.1 Brown Alumina

a) Particle Size Distribution

The average particle size of brown alumina after sieving is 181.38 µm. PSD of brown alumina is shown in Figure 6.1.

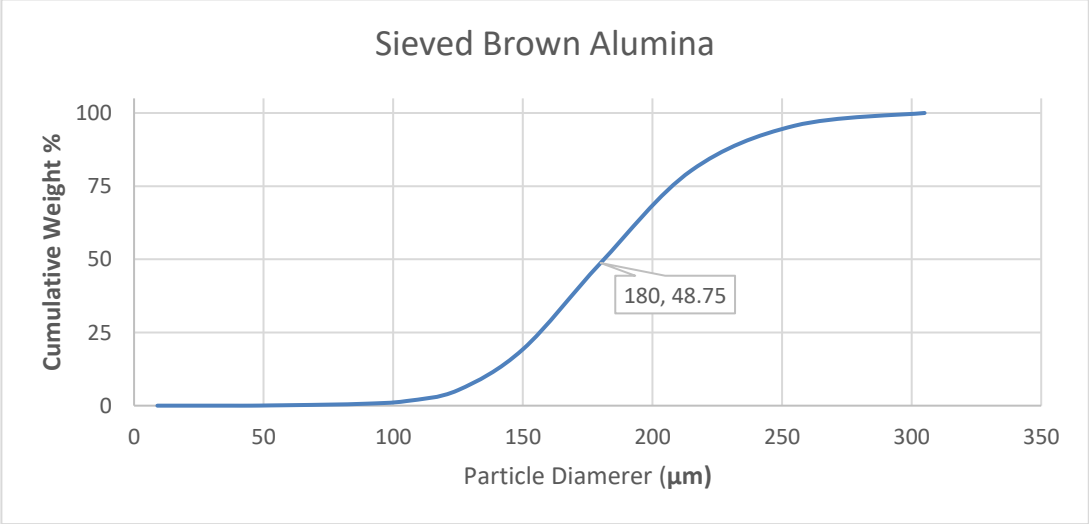

Figure 6.1: PSD of Sieved Brown Alumina

b) Fluidized Bed

The minimum fluidization velocity was obtained at ~0.08m/s. This is shown by the pressure drop profile in Figure 6.3 and the visual observation showing that fluidization occurred around 0.08m/s. The flow velocity of the gas was increased until satisfactory mixing conditions were observed at 0.59 m / s, which is seen in Figure 6.2 as the bed height increased.

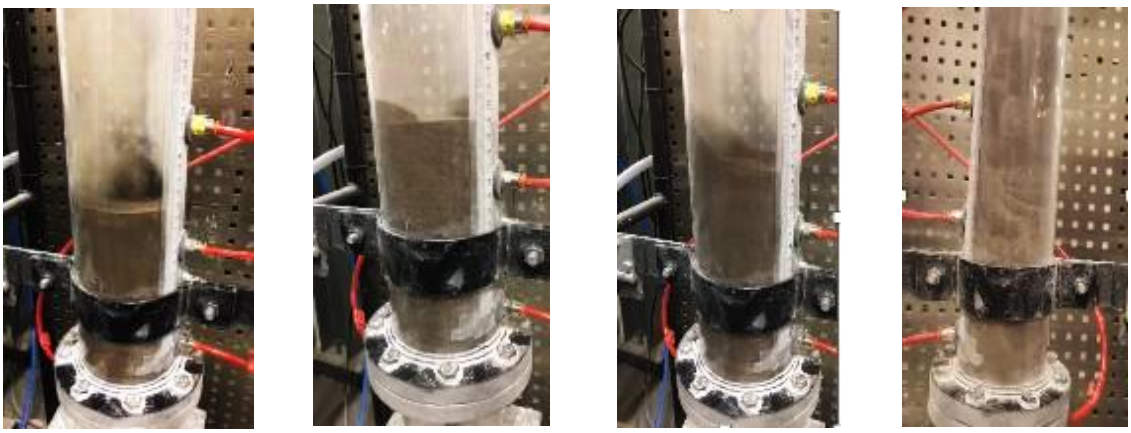

Figure 6.2:Fluidization Behavior of Brown alumina

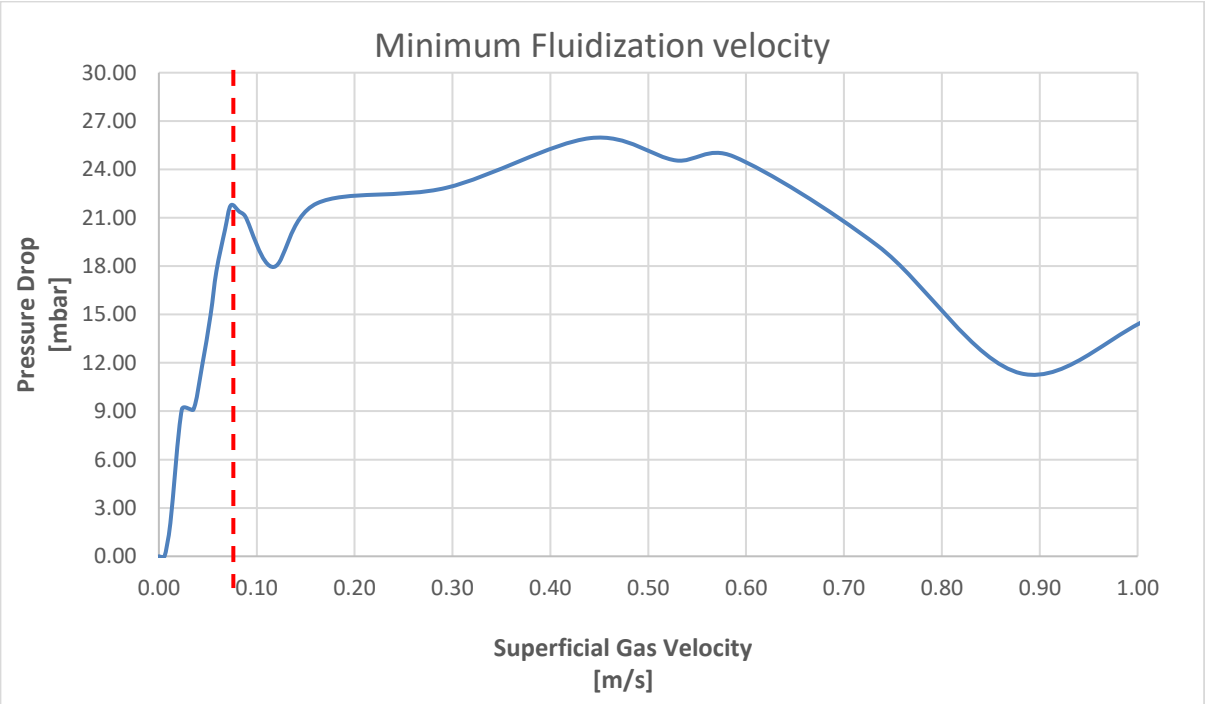

Figure 6.3:Pressure Drop profile- Brown Alumina

Table 6.2:Mass collected at each segregation velocity- Brown alumina.

Flow rate (L/min)	Flow rate (m/s)	Entrained (gm)	Remaining Mass (gm)	Mass fraction	Mass Collected (%)	To be used for Binary(gm)
0	0.00	0	4020	0%	0%	
300	0.88	780	3240	19%	19%	647
350	1.03	500	2740	15%	12%	405
400	1.17	495	2245	18%	12%	351
450	1.32	450	1795	20%	11%	97
550	1.62	1000	795	56%	25%	
600	1.76	285	510	36%	7%	
650	1.91	200	310	39%	5%	
700	2.06	100	210	32%	2%	
750	2.20	210	0	100%	5%	
						1500

From Table 6.2 we can see that the brown particles started to entrain from 0.88m/s and at around 2.2m/s, all the bed weight was collected. 1500gm of coarse particle was collected after sieving which was required for the binary experiment. Figure 6.4 shows the mass accumulated with respect to the time during entrainment.

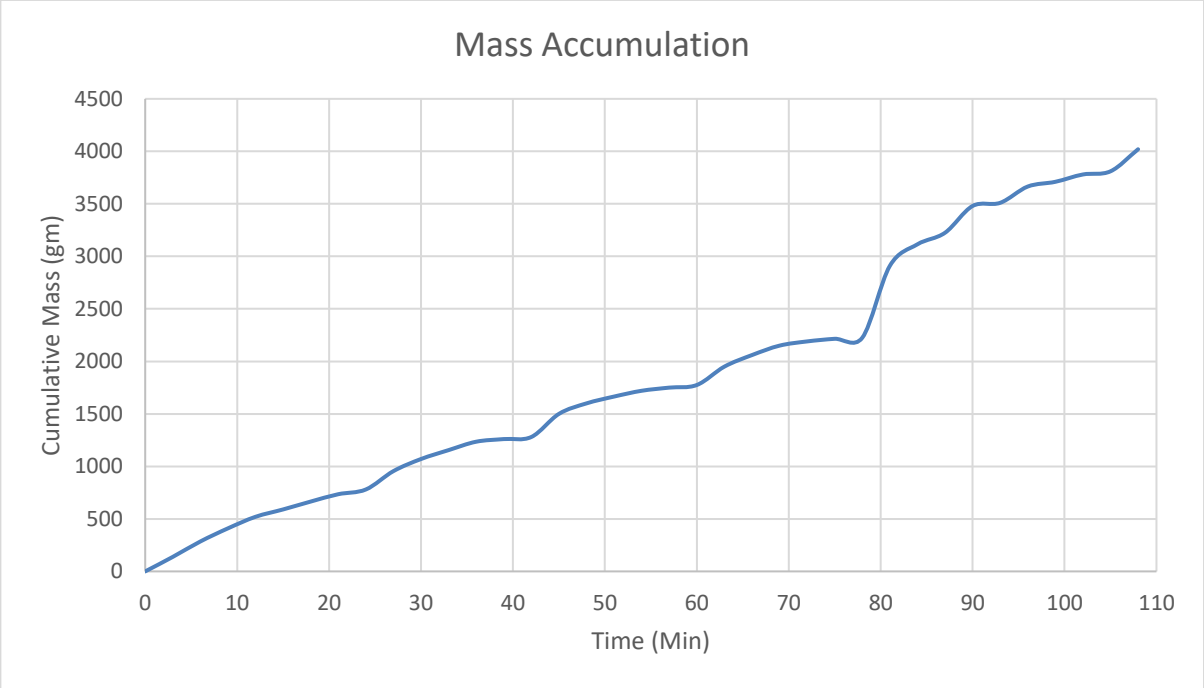

Figure 6.4: Mass accumulation- Brown Alumina

6.1.2 White Alumina

a) Particle Size Distribution

The average particle size of white alumina after sieving is 6.38 µm. PSD of the white alumina is shown in Figure 6.5.

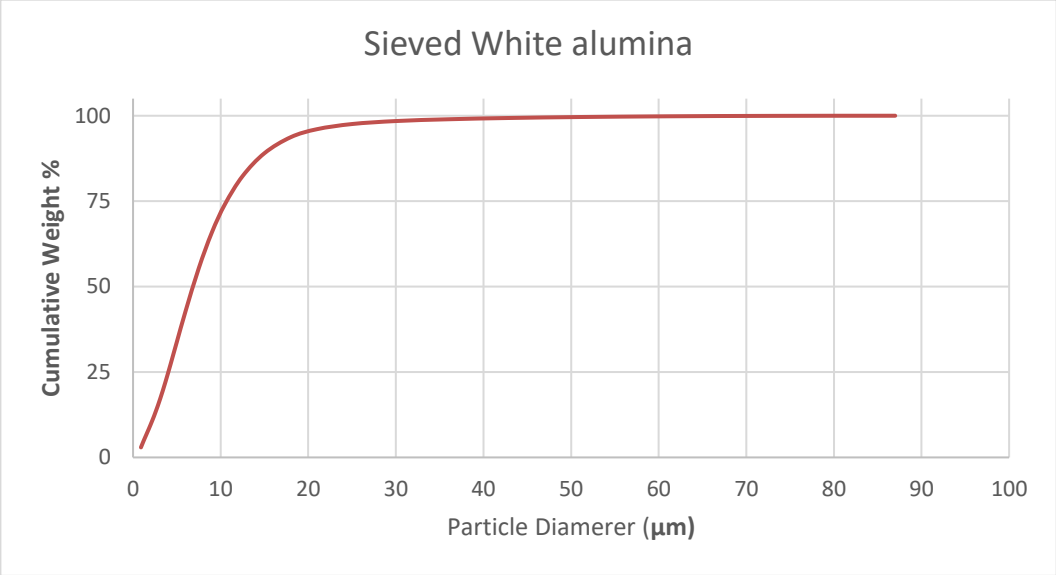

Figure 6.5: PSD of Sieved White Alumina

b) Fluidized Bed

The minimum fluidization velocity was difficult to determine experimentally because of the cohesive forces of the white alumina. This is shown by the pressure drop profile in Figure 6.7. The flow velocity of the gas was raised, and the rat holes were seen at around 0.02m/s as shown in Figure 6.6, where there was a reduction in the pressure drop. Also, at 0.1m/s another rat hole was formed, and a larger pressure drop is visible as shown in Figure 6.7. Few bed cracks are visible at 0.088m/s and at 0.21m/s mixing is seen.

0.02m/s (Rat Holes) 0.088m/s (Bed Cracks) 0.21m/s

Figure 6.6 :Fluidization Behavior of White Alumina

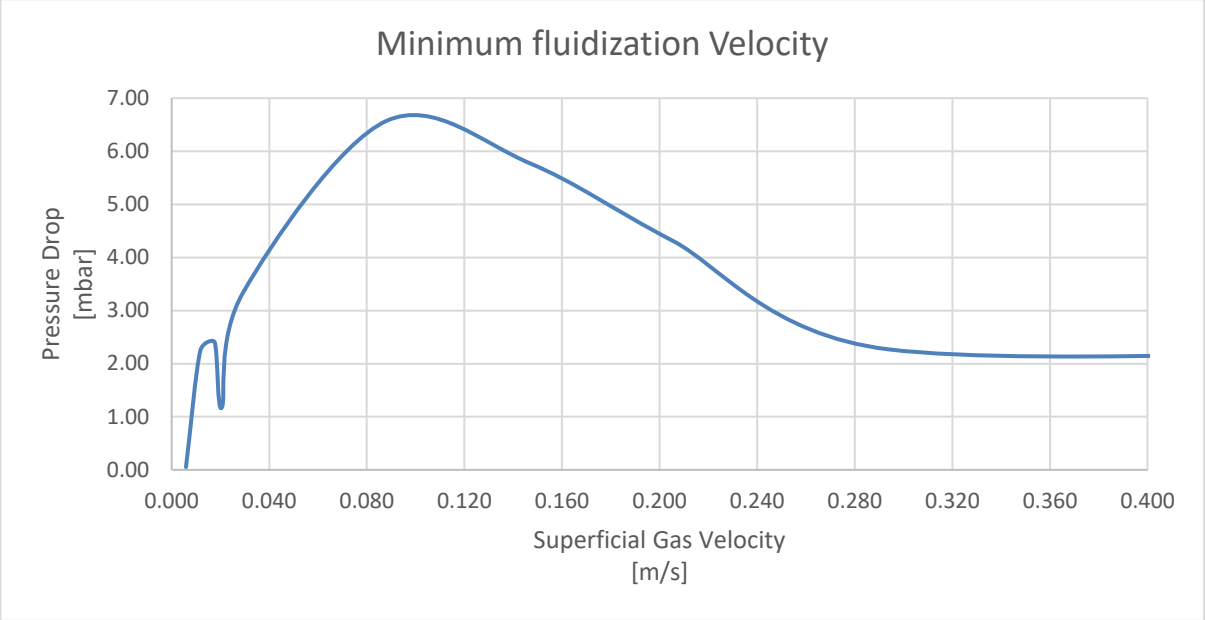

Figure 6.7: Pressure drop profile- White Alumina

From Table 6.3 we can see that the white alumina started to entrain from 0.29m/s and at around 1.32m/s all the bed weight was collected. 500 gm of fine white alumina was collected after sieving which was required for the binary experiment. Figure 6.8 shows the mass accumulated with respect to the time during the entrainment.

Table 6.3: Mass collected at each segregation velocity- White alumina.

Flow rate (L/min)	Flow rate (m/s)	Entrained (gm)	Remaining Mass (gm)	Mass fraction	Mass Collected (%)	To be used for binary expt. (gm)
0	0.00	0	2000	0%	0%	
100	0.29	40	1960	2%	2%	
200	0.59	190	1770	10%	10%	143
250	0.73	925	845	52%	46%	357
300	0.88	565	280	67%	28%	
350	1.03	120	160	43%	6%	
400	1.17	90	70	56%	5%	
450	1.32	70	0	100%	4%	
						500

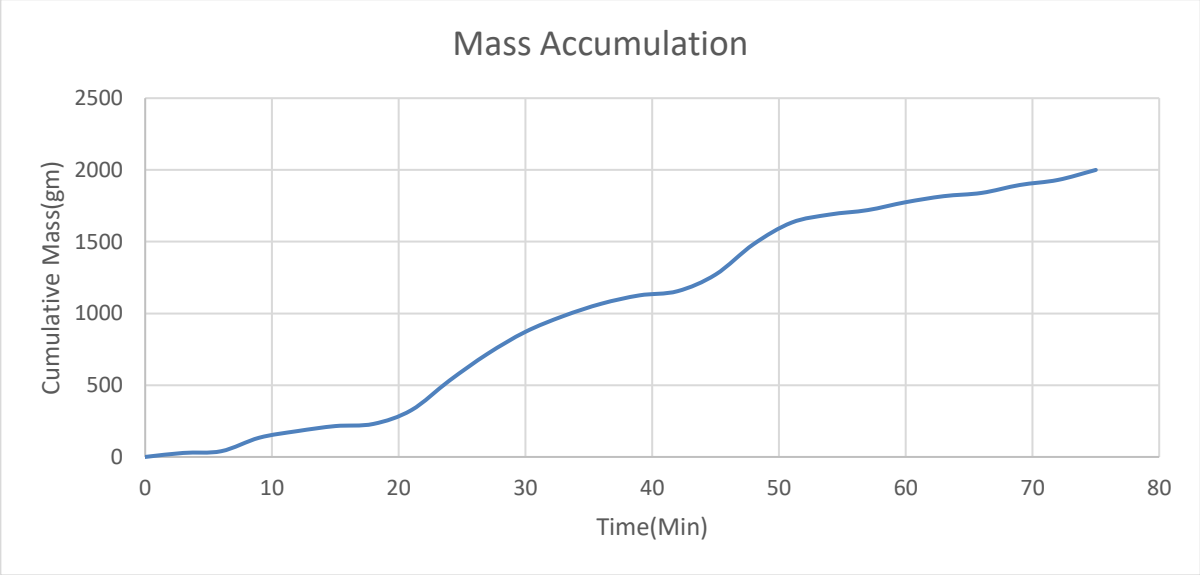

Figure 6.8: Mass accumulation- White Alumina

6.2 Binary Mixtures Particles

Exploring the flow pattern of binary particles in the Bubbling fluidized Bed (BFB) is critical for not only understanding mixing behavior but also designing and optimizing the binary system [14].. The quick expansion of mixture particles appears to raise the bed height after introducing the gas flow from the bottom of distributor. Meanwhile, the small particles in the bottom region penetrate the large particles in the upper layer because of the formation of a void structure between the interface of small particles and large particles.

The pressure characteristic is of great importance for the evaluation of gas-solid behaviors in the fluidization[25]. Figure 6.9 shows the influence of superficial gas velocity on the instantaneous pressure drop. It is found that the pressure drop under different conditions randomly fluctuates around a fixed value. The oscillation of pressure drop mainly depends on the disturbance caused by the formation and collapse of bubbles in the BFB.

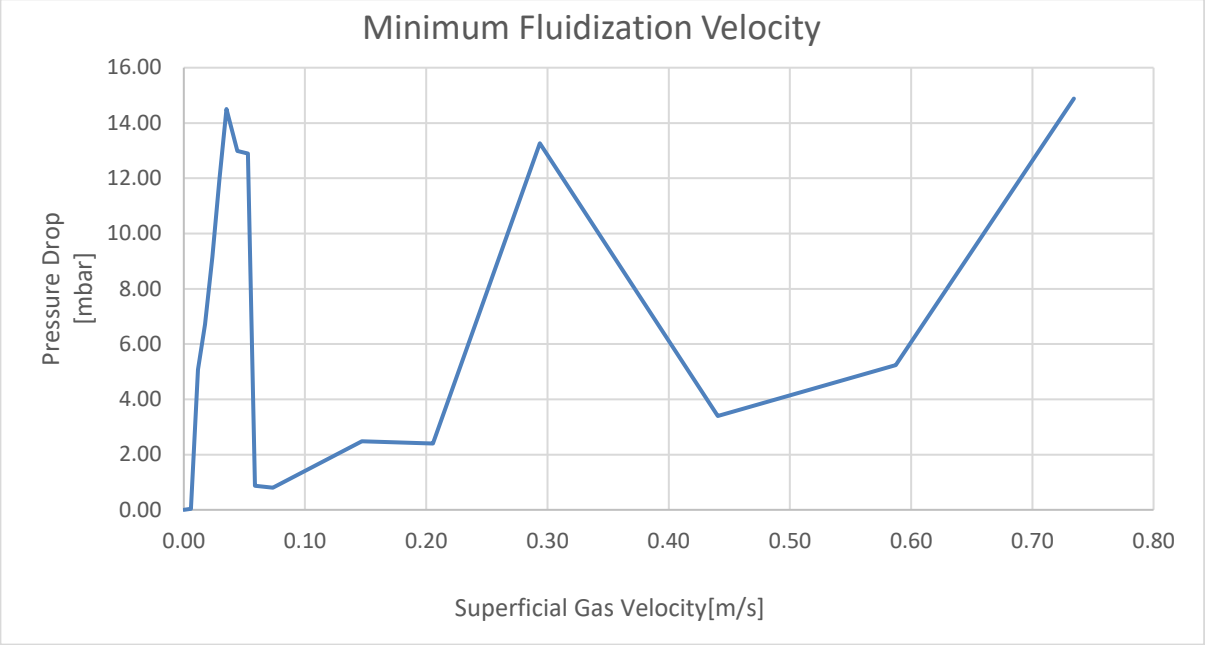

Figure 6.9: Pressure drop profile- Binary Mixture

In Figure 6.10 the particles started mixing at 0.07m/s and the optimal mixing was at 0.15m/s, which can be determined by the increase in the bed height. Fine particles started to segregate at 0.29m/s and only brown particles were left in the reactor at 0.73m/s.

0.03m/s Mixing-0.15m/s 0.29m/s 0.73m/s

Figure 6.10 :Fluidization Behavior of Binary Mixture

In Figure 6.11 we can see that at 0.73m / s, 480 g of 500 g of fine particles were collected, representing 96% of the total fine particles in the bed. The remainder is presumed to have been lost or clinging to the bed's walls and filter.

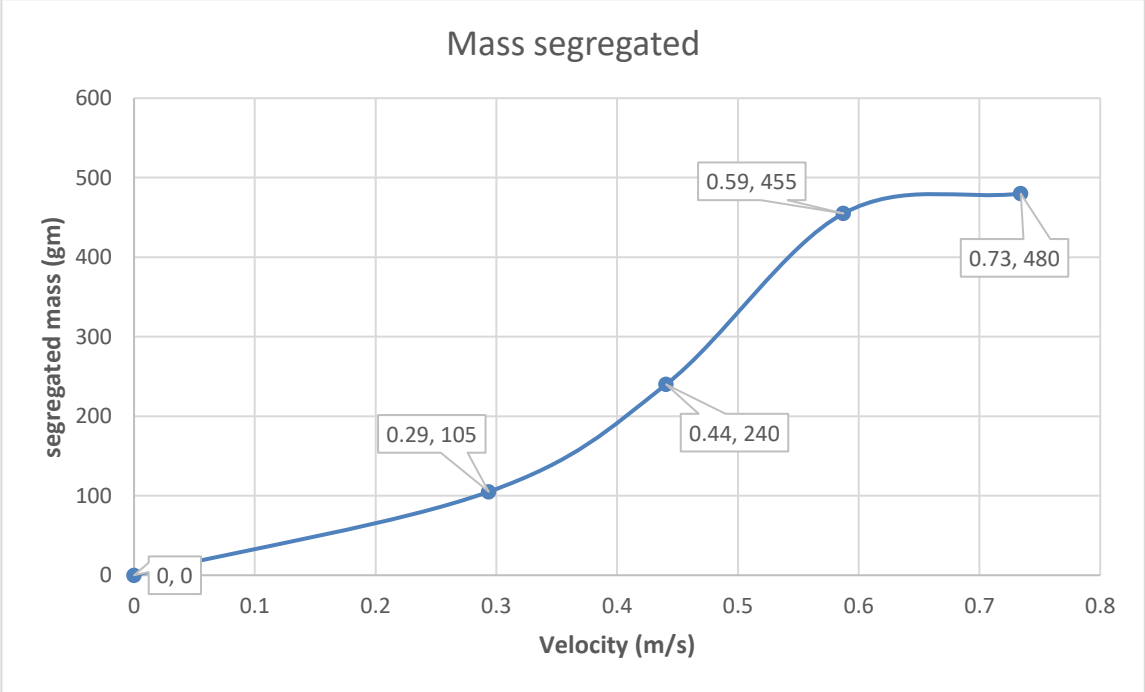

Figure 6.11: Mass collected at each segregation velocity- Binary Experiment

The binary mixture has segregated portions, namely the finer fraction of fine particles and the coarser fraction of coarse particles. Figure 6.12 shows the overlap fractions in fine and coarse particles, which should be excluded to get higher segregation efficiency. It represents the operating window between 250 to 300 L/min.

The entrained mass of pure fine particles at segregation flow rate of 100L/min, 200L/min, and 250L/min are to be considered for binary mixture. Similarly, the entrained mass of pure coarse particles at 450L/min, 550L/min,700L/min, and 750L/min can be used for the binary mixture.

Further the selected mass fractions of both pure fine and coarse particles are subjected to the PSD analysis. In Figure 6.13 we can see that there is slight overlap in terms of the particle size between fine and coarse particles. The largest fine particle is 103µm which is slightly greater than the possibly smallest coarse particle at 90µm. Therefore, further sieving was required to remove the overlapping.

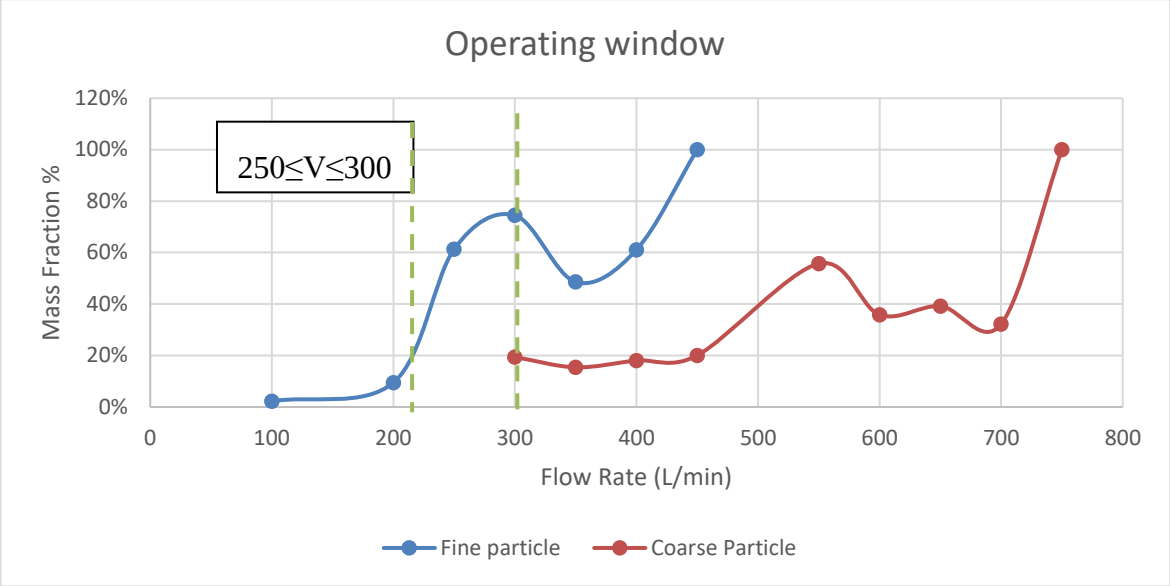

Figure 6.12: Operating Window after Segregation

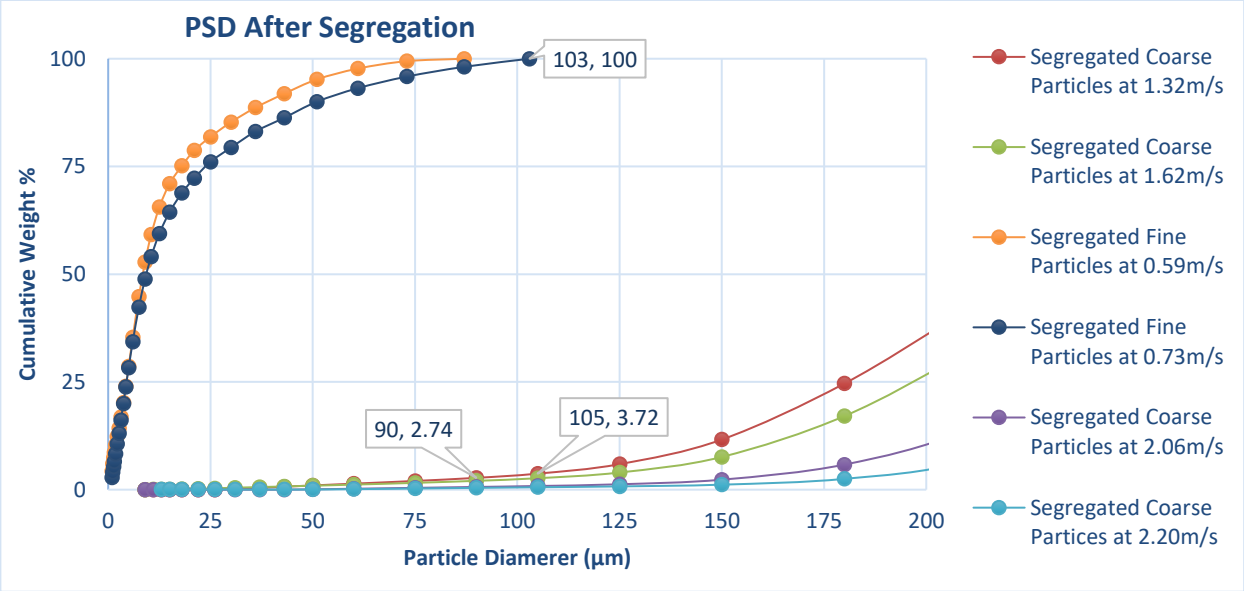

Figure 6.13: PSD After Segregation (Pre-binary Expt.)

6.3 Void Fraction

Voidage (ε) is defined as the fraction of the total volume that is free space available for the flow of fluids, and thus the fractional volume of the bed occupied by solid material is (1 − ε). Depending upon the nature of the porous medium, the voidage may range from near zero to almost unity [26]. The higher the value of voidage, the lower is the resistance to flow of a fluid. The voidage of a particle bed is significantly affected by particle shape, orientation, and size distribution. However, voidage has a strong correlation with sphericity [27].

Table 6.4 shows the results, which show that coarse particles have a smaller proportion than fine particles. Similarly, due to the size difference between the fine and coarse particles, the void fraction

of the mixture is lower than that of the coarse particles, resulting in the flow of smaller bubbles in the fluidized bed [27], [28].

Table 6.4: Void Fraction Calculations

Parameters	Unit	Brown alumina	White Alumina	Binary Experiment
Weight of particle in Bed	kg	4	2	2
Particle Density	kg/m^3	3800	3950	3950
Particle Volume	m^3	0.0011	0.0005	0.0005
Bed Height(m)	m	0.384	0.224	0.174
Internal Diameter of Rig	m	0.0850	0.0850	0.0850
Area	m^2	0.0057	0.0057	0.0057
Bed Volume	m^3	0.0023	0.0013	0.0010
Bulk Density	kg/ m^3	1754	1573	2026
Void	m^3	0.0012	0.0008	0.0005
Void Fraction		0.51	0.60	0.49

6.4 Chemical Composition

The chemical composition of white and brown alumina was calculated for a pre binary experiment as shown in sub-chapter 5.5.

The chemical composition of 143 g collected at 200L/min and 357 gm collected at 250L/min for the binary experiment is shown in Table 6.5. A total of 500 g of fine particles were used and their final composition was calculated.

Table 6.5: Chemical composition of Fine particles in pre binary experiment

Compound	Pure Fine at 200 L/min (%)	Mass at-200L/min (gm)	Pure Fine at 250 L/min (%)	Mass at-250L/min (gm)	Total Mass (gm)	Final composition (%)
SiO2	0.55	0.79	0.15	0.54	1.32	0.26
Al2O3	98.61	141.01	99.54	355.36	496.37	99.27
Fe2O3	0.30	0.43	0.05	0.18	0.61	0.12
CaO	0.00	0.00	0.00	0.00	0.00	0.00
SO3	0.01	0.01	0.00	0.00	0.01	0.00
MgO	0.24	0.34	0.00	0.00	0.34	0.07
K2O	0.017	0.02	0.008	0.03	0.05	0.01
Na2O	0.244	0.35	0.228	0.81	1.16	0.23
P2O5	0.000	0.00	0.004	0.01	0.01	0.00
Mn2O3	0.010	0.01	0.003	0.01	0.03	0.01
SrO	0.003	0.00	0.002	0.01	0.01	0.00
TiO2	0.004	0.01	0.007	0.02	0.03	0.01
ZnO	0.007	0.01	0.007	0.02	0.04	0.01
		143gm		**357gm**	**500gm**	

The chemical composition of coarse particles collected at different flow rates is shown in table 6.6. A total of 1500 gm of coarse particle was used, and its final composition was calculated.

Table 6.6: Chemical composition of Coarse particles in pre binary experiment

Compound	Pure Coarse 300 L/min (%)	Mass at -300 L/min (gm)	Pure Coarse 350 L/min (%)	Mass at -350 L/min (gm)	Pure Coarse 400 L/min (%)	Mass at -400 L/min (gm)	Pure Coarse 450 L/min (%)	Mass at -450 L/min (gm)	Total Mass (gm)	Final Composition (%)
SiO2	26.74	173.03	25.92	104.98	27.40	96.17	25.33	24.57	398.76	26.58
Al2O3	41.00	265.30	40.15	162.61	39.43	138.40	39.09	37.92	604.22	40.28
Fe2O3	7.95	51.46	7.38	29.89	7.19	25.24	8.62	8.36	114.95	7.66
CaO	1.19	7.73	1.23	4.99	1.28	4.49	1.17	1.13	18.34	1.22
SO3	0.43	2.81	0.56	2.27	0.52	1.82	0.69	0.67	7.57	0.50
MgO	18.85	121.99	20.01	81.05	19.49	68.41	19.58	18.99	290.43	19.36
K2O	0.71	4.56	0.79	3.21	0.91	3.19	0.89	0.86	11.82	0.79
Na2O	0.56	3.61	0.71	2.89	0.69	2.44	0.81	0.78	9.73	0.65
P2O5	0.19	1.25	0.34	1.37	0.30	1.07	0.45	0.44	4.13	0.28
Mn2O3	0.47	3.06	0.61	2.47	0.57	2.01	0.74	0.72	8.26	0.55
SrO	0.22	1.41	0.36	1.47	0.33	1.17	0.48	0.46	4.52	0.30
TiO2	1.48	9.55	1.59	6.42	1.57	5.51	1.71	1.65	23.14	1.54
ZnO	0.19	1.24	0.34	1.37	0.31	1.08	0.46	0.44	4.13	0.28
		647gm		**405gm**		**351gm**		**97gm**	**1500gm**	

Table 6.7 shows the change in the composition of the compounds after the binary experiments.

Table 6.7: Chemical composition of the post-binary experiment

Compound	Pre-Binary-Fine (%)	Post Binary - Fine (%)	Pre-Binary-Coarse (%)	Post Binary - Coarse (%)
SiO2	0.26	0.26	26.58	26.59
Al2O3	99.27	98.87	40.28	41.73
Fe2O3	0.12	0.09	7.66	7.68
CaO	0.00	0.00	1.22	1.22
SO3	0.00	0.00	0.50	0.51
MgO	0.07	0.00	19.36	19.39
K2O	0.01	0.009	0.79	0.79
Na2O	0.23	0.24	0.65	0.65
P2O5	0.00	0.001	0.28	0.28
Mn2O3	0.01	0.003	0.55	0.55
SrO	0.00	0.002	0.30	0.30
TiO2	0.01	0.038	1.54	1.53
ZnO	0.01	0.006	0.28	0.28
Mass	**500gm**	**480gm**	**1500gm**	**1500gm**

7 Discussion

From the experimental results, there are three areas of particular interest: (1) the particle size distribution (2) the Fluidization and (3) chemical composition. These will now be addressed in turn.

7.1 Particle Size Distribution

When white and brown alumina were purchased, their particle sizes differed from those calculated.

7.1.1 Brown Alumina

The average particle size of the brown alumina was specified to be between 180 to 212 µm, but after testing the average size was 224.34 µm. The cumulative distribution showed that the particle size ranges from 4.5 µm to 615 µm. The PSD analysis report can be found in Appendix H. However, the desired average particle size with respect to the scaled calculation was 167 µm. Brown alumina obtained from segregation at different flow rates had different set of PSD in ascending order with respect to the flow rates. Therefore, the particles' sizes were smaller at low flow rates and larger at high flow rates. So, to obtain the desired size, sieving was performed to remove both finer and coarser particles from the brown alumina. It is evident that many coarser particles must be removed from the segregated samples to achieve the desired size from Figure 7.1. The average particle size of all the segregated Brown Alumina is over 200 µm. After sieving the average particle size of 181.38 µm (Appendix I) was obtained, which is still higher than the desire size of 167 µm. This was done to maintain the 1500gm of brown alumina required to conduct the experiment. It was of the notion to conduct at least two experiments out of the total available sample.

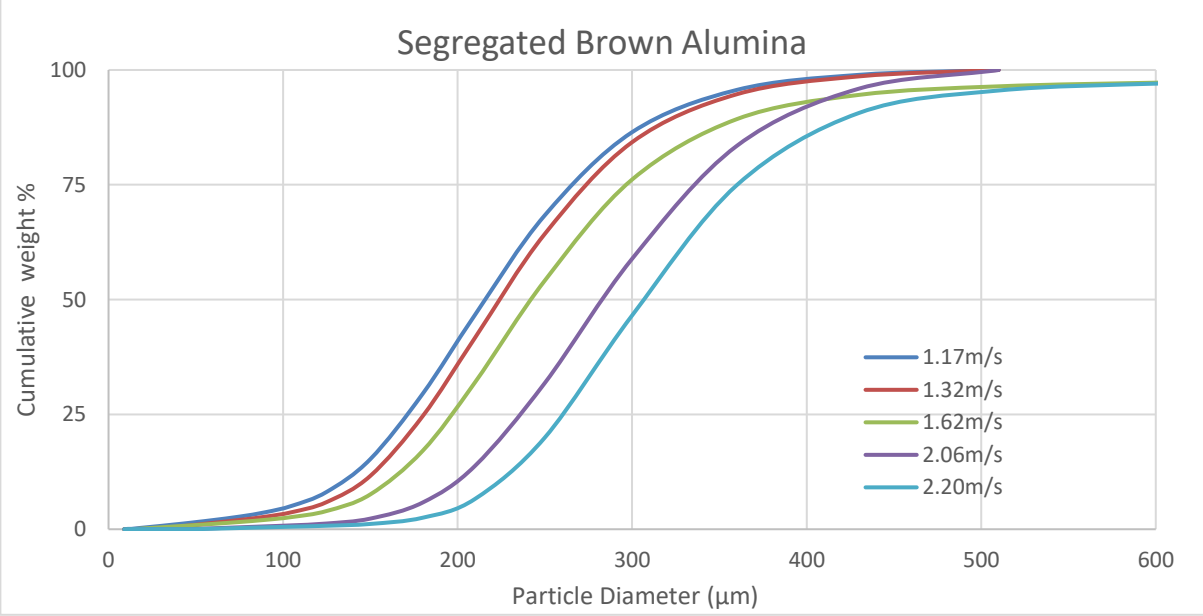

Figure 7.1: PSD of Segregated Brown Alumina

7.1.2 White Alumina

The average particle size of the white alumina was specified to be 5µm, but upon testing the average size was 7.63 µm. The cumulative distribution showed that the particle size ranges from 0.9 µm to 175 µm. The PSD analysis report can be found in Appendix K. However, the desired average particle size with respect to the scaled calculation was 5.8 µm. White alumina obtained from segregation at

different flow rates had different set of PSD in ascending order with respect to the flow rates. Therefore, the particles' sizes were smaller at low flow rates and larger at high flow rates. So, to obtain the desired size, sieving was performed to remove the coarser particles from the white alumina. It is evident that many coarser particles must be removed from the segregated samples to achieve the desired size from Figure 7.2. The average particle size of all the segregated white alumina is around 10µm. After sieving the average particle size of 6.38 µm (Appendix L) was obtained, which is still higher than the desire size of 5.8µm. The white Alumina particles could not be further sieved due to the ultra-fine sizes and sieving of sizes below 20µm was not available. Then again, sieving of such fine particles would pose a challenge due to the agglomeration effect because they stick together to form a film.

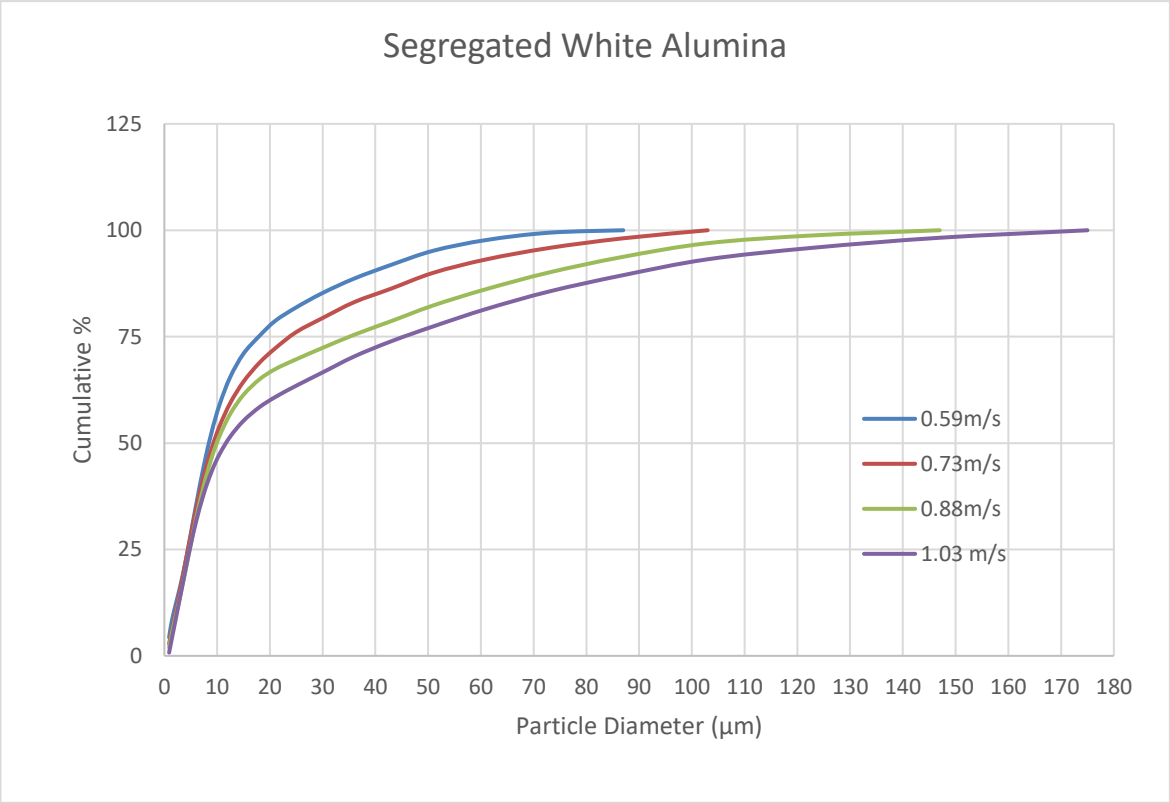

Figure 7.2: PSD of Segregated White Alumina

7.2 Fluidization

The pressure drop (Δp) against surface gas velocity (u_0) graph can be used to determine the transition from fixed to fluidized beds. The fluidization properties are governed by both particle properties such as particle size, particle density, particle shape etc. and fluid properties. Geldart has worked towards classifying the particles according to both size and density and has also discussed the effect of the particle size distribution in fluidized beds.

7.2.1 Brown Alumina

The minimum fluidization velocity of brown alumina during the experiment was 0.08m/s (Figure 6.3), which is different from the theoretical average value of 0.036m/s (Appendix E). The particle density was 3950 kg/m^3 and it was further assumed that the particles are spherical (0.84). But the

scaled density of the particle was 4036 kg/m^3. As we know that the minimum fluidization velocity is proportional to the particle density, the theoretical and experimental values are different. Also, the scaled average particle size (167µm) is smaller than experimental average particle sizes (181.38µm) the difference in the MFV is eminent. Furthermore, as evident in the videos, after fluidization was observed, the velocity increased, and bubbling was observed. This is characteristic of particles categorized as Geldart group A. Geldart group A particles are aeratable and fluidized well. They also exhibit significant bed expansion prior to bubble formation. The bed pressure drop during fixed bed operation corresponds to the gas velocity. When the bed reaches the minimum fluidization velocity, the pressure drop in the bed decreases slightly and stabilizes at the static bed pressure [3], [29]. The pressure in the bed remains constant until particle entrainment occurs. At 0.88m/s the pressure drop increases slightly as the entrainment starts and then it decreases as the bed height decreases following the entrainment.

7.2.2 White Alumina

Particles with particle sizes smaller than around 20 µm cannot be fluidized by a gas, because interparticle forces are too strong in comparison to particle weight, resulting in cohesive aggregation. The gas cannot disrupt the cohesive aggregates that reach a considerable size. The gas flow becomes heterogeneously dispersed in the bed and typically bypasses it through channels, reducing the efficiency of gas-solid interaction. The average particle size of white alumina was 6.38 µm, and it exhibits the typical characteristics of the Geldart's group C particles.

Ratholing is a common problem that occurs during fluidization of fine particles. Ratholing refers to the formation of channels or voids in the fluidized bed, which can limit the fluidization process and result in poor mixing and mass transfer. The formation of ratholes is often attributed to the cohesive forces between fine particles, which can cause them to stick together and form arches or bridges that block the flow of fluid. In figure 6.6 we can see the rat hole formation at 0.02m/s. When fluidization occurs, the particles at the bottom of the bed are lifted and suspended in the fluid, leaving behind a void that can quickly fill up with the remaining, unfluidized particles. This can result in the formation of bed cracks that can persist even at high fluid velocities. Hence, another rathole formation at higher velocity at around 0.1m/s. This persistent formation of rat holes and in between stabilization leads to the fluctuations in pressure drop.

At 0.21m/s a better mixing can be observed as the bed height rises significantly. With further increase in the velocity of gas to 0.29m/s, entrainment starts, and the pressure drop seems to decrease over the period.

7.2.3 Binary Mixture particles

Fluidization of binary mixtures, which contain two types of particles, might be more difficult than fluidization of single-particle systems. Several factors influence the fluidization behavior of binary mixtures, including particle size, density, shape, and surface properties of each component, as well as the relative proportions of the two components. The two types of particles in binary mixture fluidization might react differently based on their physical and chemical qualities. For example, one component may be denser or more cohesive than another, resulting in various fluidization behaviors. Therefore, the drag force from the fine particles makes the larger particles fluidize at lower gas velocities when those are in a mixture.

An abrupt drop in pressure at 0.04m/s can be seen in figure 6.9 due to the formation of the rat holes in the upper layer of the fine particles. Meanwhile, the small particles in the bottom region penetrate the large particles in the upper layer due to the formation of a void structure which results in the

mixing at 0.15m/s, which was a significant improvement over the pure white alumina mixing condition of 0.21 m/s.

The two components may separate during fluidization in some situations, with one component collecting at the top or bottom of the fluidized bed. Differences in properties of the respective particles strongly influence the hydrodynamic behavior of binary fluidized beds. Particles of different size and density can cause segregation during fluidization.[16] Relatively large differences in the tendency for segregation become correspondingly strong and eventually cause a binary fluidized bed to separate completely.[17]

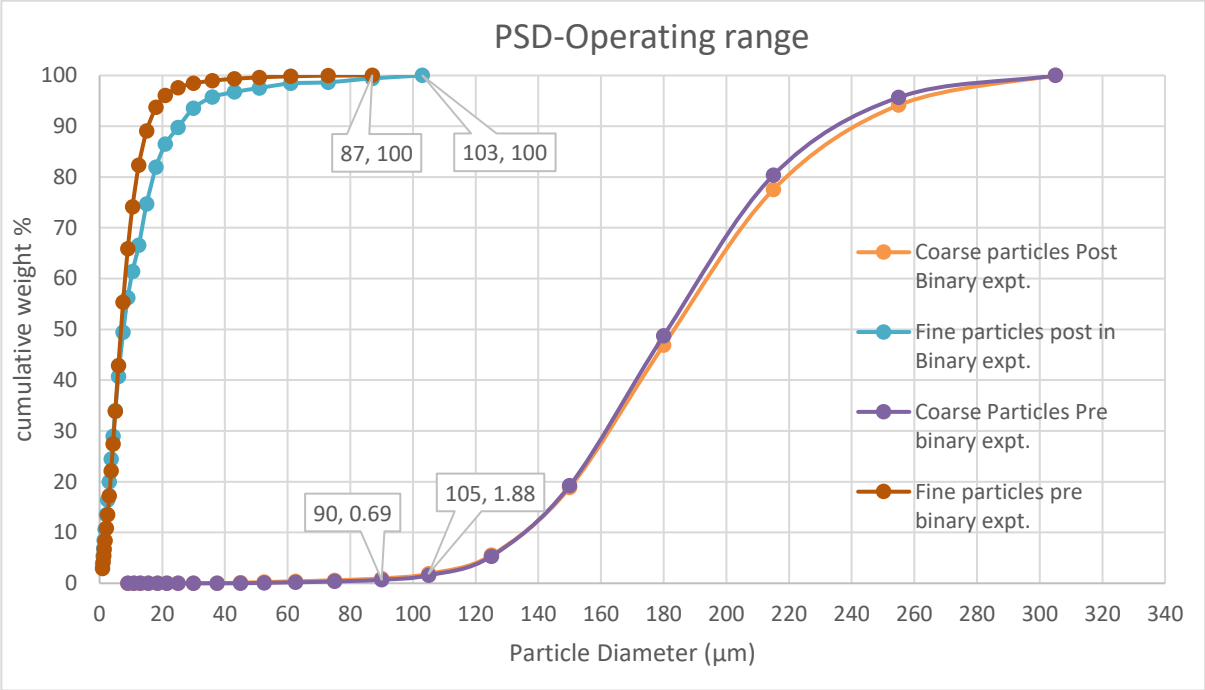

Figure 7.3: Comparison of PSD Pre and Post Binary experiment

In Figure 6.13 there is slight overlap in terms of the particle size between fine and coarse particles which can reduce the segregation efficiency. This was evident during the chemical and PSD analysis. Therefore, further sieving was required to remove the overlapping. A comparison of the PSD before and after the binary experiment is shown in Figure 7.3.

The largest particle size for the sieved fine particle is now 87µm which is smaller than that of the sieved coarse particle at 90µm. Evidently less than 1% of the brown alumina may be mixed up with the white alumina. This suggests that only a few and the very finer particles of the brown particles might be segregated along with the white alumina. The sieved PSD would improve the segregation efficiency.

After the binary experiments the PSD of the largest fine particles was 103µm and the lowest possible coarse particle was 105µm, resulting in the slightly changes in the PSD. This concludes that a small amount of white alumina might have been mixed with the brown alumina.

7.3 Purity Analysis

Norcem examined the brown, white, and binary particles. To evaluate the elemental composition of materials, XRF (X-Ray Fluorescence) analysis was done. The sizes and compositions of pure particles were discovered to deviate from the initial measurements.

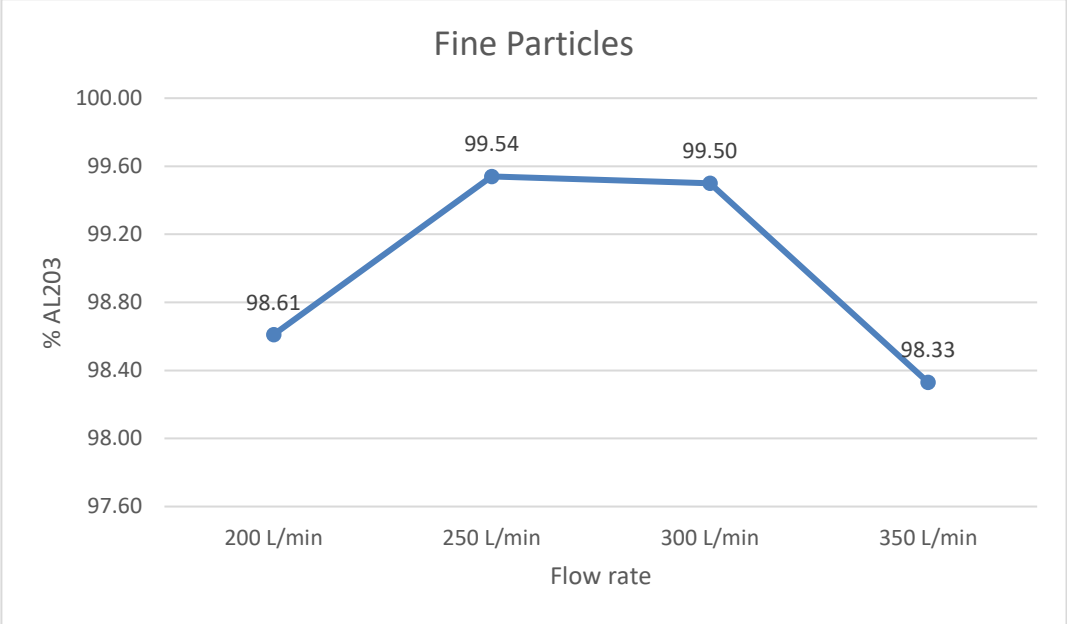

Figure 7.4: Percentage of White Alumina

The percentage of the pure alumina present in the fine and coarse particles with respect to the segregated flow rate is shown in the figure 7.4 and 7.5 respectively. When the flow rate is 200L/min, the percentage of alumina in the fine particles is 98.61%. At a flow rate of 250L/min, the percentage of alumina increases to 99.54%, which is the highest value in the list. At higher flow rates of 300L/min and 350L/min, the percentage of alumina decreases, with values of 99.5% and 98.33%, respectively.

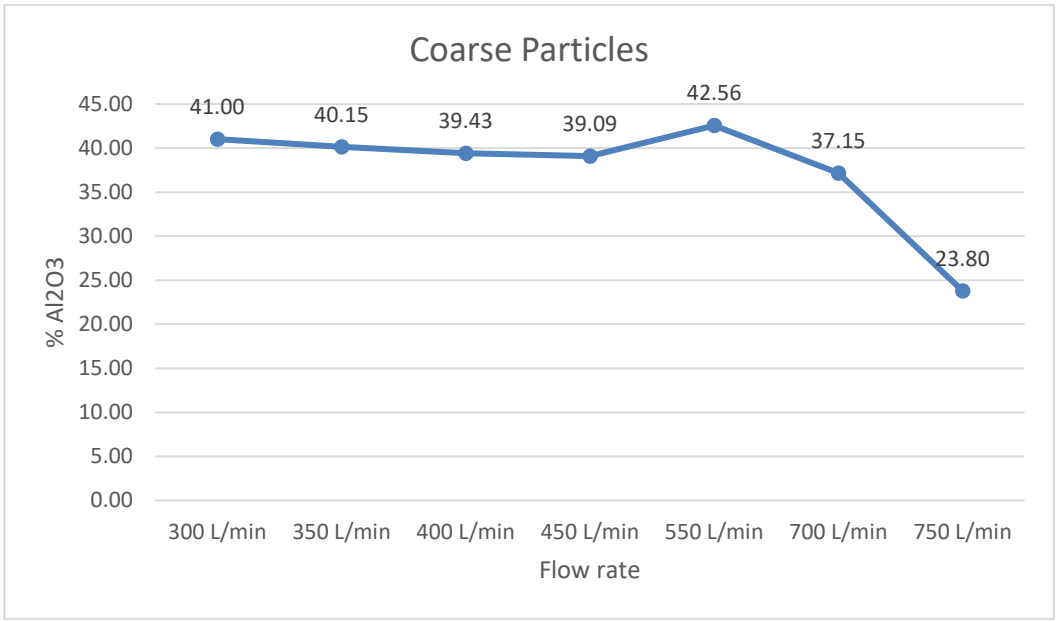

Figure 7.5: Percentage of Brown Alumina

At a flow rate of 300L/min, the percentage of alumina in the coarse particles is 41%. At higher flow rates of 350L/min, 400L/min, the percentage of alumina in the coarse particles changes very slightly, with values of 40.15%, 39.43% respectively. There is a slight decrease at 450L/min.

At a flow rate of 550L/min, the percentage of alumina in the coarse particles reaches the highest value of 42.56%. As the flow rate is increased further to 700L/min and 750L/min, the percentage of alumina in the coarse particles drops sharply to 37.15 % and 23.80%, respectively. This suggests that the high

flow rates may cause the particles to break down or erode, leading to a decrease in alumina content and presence of other impurities in the bed.

As during the fluidization there is mixing and segregation it is very important to learn about the change in chemical composition before and after the experiment. The Chemical composition before and after the binary experiment is as shown in figure 7.6 and 7.7.

The presence of Alumina (Al_2O_3) in the White alumina before the binary experiment is 99.27%, which decreases to 98.87 % after the experiment. The presence of other chemicals in the white alumina is very negligible. This suggests that the process did not involve any chemical reactions or alterations to the composition of the particle.

The composition of the Brown Alumina before binary experiment deviates slightly from the post binary experiment. It indicates the presence of impurities in the particles. There is an increase in the presence of Alumina (Al_2O_3) from 40.28% to 41.73%. The composition of other chemical does not change much as brown Alumina consists of 27% Silicon Dioxide (SiO_2), 8% Ferric Oxide (Fe_2O_3), and 20% Magnesium Oxide (MgO) as major impurities.

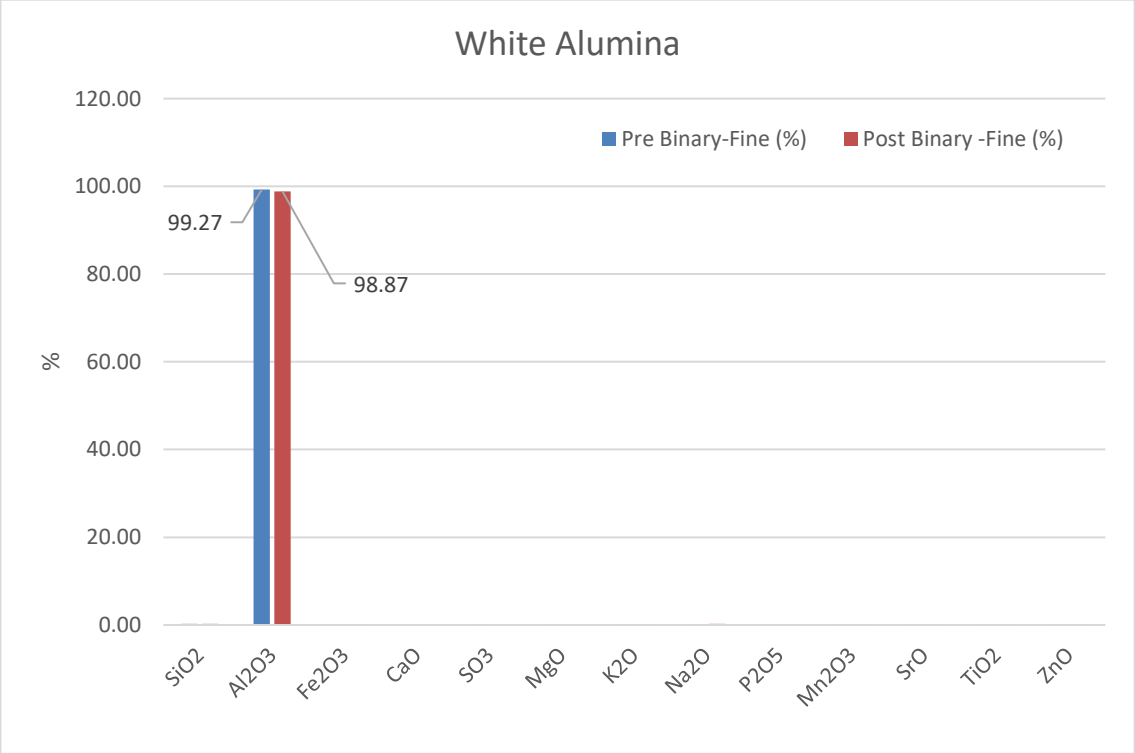

Figure 7.6: Chemical composition of white alumina

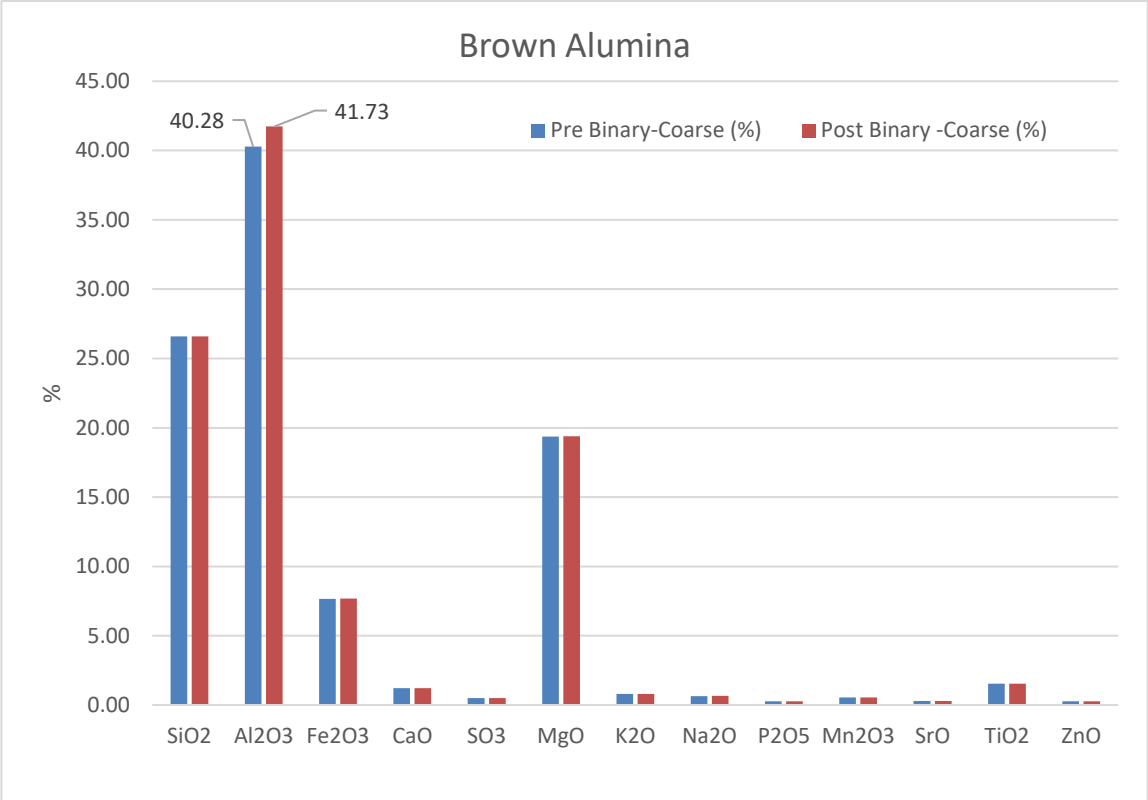

Figure 7.7: Chemical composition of brown alumina

500 gm of fine particle is mixed with 1500 gm of coarse particles. Then the fine particles were segregated in fluidized bed. The fine particles segregated was only 480 gm. The major content in the fine particles is alumina (Al_2O_3), which changes after the binary experiment. So, there is presence of (Al_2O_3) in the segregated mass from both fine and coarse particles. The chemical composition of alumina (Al_2O_3) in both fine and coarse was different from before and after the experiment. As per the calculation 479.97 gm of alumina (Al_2O_3) was present from the fine particle and rest from the coarse particles. This represents a purity of 99.99%.

8 Conclusion

Experiments of particles fluidization were performed in a narrow rectangular column that sat on a uniform distributor. Scaling from hot flow to cold flow conditions gives experimentally difficult demands such as specific density and ultra-fine particles. The scaling law used has few assumptions which cannot be ignored.

The pure coarse particles have a minimum fluidization velocity (umf) of 0.08 m/s. Because the motions in the bed began at the lowest superficial gas velocity of 0.01 m/s, the fine particles' minimum fluidizing velocity (umf) could not be determined precisely. When the velocity is high, the pressure drop fluctuations for coarse particles are large. Fine particles, on the other hand, have modest fluctuations due to cohesive forces causing the formation of rat holes. These findings imply that coarse particles have great fluidization behavior while fine particles have poor fluidization behavior. This is further evident by visual observation of the bed.

Fluidizing fine particles by mixing with coarse particles appears to be practically feasible but the minimum fluidizing velocity (u_{mf}) could not be accurately determined as the bed motion started at very low velocity. For the binary mixtures, stable fluidization was observed with a superficial gas velocity higher than 0.29 m/s. Increasing the gas flow rate causes the circulation of particles within the bed, but the fine particles get trapped in the void of coarse particles in certain areas of the bed. This phenomenon is called entrapment. This can lead to regions of poor mixing and reduced fluidization performance. The sudden spikes in the pressure drop profile is the representation of the same. However, mixing conditions had improved compared to pure fine particles mixing conditions.

Segregation can occur due to the differences in the fluidization behavior of particles of different sizes or densities. To maximize the operating window that can generate segregation, the mean diameter of the fine particle is 5μm and that for the coarse particle is 181μm representing a wide range of particle size. This was critical since the densities of white Alumina and brown Alumina were identical. As a result, increasing the particle size difference increases the possibility of segregation. The segregation efficiency was 96%.

Overall, understanding the chemical composition of particles in a fluidized bed reactor is important for optimizing the reactor performance and ensuring safe and efficient operation. It's worth noting that the relationship between flow rate and alumina (Al_2O_3) content in both fine and coarse particles may be complex, and other factors such as particle size, composition, and bed height could also be important. To assess the purity of the material, comparison of the chemical composition of the particle before and after the binary experiment is required. Despite the no chemical reactions, there is a small change in the chemical composition of segregated particles. During fluidization the particles may erode or break down which causes the change in the size and shape of the particles leading to their change in chemical composition. The change in alumina (Al_2O_3) content in fine particles is less than 0.5%, whereas in coarse particles it is about 1.5%. A purity of 99.99% in terms of Alumina (Al_2O_3) present in the segregated mass suggest that the segregation process used in the experiment is very much effective.

A further comparison of the results with the previous experiment suggests a better segregation efficiency, since a coarser particle was used. The Alumina (Al_2O_3) content was higher, and the presence of other impurities was less as compared to the previous experiment.

9 Future Works

In this study, we investigated the fluidization behavior of the binary particles in cold flow conditions which emulate the particles in the hot flow conditions. The experimental results indicate that mixing of fine and coarse particles is possible at low velocities, and separation is possible at higher velocities, while resulting in a high level of purity of the alumina (Al_2O_3) in fine particles.

However, our study can be improved in several ways. First, we can investigate other particles that have closer densities to the scaled densities for both fine and coarse particles. Second, the fluidized bed used for the experiments was circular, whereas the hot flow reactor is non-circular and has different dimensions. The parameters of the Hot flow reactor are in Appendix G.

The scaling law assumes that the behavior of particles is determined solely by their size and shape and does not consider other factors such as particle-particle interactions, surface chemistry, and environmental conditions. Particle size and shape can change due to various factors such as agglomeration, attrition, and erosion. The scaling law is unable to account for these dynamic changes, leading to inaccurate predictions of particle behavior. Therefore, these interparticle forces should be tested to determine the extent to which they affect the fluid dynamics of the bed. The sphericity of the particle could be measured to determine the shape.

There is a change in the chemical composition of particles with the change in flow rates. This could be analyzed to determine the relationship between flow rate and chemical composition.

Binary entrainment of fine particles could also be weighted separately for each segregation velocity. It could help to analyze the chemical composition and purity of the segregated mass even better. Also, the purity in terms of PSD could be analyzed to compare it with the chemical purity.

References

[1] L.-A. Tokheim, A. Mathisen, L. E. Øi, C. Jayarathna, and N. Eldrup, "COMBINED CALCINATION AND CO2 CAPTURE IN CEMENT CLINKER PRODUCTION BY USE OF ELECTRICAL ENERGY," 2019.

[2] R. M. Jacob, B. M. E. Moldestad, and L.-A. Tokheim, "Fluidization of Fine Calciner Raw Meal Particles by mixing with coarser Inert Particles – Experiments and CPFD Simulations," presented at the The First SIMS EUROSIM Conference on Modelling and Simulation, SIMS EUROSIM 2021, and 62nd International Conference of Scandinavian Simulation Society, SIMS 2021, September 21-23, Virtual Conference, Finland, Mar. 2022, pp. 333–340. doi: 10.3384/ecp21185333.

[3] D. Kunii and O. Levenspiel, *Fluidization engineering*, 2. ed., Reprinted. in Butterworth-Heinemann series in chemical engineering. Amsterdam Heidelberg: Elsevier ; Butterworth-Heinemann, 2012.

[4] S. Maurer, "Hydrodynamic Characterization and Scale-Up of Bubbling Fluidized Beds for Catalytic Conversion," ETH Zurich, 2015. doi: 10.3929/ETHZ-A-010453120.

[5] Masayuki. Horio, "Fluidization in Natural Phenomena," in *Reference Module in Chemistry, Molecular Sciences and Chemical Engineering*, Elsevier, 2017, p. B9780124095472122000. doi: 10.1016/B978-0-12-409547-2.12185-7.

[6] C. Dechsiri, "Particle Transport in Fluidized Beds," 2004.

[7] L. Stepien, "FLUIDIZATION," 2015. https://docplayer.net/50905253-Agh-university-fluidization-author-mgr-inz-leszek-stepien-supervisor-dr-hab-inz-marek-sciazko-department-of-energy-nad-fuels.html (accessed Feb. 07, 2023).

[8] D. Geldart, "Types of gas fluidization," *Powder Technology*, vol. 7, no. 5, pp. 285–292, May 1973, doi: 10.1016/0032-5910(73)80037-3.

[9] R. Cocco, S. B. R. Karri, and T. Knowlton, "Introduction to Fluidization," *Back to Basics*, 2014.

[10] R. Niven, "Physical insight into the Ergun and Wen and Yu Equations for Fluid Flow in Packed and Fluidized Beds," *Chemical Engineering Science - CHEM ENG SCI*, vol. 57, pp. 527–534, Feb. 2002, doi: 10.1016/S0009-2509(01)00371-2.

[11] T. M. Knowlton, "10 - Fluidized bed reactor design and scale-up," in *Fluidized Bed Technologies for Near-Zero Emission Combustion and Gasification*, F. Scala, Ed., in Woodhead Publishing Series in Energy. Woodhead Publishing, 2013, pp. 481–523. doi: 10.1533/9780857098801.2.481.

[12] P. Bourgeois and P. Grenier, "The ratio of terminal velocity to minimum fluidising velocity for spherical particles," *Can. J. Chem. Eng.*, vol. 46, no. 5, pp. 325–328, Oct. 1968, doi: 10.1002/cjce.5450460508.

[13] A. Haider and O. Levenspiel, "Drag coefficient and terminal velocity of spherical and nonspherical particles," *Powder Technology*, vol. 58, no. 1, pp. 63–70, May 1989, doi: 10.1016/0032-5910(89)80008-7.

[14] J. Lin, K. Luo, S. Wang, L. Sun, and J. Fan, "Particle-Scale Simulation of Solid Mixing Characteristics of Binary Particles in a Bubbling Fluidized Bed," *Energies*, vol. 13, no. 17, Art. no. 17, Jan. 2020, doi: 10.3390/en13174442.

[15] J. Tang, X. N. Chen, C. X. Lu, and Y. M. Zhang, “Minimum Fluidization Velocity of Binary Particles with Different Geldart Classification,” *AMR*, vol. 482–484, pp. 655–662, Feb. 2012, doi: 10.4028/www.scientific.net/AMR.482-484.655.

[16] C. C. Obuseh, Z.-G. Feng, and B. D. Paudel, “An Experimental Study on Fluidization of Binary Mixture in Particulate Flows,” *Journal of Dispersion Science and Technology*, vol. 33, no. 9, pp. 1379–1384, Sep. 2012, doi: 10.1080/01932691003800163.

[17] J. Grace, X. Bi, and N. Ellis, “Essentials of Fluidization Technology | Wiley,” *Wiley.com*. https://www.wiley.com/en-us/Essentials+of+Fluidization+Technology-p-9783527699490 (accessed May 15, 2023).

[18] L. R. Glicksman, “Scaling relationships for fluidized beds,” *Chemical Engineering Science*, vol. 43, no. 6, pp. 1419–1421, Jan. 1988, doi: 10.1016/0009-2509(88)85118-2.

[19] J. Sanderson and M. Rhodes, “Bubbling fluidized bed scaling laws: Evaluation at large scales,” *AIChE Journal*, vol. 51, no. 10, pp. 2686–2694, 2005, doi: 10.1002/aic.10511.

[20] M. Horio, A. Nonaka, Y. Sawa, and I. Muchi, “A new similarity rule for fluidized bed scale-up,” *AIChE Journal*, vol. 32, no. 9, pp. 1466–1482, 1986, doi: 10.1002/aic.690320908.

[21] R. K. Thapa and B. M. Halvorsen, “Scaling of bubbling fluidized bed reactors with glicksman’s viscous limit set and CFD simulation,” *Int. J. CMEM*, vol. 2, no. 2, pp. 135–144, Jun. 2014, doi: 10.2495/CMEM-V2-N2-135-144.

[22] J. R. van Ommen, M. Teuling, J. Nijenhuis, and B. G. M. van Wachem, “Computational validation of the scaling rules for fluidized beds,” *Powder Technology*, vol. 163, no. 1–2, pp. 32–40, Apr. 2006, doi: 10.1016/j.powtec.2006.01.010.

[23] “MP-20-22 Fluidization of scaled binary particles.pdf.”

[24] N. Ahmadpour Samani, C. K. Jayarathna, and L.-A. Tokheim, “Fluidized bed calcination of cement raw meal: Laboratory experiments and CPFD simulations,” presented at the SIMS Conference on Simulation and Modelling SIMS 2020, September 22-24, Virtual Conference, Finland, Mar. 2021, pp. 407–413. doi: 10.3384/ecp20176407.

[25] S. Wang, K. Luo, C. Hu, and J. Fan, “CFD-DEM study of the effect of ring baffles on system performance of a full-loop circulating fluidized bed,” *Chemical Engineering Science*, vol. 196, pp. 130–144, Mar. 2019, doi: 10.1016/j.ces.2018.10.056.

[26] R. P. Chhabra and J. F. Richardson, “Particulate systems,” in *Non-Newtonian Flow in the Process Industries*, Elsevier, 1999, pp. 206–259. doi: 10.1016/B978-075063770-1/50006-3.

[27] C. E. Agu, C. Pfeifer, and B. M. E. Moldestad, “Prediction of void fraction and minimum fluidization velocity of a binary mixture of particles: Bed material and fuel particles,” *Powder Technology*, vol. 349, pp. 99–107, May 2019, doi: 10.1016/j.powtec.2019.03.027.

[28] L. Xie, J. Zhu, and C. Jiang, “Quantitative study of mixing/segregation behaviors of binary-mixture particles in pilot-scale fluidized bed reactor,” *Powder Technology*, vol. 377, pp. 103–114, Jan. 2021, doi: 10.1016/j.powtec.2020.08.069.

[29] J. Chandimal Bandara, M. Sørflaten Eikeland, and B. M. E. Moldestad, “Analyzing the effects of particle density, size, size distribution and shape for minimum fluidization velocity with Eulerian-Lagrangian CFD simulation,” presented at the The 58th Conference on Simulation and Modelling (SIMS 58) Reykjavik, Iceland, September 25th – 27th, 2017, Sep. 2017, pp. 60–65. doi: 10.3384/ecp1713860.

Appendices

Appendix A: Signed Task Description

FMH606 Master's Thesis

Title: Electrified calcination in a fluidized bed calciner – Experiments with scaled binary particles

USN supervisor: Lars-André Tokheim

External partner: Norcem and Heidelberg Cement Northern Europe (Christoffer Moen)

Task background:
USN is one of the partners in the research project *"Combined calcination and CO_2 capture in cement clinker production by use of CO_2-neutral electrical energy"*. The acronym ELSE[1] is used as a short name for the project. Phase 1 of the project was completed in April 2019, and Phase 2 was started in April 2020. The goal of the ELSE project is to utilize electricity (instead of carbon-containing fuels) to decarbonate the raw meal in the cement kiln process while at the same time capturing the CO_2 from decarbonation of the calcium carbonate in the calciner. Such a concept may be less expensive than a regular post-combustion system applied to CO_2 capture from the cement plant. Moreover, as the fuel generated CO_2 will be eliminated, less CO_2 is produced in the calcination process.

Different concepts to implement electrification of the calciner have been discussed in the project. One alternative is to use electricity (through resistance heating) to generate heat that is transferred to the calciner, where it is used to calcine the meal ($CaCO_3 \rightarrow CaO+CO_2$). Different reactor types may be used as a calciner, for example a fluidized bed with immersed heating elements.

As the meal particles are small (median ~20-30 µm, i.e. Geldart C particles), they are difficult to fluidize. However, it may be possible to improve the fluidization properties by mixing the small particles with coarser particles. In that case, the bed should be designed in such a way that the coarse particles remain in the bed, whereas the fine uncalcined particles are continuously fed close to the bottom of the bed and fine calcined particles are continuously discharged at top of the bed. Based on CPFD simulations, Ron M. Jacob has come up with a reactor geometry which will likely fulfil the requirements described above.

In a student project from fall 2022, experiments with scaled particles were run in a cold flow fluidized bed in USN's process lab. (Scaling is necessary to emulate the hot-flow particle at cold-flow conditions.) The experimental results were very promising as it appears that mixing of small and large particles is possible at low velocities, and separation is possible at higher velocities. Now, we hope to do additional experimental work with the current setup to understand more about the powder behaviour and prepare for future hot-flow experiments.

[1] ELSE is short for 'ELektrifisert SEmentproduksjon' (Norwegian) meaning 'electrified cement production'.

Task description:

The task may include the following:

- Fluidized bed theory.
- Summary of relevant previous experimental work
- Description of the current experimental setup
- Particle characterization and preparation
- Cold-flow lab-scale experiments with scaled particles
- Design of a hot-flow lab-scale rig based on the binary particle concept.

Student category: EET or PT students (relevant lab experience is an advantage)

Is the task suitable for online students (not present at the campus)? No, experimental work will have to be carried out at the USN campus.

Practical arrangements:

There will be meetings with Norcem to discuss the task and the progress, most likely via Teams.

Supervision:

As a general rule, the student is entitled to 15-20 hours of supervision. This includes necessary time for the supervisor to prepare for supervision meetings (reading material to be discussed, etc).

Signatures:

Supervisor (date and signature): 26 January 2023, 

Student (write clearly in all capitalized letters): NITISH KUMAR JHA

Student (date and signature): 26 January 2023, 

Appendix B: WBS

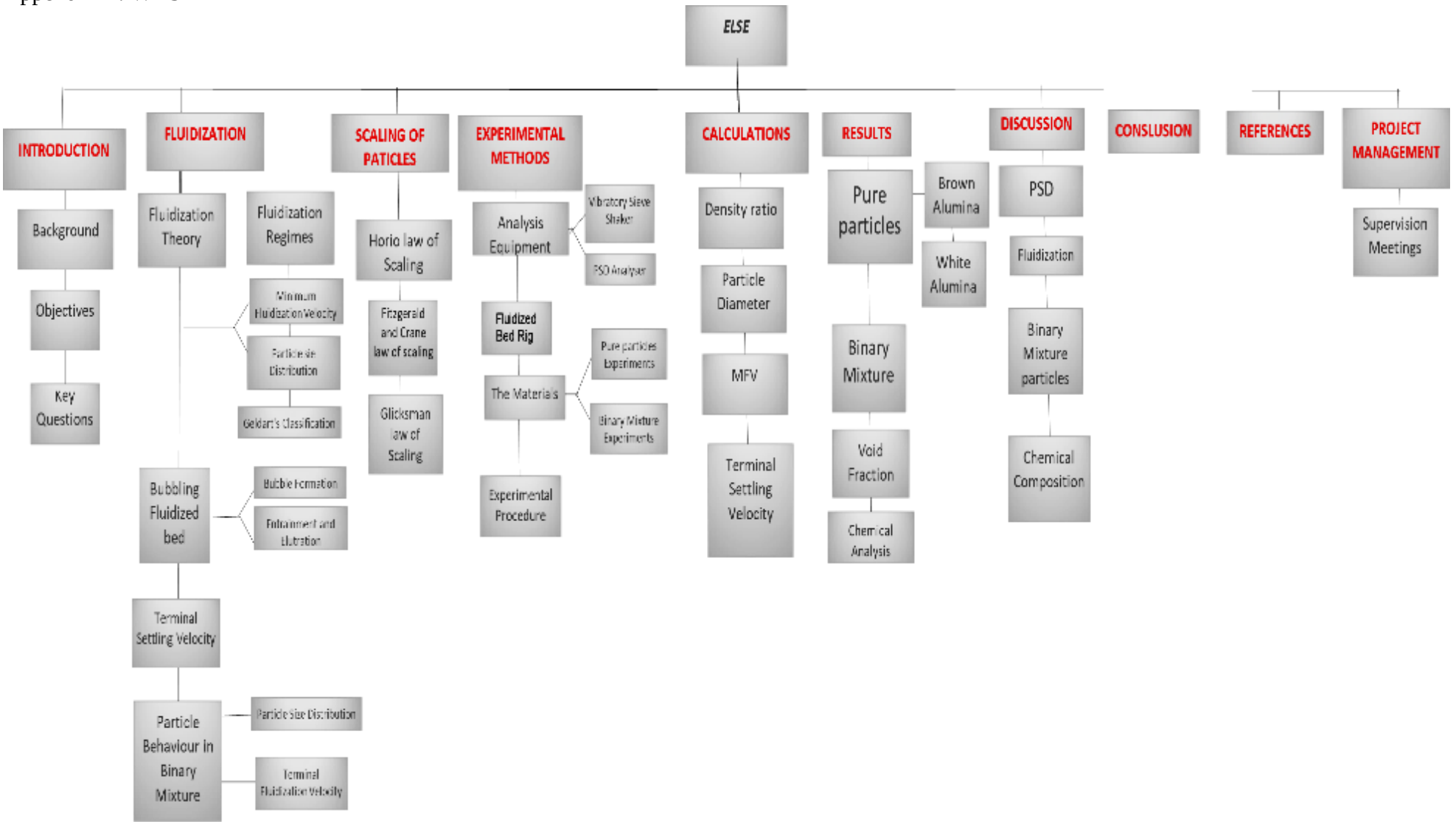

Appendix C: XRF result of pure and binary mixture particles (Norcem)

	SiO2	Al2O3	Fe2O3	CaO	SO3	MgO	K2O	Na2O	P2O5	Mn2O3	SrO	TiO2	ZnO
Coarse 300 L/min	26.74	41.00	7.95	1.19	0.43	18.85	0.71	0.56	0.19	0.47	0.22	1.48	0.19
Coarse 350 L/min	25.92	40.15	7.38	1.23	0.56	20.01	0.79	0.71	0.34	0.61	0.36	1.59	0.34
Coarse 400 L/min	27.40	39.43	7.19	1.28	0.52	19.49	0.91	0.69	0.30	0.57	0.33	1.57	0.31
Coarse 450 L/min	25.33	39.09	8.62	1.17	0.69	19.58	0.89	0.81	0.45	0.74	0.48	1.71	0.46
Coarse 550 L/min	26.10	42.56	11.54	0.59	0.23	16.42	0.430	0.320	0.026	0.349	0.036	1.372	0.021
Coarse 700 L/min	28.11	37.15	25.18	0.39	0.10	6.52	0.220	0.121	0.063	0.604	0.016	1.499	0.014
Coarse 750 L/min	33.96	23.80	36.22	0.52	0.02	2.55	0.063	0.048	0.140	0.817	0.002	1.836	0.007
Fine 200 L/min	0.55	98.61	0.30	0.00	0.01	0.24	0.017	0.244	0.000	0.010	0.003	0.004	0.007
Fine 250 L/min	0.15	99.54	0.05	0.00	0.00	0.00	0.008	0.228	0.004	0.003	0.002	0.007	0.007
Fine 300 L/min	0.06	99.50	0.08	0.00	0.00	0.00	0.004	0.238	0.000	0.003	0.002	0.005	0.007
Fine 350 L/min	1.13	98.33	0.22	0.00	0.00	0.01	0.056	0.243	0.001	0.005	0.003	0.026	0.006
Fine Pre-Binary Expt.	0.26	99.27	0.12	0.00	0.00	0.07	0.01	0.23	0.00	0.01	0.00	0.01	0.01
Coarse Pre-Binary Expt.	26.58	40.28	7.66	1.22	0.50	19.36	0.79	0.65	0.28	0.55	0.30	1.54	0.28
Fine post Binary Expt.	0.26	98.87	0.09	0.00	0.00	0.00	0.009	0.24	0.001	0.003	0.002	0.038	0.006
Coarse post Binary Expt.	26.59	41.73	7.675	1.22	0.51	19.39	0.789	0.649	0.276	0.5515	0.301	1.5325	0.2757

Appendix D: Theoretical calculation of Minimum Fluidization Velocity and Terminal Velocity with PSD for **Fine particles**

HOT FLOW		COLD FLOW				Hot	Cold					Hot Flow			Cold Flow		
Particle Diameter dp (μm)	MIN.Flu. Velocity umf (m/s)	Scaled Particle Diameter dp (μm)	Scaled Min. Flu. Velocity umf (m/s)	Cumulative Weight (%)	Weight %	hot (mean Dia) μm	cold (mean Dia)μm	Archimedes number	dp*	Ut*(0.5<øs<1)	Reynolds no. p	Ut	Ut average	Umf Average	Ut	Ut average	Umf Average
0.4	3.17E-08	0	1.67E-08	0.00%	0.00%	0.00E+00	0.00E+00	1.95E-07	5.80E-03	1.87E-06	1.18E-10	2.91E-06	0.00E+00	0.00E+00	1.53E-06	0.00E+00	0.00E+00
0.5	4.95E-08	0	2.61E-08	0.03%	0.03%	1.50E-04	4.15E-05	3.82E-07	7.25E-03	2.92E-06	2.31E-10	4.54E-06	1.36E-09	1.49E-11	2.39E-06	7.16E-10	7.82E-12
0.6	7.13E-08	0	3.75E-08	0.37%	0.34%	2.04E-03	5.65E-04	6.59E-07	8.70E-03	4.21E-06	3.99E-10	6.54E-06	2.22E-08	2.42E-10	3.44E-06	1.17E-08	1.28E-10
0.7	9.71E-08	0	5.11E-08	1.50%	1.13%	7.91E-03	2.19E-03	1.05E-06	1.02E-02	5.73E-06	6.34E-10	8.90E-06	1.01E-07	1.10E-09	4.68E-06	5.29E-08	5.77E-10
0.8	1.27E-07	0	6.67E-08	2.26%	0.76%	6.08E-03	1.68E-03	1.56E-06	1.16E-02	7.48E-06	9.46E-10	1.16E-05	8.83E-08	9.63E-10	6.11E-06	4.65E-08	5.07E-10
0.9	1.60E-07	0	8.44E-08	3.13%	0.87%	7.83E-03	2.17E-03	2.23E-06	1.31E-02	9.47E-06	1.35E-09	1.47E-05	1.28E-07	1.40E-09	7.74E-06	6.73E-08	7.34E-10
1.0	1.98E-07	0	1.04E-07	4.05%	0.92%	9.20E-03	2.55E-03	3.05E-06	1.45E-02	1.17E-05	1.85E-09	1.82E-05	1.67E-07	1.82E-09	9.55E-06	8.79E-08	9.59E-10
1.0	1.98E-07	0	1.04E-07	4.07%	0.02%	2.00E-04	5.54E-05	3.05E-06	1.45E-02	1.17E-05	1.85E-09	1.82E-05	3.63E-09	3.96E-11	9.55E-06	1.91E-09	2.08E-11
1.1	2.40E-07	0	1.26E-07	5.09%	1.02%	1.12E-02	3.11E-03	4.06E-06	1.60E-02	1.41E-05	2.46E-09	2.20E-05	2.24E-07	2.44E-09	1.16E-05	1.18E-07	1.29E-09
1.3	3.35E-07	0	1.76E-07	6.16%	1.07%	1.39E-02	3.85E-03	6.71E-06	1.89E-02	1.98E-05	4.06E-09	3.07E-05	3.28E-07	3.58E-09	1.61E-05	1.73E-07	1.88E-09
1.4	3.88E-07	0	2.04E-07	7.31%	1.15%	1.61E-02	4.46E-03	8.38E-06	2.03E-02	2.29E-05	5.07E-09	3.56E-05	4.09E-07	4.46E-09	1.87E-05	2.15E-07	2.35E-09
1.5	4.46E-07	0	2.34E-07	7.92%	0.61%	9.15E-03	2.53E-03	1.03E-05	2.18E-02	2.63E-05	6.24E-09	4.08E-05	2.49E-07	2.72E-09	2.15E-05	1.31E-07	1.43E-09

1.8	6.42E-07	0	3.38E-07	9.86%	1.94%	3.49E-02	9.66E-03	1.78E-05	2.61E-02	3.79E-05	1.08E-08	5.88E-05	1.14E-06	1.25E-08	3.09E-05	6.00E-07	6.55E-09
2.0	7.92E-07	1	4.17E-07	11.27%	1.41%	2.82E-02	7.80E-03	2.44E-05	2.90E-02	4.67E-05	1.48E-08	7.26E-05	1.02E-06	1.12E-08	3.82E-05	5.39E-07	5.88E-09
2.2	9.59E-07	1	5.04E-07	12.78%	1.51%	3.32E-02	9.19E-03	3.25E-05	3.19E-02	5.66E-05	1.97E-08	8.79E-05	1.33E-06	1.45E-08	4.62E-05	6.98E-07	7.62E-09
2.5	1.24E-06	1	6.51E-07	14.41%	1.63%	4.08E-02	1.13E-02	4.77E-05	3.63E-02	7.30E-05	2.89E-08	1.13E-04	1.85E-06	2.02E-08	5.97E-05	9.73E-07	1.06E-08
2.8	1.55E-06	1	8.17E-07	16.15%	1.74%	4.87E-02	1.35E-02	6.70E-05	4.06E-02	9.16E-05	4.06E-08	1.42E-04	2.48E-06	2.70E-08	7.49E-05	1.30E-06	1.42E-08
3.0	1.78E-06	1	9.38E-07	17.11%	0.96%	2.88E-02	7.97E-03	8.24E-05	4.35E-02	1.05E-04	4.99E-08	1.63E-04	1.57E-06	1.71E-08	8.59E-05	8.25E-07	9.00E-09
3.2	2.03E-06	1	1.07E-06	18.02%	0.91%	2.91E-02	8.06E-03	1.00E-04	4.64E-02	1.20E-04	6.05E-08	1.86E-04	1.69E-06	1.85E-08	9.78E-05	8.90E-07	9.71E-09
3.6	2.57E-06	1	1.35E-06	20.00%	1.98%	7.13E-02	1.97E-02	1.42E-04	5.22E-02	1.51E-04	8.62E-08	2.35E-04	4.66E-06	5.08E-08	1.24E-04	2.45E-06	2.67E-08
4.0	3.17E-06	1	1.67E-06	22.10%	2.10%	8.40E-02	2.32E-02	1.95E-04	5.80E-02	1.87E-04	1.18E-07	2.90E-04	6.10E-06	6.66E-08	1.53E-04	3.21E-06	3.50E-08
4.0	3.17E-06	1	1.67E-06	22.14%	0.04%	1.60E-03	4.43E-04	1.95E-04	5.80E-02	1.87E-04	1.18E-07	2.90E-04	1.16E-07	1.27E-09	1.53E-04	6.11E-08	6.67E-10
4.5	4.01E-06	1	2.11E-06	24.31%	2.17%	9.77E-02	2.70E-02	2.78E-04	6.53E-02	2.37E-04	1.68E-07	3.67E-04	7.97E-06	8.70E-08	1.93E-04	4.19E-06	4.58E-08
5.0	4.95E-06	1	2.61E-06	26.54%	2.23%	1.12E-01	3.09E-02	3.82E-04	7.25E-02	2.92E-04	2.31E-07	4.54E-04	1.01E-05	1.10E-07	2.39E-04	5.32E-06	5.81E-08
5.0	4.95E-06	1	2.61E-06	26.64%	0.10%	5.00E-03	1.38E-03	3.82E-04	7.25E-02	2.92E-04	2.31E-07	4.54E-04	4.54E-07	4.95E-09	2.39E-04	2.39E-07	2.61E-09
6.0	7.13E-06	2	3.75E-06	30.48%	3.84%	2.30E-01	6.38E-02	6.59E-04	8.70E-02	4.20E-04	3.99E-07	6.53E-04	2.51E-05	2.74E-07	3.43E-04	1.32E-05	1.44E-07
6.3	7.86E-06	2	4.14E-06	31.68%	1.20%	7.56E-02	2.09E-02	7.63E-04	9.14E-02	4.63E-04	4.62E-07	7.20E-04	8.64E-06	9.43E-08	3.79E-04	4.54E-06	4.96E-08
7.1	9.99E-06	2	5.25E-06	34.39%	2.71%	1.92E-01	5.33E-02	1.09E-03	1.03E-01	5.88E-04	6.61E-07	9.14E-04	2.48E-05	2.71E-07	4.81E-04	1.30E-05	1.42E-07
8.0	1.27E-05	2	6.67E-06	37.24%	2.85%	2.28E-01	6.31E-02	1.56E-03	1.16E-01	7.47E-04	9.46E-07	1.16E-03	3.31E-05	3.61E-07	6.10E-04	1.74E-05	1.90E-07
8.0	1.27E-05	2	6.67E-06	37.36%	0.12%	9.60E-03	2.66E-03	1.56E-03	1.16E-01	7.47E-04	9.46E-07	1.16E-03	1.39E-06	1.52E-08	6.10E-04	7.32E-07	8.00E-09

8.9	1.57E-05	2	8.25E-06	40.24%	2.88%	2.56E-01	7.09E-02	2.15E-03	1.29E-01	9.24E-04	1.30E-06	1.44E-03	4.13E-05	4.52E-07	7.55E-04	2.17E-05	2.38E-07
10.0	1.98E-05	3	1.04E-05	43.32%	3.08%	3.08E-01	8.52E-02	3.05E-03	1.45E-01	1.17E-03	1.85E-06	1.81E-03	5.58E-05	6.10E-07	9.53E-04	2.93E-05	3.21E-07
11.2	2.48E-05	3	1.31E-05	46.69%	3.37%	3.77E-01	1.04E-01	4.29E-03	1.62E-01	1.46E-03	2.60E-06	2.27E-03	7.65E-05	8.37E-07	1.19E-03	4.03E-05	4.41E-07
12.0	2.85E-05	3	1.50E-05	48.62%	1.93%	2.32E-01	6.41E-02	5.27E-03	1.74E-01	1.68E-03	3.19E-06	2.61E-03	5.03E-05	5.51E-07	1.37E-03	2.65E-05	2.90E-07
12.6	3.14E-05	3	1.65E-05	50.15%	1.53%	1.93E-01	5.34E-02	6.11E-03	1.83E-01	1.85E-03	3.70E-06	2.87E-03	4.39E-05	4.81E-07	1.51E-03	2.31E-05	2.53E-07
14.2	3.99E-05	4	2.10E-05	53.73%	3.58%	5.08E-01	1.41E-01	8.74E-03	2.06E-01	2.35E-03	5.29E-06	3.64E-03	1.30E-04	1.43E-06	1.92E-03	6.86E-05	7.52E-07
15.0	4.46E-05	4	2.34E-05	55.57%	1.84%	2.76E-01	7.64E-02	1.03E-02	2.18E-01	2.62E-03	6.24E-06	4.07E-03	7.48E-05	8.20E-07	2.14E-03	3.94E-05	4.31E-07
16.0	5.07E-05	4	2.67E-05	57.66%	2.09%	3.34E-01	9.26E-02	1.25E-02	2.32E-01	2.98E-03	7.57E-06	4.62E-03	9.66E-05	1.06E-06	2.43E-03	5.08E-05	5.58E-07
17.8	6.28E-05	5	3.30E-05	61.21%	3.55%	6.32E-01	1.75E-01	1.72E-02	2.58E-01	3.68E-03	1.04E-05	5.72E-03	2.03E-04	2.23E-06	3.01E-03	1.07E-04	1.17E-06
18.0	6.42E-05	5	3.38E-05	61.53%	0.32%	5.76E-02	1.59E-02	1.78E-02	2.61E-01	3.76E-03	1.08E-05	5.85E-03	1.87E-05	2.05E-07	3.08E-03	9.84E-06	1.08E-07
19.0	7.15E-05	5	3.76E-05	63.32%	1.79%	3.40E-01	9.41E-02	2.09E-02	2.76E-01	4.19E-03	1.27E-05	6.51E-03	1.17E-04	1.28E-06	3.42E-03	6.13E-05	6.73E-07
20.0	7.92E-05	6	4.17E-05	65.03%	1.71%	3.42E-01	9.47E-02	2.44E-02	2.90E-01	4.64E-03	1.48E-05	7.21E-03	1.23E-04	1.35E-06	3.79E-03	6.48E-05	7.13E-07
22.4	9.94E-05	6	5.23E-05	68.85%	3.82%	8.56E-01	2.37E-01	3.43E-02	3.25E-01	5.81E-03	2.08E-05	9.03E-03	3.45E-04	3.80E-06	4.75E-03	1.81E-04	2.00E-06
24.0	1.14E-04	7	6.00E-05	71.06%	2.21%	5.30E-01	1.47E-01	4.22E-02	3.48E-01	6.67E-03	2.55E-05	1.04E-02	2.29E-04	2.52E-06	5.45E-03	1.20E-04	1.33E-06
25.0	1.24E-04	7	6.51E-05	72.39%	1.33%	3.32E-01	9.20E-02	4.77E-02	3.63E-01	7.23E-03	2.89E-05	1.12E-02	1.49E-04	1.65E-06	5.91E-03	7.86E-05	8.66E-07
25.2	1.26E-04	7	6.62E-05	72.62%	0.23%	5.80E-02	1.60E-02	4.88E-02	3.66E-01	7.35E-03	2.96E-05	1.14E-02	2.62E-05	2.89E-07	6.00E-03	1.38E-05	1.52E-07
26.0	1.34E-04	7	7.04E-05	73.66%	1.04%	2.70E-01	7.48E-02	5.36E-02	3.77E-01	7.81E-03	3.25E-05	1.21E-02	1.26E-04	1.39E-06	6.39E-03	6.64E-05	7.33E-07
27.0	1.44E-04	7	7.60E-05	74.86%	1.20%	3.24E-01	8.97E-02	6.01E-02	3.92E-01	8.42E-03	3.64E-05	1.31E-02	1.57E-04	1.73E-06	6.88E-03	8.26E-05	9.12E-07

28.3	1.59E-04	8	8.35E-05	76.28%	1.42%	4.02E-01	1.11E-01	6.92E-02	4.11E-01	9.24E-03	4.19E-05	1.44E-02	2.04E-04	2.25E-06	7.55E-03	1.07E-04	1.19E-06
30.0	1.78E-04	8	9.38E-05	78.14%	1.86%	5.58E-01	1.54E-01	8.24E-02	4.35E-01	1.04E-02	4.99E-05	1.61E-02	3.00E-04	3.32E-06	8.48E-03	1.58E-04	1.74E-06
32.0	2.03E-04	9	1.07E-04	80.07%	1.93%	6.18E-01	1.71E-01	1.00E-01	4.64E-01	1.18E-02	6.05E-05	1.83E-02	3.53E-04	3.91E-06	9.63E-03	1.86E-04	2.06E-06
35.6	2.51E-04	10	1.32E-04	83.08%	3.01%	1.07E+00	2.97E-01	1.38E-01	5.16E-01	1.46E-02	8.34E-05	2.26E-02	6.80E-04	7.56E-06	1.19E-02	3.58E-04	3.98E-06
39.9	3.15E-04	11	1.66E-04	86.10%	3.02%	1.20E+00	3.34E-01	1.94E-01	5.79E-01	1.82E-02	1.17E-04	2.83E-02	8.55E-04	9.52E-06	1.49E-02	4.50E-04	5.01E-06
40.0	3.17E-04	11	1.67E-04	86.16%	0.06%	2.40E-02	6.64E-03	1.95E-01	5.80E-01	1.83E-02	1.18E-04	2.84E-02	1.71E-05	1.90E-07	1.50E-02	8.98E-06	1.00E-07
45.0	4.01E-04	12	2.11E-04	88.94%	2.78%	1.25E+00	3.46E-01	2.78E-01	6.53E-01	2.31E-02	1.68E-04	3.59E-02	9.97E-04	1.12E-05	1.89E-02	5.24E-04	5.87E-06
48.0	4.56E-04	13	2.40E-04	90.32%	1.38%	6.62E-01	1.83E-01	3.38E-01	6.96E-01	2.62E-02	2.04E-04	4.07E-02	5.62E-04	6.30E-06	2.14E-02	2.95E-04	3.31E-06
50.2	4.99E-04	14	2.63E-04	91.23%	0.91%	4.57E-01	1.26E-01	3.86E-01	7.28E-01	2.86E-02	2.34E-04	4.44E-02	4.04E-04	4.54E-06	2.34E-02	2.13E-04	2.39E-06
56.4	6.30E-04	16	3.31E-04	93.28%	2.05%	1.16E+00	3.20E-01	5.48E-01	8.18E-01	3.59E-02	3.31E-04	5.58E-02	1.14E-03	1.29E-05	2.93E-02	6.01E-04	6.80E-06
63.0	7.86E-04	17	4.14E-04	94.94%	1.66%	1.05E+00	2.89E-01	7.63E-01	9.14E-01	4.45E-02	4.62E-04	6.91E-02	1.15E-03	1.31E-05	3.64E-02	6.04E-04	6.87E-06
64.0	8.11E-04	18	4.27E-04	95.15%	0.21%	1.34E-01	3.72E-02	8.00E-01	9.28E-01	4.59E-02	4.84E-04	7.13E-02	1.50E-04	1.70E-06	3.75E-02	7.88E-05	8.96E-07
71.0	9.99E-04	20	5.25E-04	96.37%	1.22%	8.66E-01	2.40E-01	1.09E+00	1.03E+00	5.61E-02	6.61E-04	8.71E-02	1.06E-03	1.22E-05	4.58E-02	5.59E-04	6.41E-06
80.0	1.27E-03	22	6.67E-04	97.48%	1.11%	8.88E-01	2.46E-01	1.56E+00	1.16E+00	7.06E-02	9.46E-04	1.10E-01	1.22E-03	1.41E-05	5.77E-02	6.40E-04	7.40E-06
89.3	1.58E-03	25	8.31E-04	98.25%	0.77%	6.88E-01	1.90E-01	2.17E+00	1.30E+00	8.70E-02	1.32E-03	1.35E-01	1.04E-03	1.22E-05	7.11E-02	5.48E-04	6.40E-06
90.0	1.60E-03	25	8.44E-04	98.29%	0.04%	3.60E-02	9.96E-03	2.23E+00	1.31E+00	8.83E-02	1.35E-03	1.37E-01	5.49E-05	6.42E-07	7.22E-02	2.89E-05	3.38E-07
95.0	1.79E-03	26	9.40E-04	98.58%	0.29%	2.76E-01	7.63E-02	2.62E+00	1.38E+00	9.79E-02	1.58E-03	1.52E-01	4.41E-04	5.18E-06	8.00E-02	2.32E-04	2.73E-06
96.0	1.83E-03	27	9.60E-04	98.63%	0.05%	4.80E-02	1.33E-02	2.70E+00	1.39E+00	9.98E-02	1.63E-03	1.55E-01	7.75E-05	9.13E-07	8.16E-02	4.08E-05	4.80E-07

100.0	1.98E-03	28	1.04E-03	98.81%	0.18%	1.80E-01	4.98E-02	3.05E+00	1.45E+00	1.08E-01	1.85E-03	1.67E-01	3.01E-04	3.57E-06	8.81E-02	1.59E-04	1.88E-06
112.5	2.51E-03	31	1.32E-03	99.22%	0.41%	4.61E-01	1.28E-01	4.35E+00	1.63E+00	1.34E-01	2.63E-03	2.09E-01	8.56E-04	1.03E-05	1.10E-01	4.50E-04	5.41E-06
125.0	3.10E-03	35	1.63E-03	99.46%	0.24%	3.00E-01	8.30E-02	5.96E+00	1.81E+00	1.63E-01	3.61E-03	2.54E-01	6.09E-04	7.43E-06	1.34E-01	3.20E-04	3.91E-06
128.0	3.25E-03	35	1.71E-03	99.50%	0.04%	5.12E-02	1.42E-02	6.40E+00	1.86E+00	1.71E-01	3.87E-03	2.65E-01	1.06E-04	1.30E-06	1.39E-01	5.58E-05	6.83E-07
141.6	3.97E-03	39	2.09E-03	99.64%	0.14%	1.98E-01	5.49E-02	8.67E+00	2.05E+00	2.05E-01	5.25E-03	3.19E-01	4.46E-04	5.56E-06	1.68E-01	2.35E-04	2.93E-06
158.9	5.00E-03	44	2.63E-03	99.74%	0.10%	1.59E-01	4.40E-02	1.22E+01	2.30E+00	2.52E-01	7.41E-03	3.92E-01	3.92E-04	5.00E-06	2.06E-01	2.06E-04	2.63E-06
178.3	6.30E-03	49	3.31E-03	99.82%	0.08%	1.43E-01	3.95E-02	1.73E+01	2.59E+00	3.09E-01	1.05E-02	4.81E-01	3.84E-04	5.04E-06	2.53E-01	2.02E-04	2.65E-06
200.0	7.92E-03	55	4.17E-03	99.90%	0.08%	1.60E-01	4.43E-02	2.44E+01	2.90E+00	3.77E-01	1.48E-02	5.86E-01	4.69E-04	6.34E-06	3.08E-01	2.47E-04	3.33E-06
224.4	9.97E-03	62	5.25E-03	99.97%	0.07%	1.57E-01	4.35E-02	3.45E+01	3.26E+00	4.59E-01	2.09E-02	7.12E-01	4.99E-04	6.98E-06	3.75E-01	2.62E-04	3.67E-06
250.0	1.24E-02	69	6.51E-03	100.00%	0.03%	7.50E-02	2.08E-02	4.77E+01	3.63E+00	5.48E-01	2.89E-02	8.51E-01	2.55E-04	3.71E-06	4.48E-01	1.34E-04	1.95E-06
282.5	1.58E-02	78	8.32E-03	100.00%	0.00%	0.00E+00	0.00E+00	6.88E+01	4.10E+00	6.66E-01	4.16E-02	1.03E+00	0.00E+00	0.00E+00	5.44E-01	0.00E+00	0.00E+00
						20.93	**5.793**						0.017	0.000		0.009	0.000

Appendix E: Theoretical calculation of Minimum Fluidization Velocity and Terminal Velocity with PSD for **Coarse particles**

HOT FLOW				COLD FLOW		Hot	Cold					HOT			COLD		
Particle Diameter dp (μm)	Cumulative Weight (%)	Weight %	MIN.Flu. Velocity umf (m/s)	Scaled Particle Diameter dp (μm)	Scaled Min. Flu. Velocity umf (m/s)	hot (mean Dia) μm	cold (mean Dia)μm	Archimedes number	dp*	Ut*(0.5<øs<1)	Reynolds no. p	Ut hot	Ut average	Umf Average	Umf average	Ut cold	Ut average
400	0%	0%	3.03E-02	111	1.59E-02	0.00	0.00	186.59	5.71	1.09	0.11	1.67	0.00	0.0000	0.0000	0.88	0.00
408	0%	0%	3.15E-02	113	1.66E-02	0.03	0.01	198.24	5.83	1.12	0.12	1.72	0.00	0.0000	0.0000	0.90	0.00
416	0%	0%	3.28E-02	115	1.73E-02	0.02	0.01	210.38	5.95	1.16	0.13	1.77	0.00	0.0000	0.0000	0.93	0.00
424	0%	0%	3.41E-02	117	1.79E-02	0.04	0.01	223.00	6.06	1.19	0.13	1.82	0.00	0.0000	0.0000	0.95	0.00
433	0%	0%	3.54E-02	120	1.86E-02	0.08	0.02	236.11	6.18	1.22	0.14	1.86	0.00	0.0000	0.0000	0.98	0.00
441	0%	0%	3.68E-02	122	1.93E-02	0.14	0.04	249.73	6.30	1.25	0.15	1.91	0.00	0.0000	0.0000	1.01	0.00
449	0%	0%	3.81E-02	124	2.01E-02	0.24	0.07	263.86	6.41	1.28	0.16	1.96	0.00	0.0000	0.0000	1.03	0.00
457	0%	0%	3.95E-02	127	2.08E-02	0.40	0.11	278.52	6.53	1.31	0.17	2.01	0.00	0.0000	0.0000	1.06	0.00
465	0%	0%	4.10E-02	129	2.16E-02	0.65	0.18	293.71	6.65	1.34	0.18	2.05	0.00	0.0001	0.0000	1.08	0.00
473	1%	0%	4.24E-02	131	2.23E-02	1.02	0.28	309.44	6.76	1.37	0.19	2.10	0.00	0.0001	0.0000	1.11	0.00
482	1%	0%	4.39E-02	133	2.31E-02	1.57	0.44	325.72	6.88	1.40	0.20	2.15	0.01	0.0001	0.0001	1.13	0.00
490	1%	0%	4.54E-02	136	2.39E-02	2.35	0.65	342.57	7.00	1.44	0.21	2.20	0.01	0.0002	0.0001	1.16	0.01
498	2%	1%	4.69E-02	138	2.47E-02	3.42	0.95	359.98	7.11	1.47	0.22	2.24	0.02	0.0003	0.0002	1.18	0.01
506	3%	1%	4.85E-02	140	2.55E-02	4.85	1.34	377.98	7.23	1.50	0.23	2.29	0.02	0.0005	0.0002	1.20	0.01

514	4%	1%	5.00E-02	142	2.63E-02	6.69	1.85	396.56	7.35	1.53	0.24	2.34	0.03	0.0007	0.0003	1.23	0.02
522	6%	2%	5.16E-02	145	2.72E-02	8.99	2.49	415.75	7.46	1.56	0.25	2.38	0.04	0.0009	0.0005	1.25	0.02
531	8%	2%	5.33E-02	147	2.80E-02	11.76	3.25	435.54	7.58	1.59	0.26	2.43	0.05	0.0012	0.0006	1.28	0.03
539	11%	3%	5.49E-02	149	2.89E-02	14.97	4.14	455.95	7.70	1.62	0.27	2.48	0.07	0.0015	0.0008	1.30	0.04
547	14%	3%	5.66E-02	151	2.98E-02	18.55	5.13	476.99	7.81	1.65	0.29	2.52	0.09	0.0019	0.0010	1.33	0.05
555	18%	4%	5.83E-02	154	3.07E-02	22.38	6.19	498.67	7.93	1.68	0.30	2.57	0.10	0.0024	0.0012	1.35	0.05
563	23%	5%	6.00E-02	156	3.16E-02	26.28	7.27	521.00	8.05	1.71	0.31	2.62	0.12	0.0028	0.0015	1.38	0.06
571	28%	5%	6.18E-02	158	3.25E-02	30.05	8.32	543.98	8.16	1.74	0.33	2.66	0.14	0.0032	0.0017	1.40	0.07
580	34%	6%	6.36E-02	160	3.34E-02	33.46	9.26	567.63	8.28	1.77	0.34	2.71	0.16	0.0037	0.0019	1.42	0.08
588	40%	6%	6.54E-02	163	3.44E-02	36.26	10.04	591.95	8.40	1.80	0.36	2.75	0.17	0.0040	0.0021	1.45	0.09
596	47%	6%	6.72E-02	165	3.53E-02	38.26	10.59	616.96	8.51	1.83	0.37	2.80	0.18	0.0043	0.0023	1.47	0.09
604	53%	7%	6.90E-02	167	3.63E-02	39.30	10.88	642.66	8.63	1.86	0.39	2.84	0.19	0.0045	0.0024	1.50	0.10
612	60%	6%	7.09E-02	169	3.73E-02	39.31	10.88	669.07	8.75	1.89	0.40	2.89	0.19	0.0046	0.0024	1.52	0.10
620	66%	6%	7.28E-02	172	3.83E-02	38.27	10.59	696.19	8.86	1.92	0.42	2.93	0.18	0.0045	0.0024	1.54	0.10
629	72%	6%	7.48E-02	174	3.93E-02	36.28	10.04	724.04	8.98	1.95	0.44	2.98	0.17	0.0043	0.0023	1.57	0.09
637	77%	5%	7.67E-02	176	4.04E-02	33.49	9.27	752.62	9.10	1.98	0.45	3.02	0.16	0.0040	0.0021	1.59	0.08
645	82%	5%	7.87E-02	178	4.14E-02	30.09	8.33	781.94	9.21	2.01	0.47	3.07	0.14	0.0037	0.0019	1.61	0.08
653	86%	4%	8.07E-02	181	4.25E-02	26.32	7.29	812.01	9.33	2.03	0.49	3.11	0.13	0.0033	0.0017	1.64	0.07
661	89%	3%	8.27E-02	183	4.35E-02	22.42	6.21	842.84	9.45	2.06	0.51	3.16	0.11	0.0028	0.0015	1.66	0.06
669	92%	3%	8.48E-02	185	4.46E-02	18.59	5.15	874.44	9.56	2.09	0.53	3.20	0.09	0.0024	0.0012	1.68	0.05

678	94%	2%	8.69E-02	188	4.57E-02	15.01	4.16	906.83	9.68	2.12	0.54	3.24	0.07	0.0019	0.0010	1.71	0.04
686	96%	2%	8.90E-02	190	4.68E-02	11.80	3.27	940.00	9.80	2.15	0.56	3.29	0.06	0.0015	0.0008	1.73	0.03
694	97%	1%	9.11E-02	192	4.79E-02	9.03	2.50	973.97	9.91	2.18	0.58	3.33	0.04	0.0012	0.0006	1.75	0.02
702	98%	1%	9.32E-02	194	4.91E-02	6.73	1.86	1008.75	10.03	2.20	0.61	3.37	0.03	0.0009	0.0005	1.77	0.02
710	99%	1%	9.54E-02	197	5.02E-02	4.88	1.35	1044.35	10.15	2.23	0.63	3.41	0.02	0.0007	0.0003	1.80	0.01
718	99%	0%	9.76E-02	199	5.14E-02	3.45	0.95	1080.78	10.26	2.26	0.65	3.46	0.02	0.0005	0.0002	1.82	0.01
727	99%	0%	9.99E-02	201	5.25E-02	2.37	0.66	1118.05	10.38	2.29	0.67	3.50	0.01	0.0003	0.0002	1.84	0.01
735	100%	0%	1.02E-01	203	5.37E-02	1.59	0.44	1156.16	10.50	2.32	0.69	3.54	0.01	0.0002	0.0001	1.86	0.00
743	100%	0%	1.04E-01	206	5.49E-02	1.04	0.29	1195.13	10.61	2.34	0.72	3.58	0.00	0.0001	0.0001	1.89	0.00
751	100%	0%	1.07E-01	208	5.61E-02	0.66	0.18	1234.96	10.73	2.37	0.74	3.62	0.00	0.0001	0.0000	1.91	0.00
759	100%	0%	1.09E-01	210	5.74E-02	0.41	0.11	1275.67	10.85	2.40	0.76	3.67	0.00	0.0001	0.0000	1.93	0.00
767	100%	0%	1.11E-01	212	5.86E-02	0.24	0.07	1317.26	10.96	2.42	0.79	3.71	0.00	0.0000	0.0000	1.95	0.00
776	100%	0%	1.14E-01	215	5.99E-02	0.14	0.04	1359.75	11.08	2.45	0.81	3.75	0.00	0.0000	0.0000	1.97	0.00
784	100%	0%	1.16E-01	217	6.11E-02	0.08	0.02	1403.15	11.20	2.48	0.84	3.79	0.00	0.0000	0.0000	1.99	0.00
792	100%	0%	1.19E-01	219	6.24E-02	0.05	0.01	1447.45	11.31	2.50	0.87	3.83	0.00	0.0000	0.0000	2.02	0.00
800	100%	0%	1.21E-01	221	6.37E-02	0.05	0.01	1492.68	11.43	2.53	0.89	3.87	0.00	0.0000	0.0000	2.04	0.00
						604.08	**167.19**						**2.84**	**0.07**	**0.04**		**1.49**

Appendix F: PSD at Hot flow condition

Raw Meal		Limestone	
Particle Diameter (µm)	Cumulative Weight (%)	Particle Diameter (µm)	Cumulative Weight (%)
0.4	0.00%	400	0.00%
0.5	0.03%	408	0.01%
0.6	0.37%	416	0.01%
0.7	1.50%	424	0.02%
0.8	2.26%	433	0.04%
0.9	3.13%	441	0.07%
1.0	4.05%	449	0.13%
1.0	4.07%	457	0.21%
1.1	5.09%	465	0.35%
1.3	6.16%	473	0.57%
1.4	7.31%	482	0.90%
1.5	7.92%	490	1.38%
1.8	9.86%	498	2.06%
2.0	11.27%	506	3.02%
2.2	12.78%	514	4.32%
2.5	14.41%	522	6.04%
2.8	16.15%	531	8.26%
3.0	17.11%	539	11.04%
3.2	18.02%	547	14.43%
3.6	20.00%	555	18.46%
4.0	22.10%	563	23.13%
4.0	22.14%	571	28.39%
4.5	24.31%	580	34.16%
5.0	26.54%	588	40.33%
5.0	26.64%	596	46.75%
6.0	30.48%	604	53.25%
6.3	31.68%	612	59.67%
7.1	34.39%	620	65.84%
8.0	37.24%	629	71.61%
8.0	37.36%	637	76.87%
8.9	40.24%	645	81.54%
10.0	43.32%	653	85.57%
11.2	46.69%	661	88.96%
12.0	48.62%	669	91.74%
12.6	50.15%	678	93.96%
14.2	53.73%	686	95.68%
15.0	55.57%	694	96.98%
16.0	57.66%	702	97.94%

17.8	61.21%	710	98.62%
18.0	61.53%	718	99.10%
19.0	63.32%	727	99.43%
20.0	65.03%	735	99.65%
22.4	68.85%	743	99.79%
24.0	71.06%	751	99.87%
25.0	72.39%	759	99.93%
25.2	72.62%	767	99.96%
26.0	73.66%	776	99.98%
27.0	74.86%	784	99.99%
28.3	76.28%	792	99.99%
30.0	78.14%	800	100.00%
32.0	80.07%		
35.6	83.08%		
39.9	86.10%		
40.0	86.16%		
45.0	88.94%		
48.0	90.32%		
50.2	91.23%		
56.4	93.28%		
63.0	94.94%		
64.0	95.15%		
71.0	96.37%		
80.0	97.48%		
89.3	98.25%		
90.0	98.29%		
95.0	98.58%		
96.0	98.63%		
100.0	98.81%		
112.5	99.22%		
125.0	99.46%		
128.0	99.50%		
141.6	99.64%		
158.9	99.74%		
178.3	99.82%		
200.0	99.90%		
224.4	99.97%		
250.0	100.00%		
282.5	100.00%		

Appendix G: Design basis for fluidized bed calciner

Table: Data to be used as a basis for the full-scale hot flow fluidized bed calciner operated with a binary particle mixture.

Characteristic	**Unit**	**Value**	**Remark**
Fine particles	-	Raw meal	See details in separate document
Coarse particles	-	Calcined limestone	See details in separate document
Fluidization gas	-	CO_2	
Gas evolution	-	CO_2	From calcination
Fine particle size	µm	0.4 – 283	See details in separate document
Coarse particle size	µm	250 – 550	See details in separate document
Coarse fraction in vessel	wt.%	75	
Reactor temperature	°C	920	
Reactor pressure	Pa	100 000	Absolute pressure
Mixing chamber width	m	2.5	
Segr. Chamber width	m	2.5	
Mixing chamber length	m	16.4	
Segr. Chamber length	m	22.1	
Mixing chamber height	m	4.2	
Segr. Chamber height	m	3.3	
Raw meal feed rate	kg/s	62	

Appendix H: PSD of pure Coarse particles Before Sieving (SINTEF)

Sympatec GmbH
System-Partikel-Technik

HELOS Particle Size Analysis
WINDOX 5

HELOS (H1223) & RODOS, R5: 0.5/4.5...875µm **2023-03-14, 13:08:00,610**
Alumina

x_{10} = 115.70 µm	x_{50} = 224.34 µm	x_{90} = 339.57 µm	SMD = 103.36 µm	VMD = 225.24 µm	
x_{16} = 143.12 µm	x_{84} = 307.39 µm	x_{99} = 450.09 µm	S_V = 0.06 m²/cm³	S_m = 137.40 cm²/g	

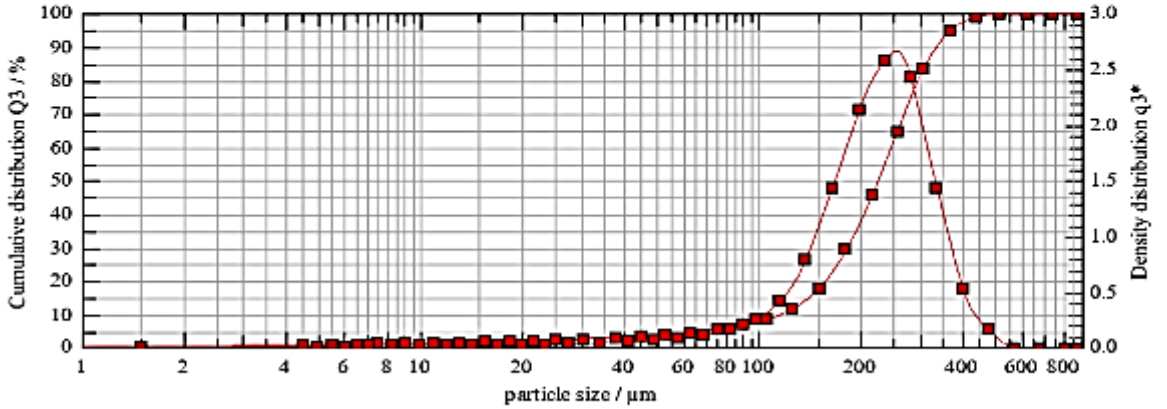

comment:	user parameters:
	P1: Alumina P2: Coarse Particles T3 P3: Nitish

cumulative distribution

x_0/µm	Q_3/%	x_0/µm	Q_3/%	x_0/µm	Q_3/%	x_0/µm	Q_3/%
4.50	0.77	18.50	1.86	75.00	5.39	305.00	83.56
5.50	0.90	21.50	2.02	90.00	6.67	365.00	94.74
6.50	1.01	25.00	2.22	105.00	8.32	435.00	98.77
7.50	1.11	30.00	2.49	125.00	11.46	515.00	100.00
9.00	1.24	37.50	2.92	150.00	17.72	615.00	100.00
11.00	1.39	45.00	3.36	180.00	29.11	735.00	100.00
13.00	1.53	52.50	3.83	215.00	45.54	875.00	100.00
15.50	1.68	62.50	4.49	255.00	64.64		

density distribution (log.)

x_m/µm	$q_3$lg	x_m/µm	$q_3$lg	x_m/µm	$q_3$lg	x_m/µm	$q_3$lg
1.50	0.01	16.93	0.02	68.47	0.11	278.88	2.43
4.97	0.01	19.94	0.03	82.16	0.16	333.65	1.43
5.98	0.02	23.18	0.03	97.21	0.25	398.47	0.53
6.98	0.02	27.39	0.03	114.56	0.41	473.31	0.17
8.22	0.02	33.54	0.04	136.93	0.79	562.78	0.00
9.95	0.02	41.08	0.06	164.32	1.44	672.33	0.00
11.96	0.02	48.61	0.07	196.72	2.13	801.95	0.00
14.20	0.02	57.28	0.09	234.15	2.58		

evaluation: WINDOX 5.7.1.0, *HRLD*		product: Alumina	
revalidation:		density:	4.22 g/cm³
reference measurement:	03-14 13:03:25	shape factor:	1.00
contamination:	0.00 %	C_{opt}= 7.03 %	

trigger condition: Test 2		dispersing method: 1 bar 50 % feeding rate	
time base: 1000.00 ms		cascade:	0
start:	c.opt >= 2%	pressure:	0.85 bar, vacuum: 0
valid:	always	revolution:	25.00 %
stop:	20s c.opt <= 1.9% or 99s real time	doser:	VIBRI, feed rate: 50.00 %

Appendix I: PSD of pure Coarse particles After Sieving (SINTEF)

Sympatec GmbH
System-Partikel-Technik

HELOS Particle Size Analysis
WINDOX 5

HELOS (H1223) & RODOS, R5: 0.5/4.5...875µm **2023-03-30, 13:41:35,302**
Alumina

x_{10} = 133.42 µm	x_{50} = 181.38 µm	x_{90} = 240.17 µm	SMD = 174.71 µm	VMD = 184.03 µm
x_{16} = 144.18 µm	x_{84} = 224.52 µm	x_{99} = 293.42 µm	S_V = 0.03 m²/cm³	S_m = 81.29 cm²/g

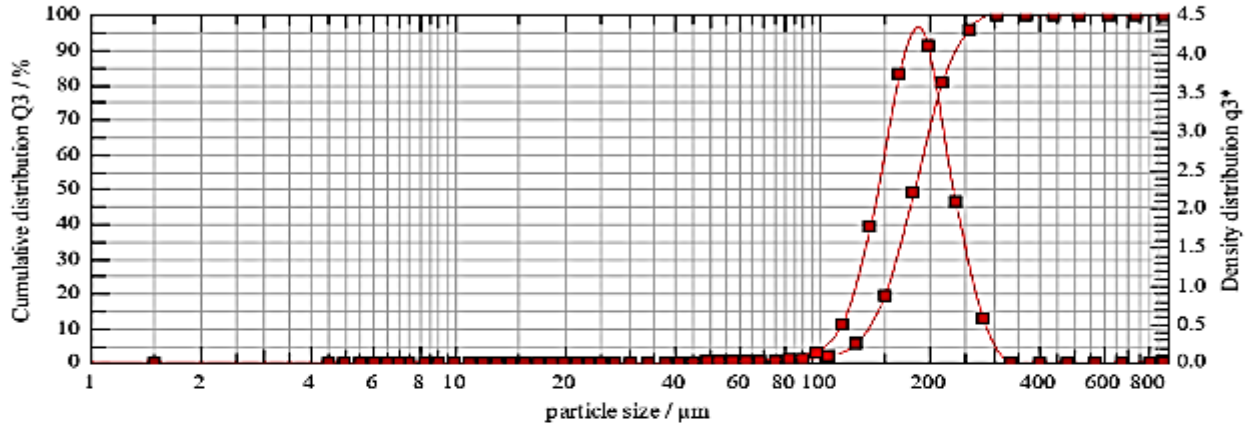

comment:	user parameters:
	P1: Alumina
	P2: Coarse particle final 12
	P3: Nitish

cumulative distribution

x_0/µm	Q_3/%	x_0/µm	Q_3/%	x_0/µm	Q_3/%	x_0/µm	Q_3/%
4.50	0.00	18.50	0.00	75.00	0.36	305.00	100.00
5.50	0.00	21.50	0.00	90.00	0.69	365.00	100.00
6.50	0.00	25.00	0.00	105.00	1.57	435.00	100.00
7.50	0.00	30.00	0.00	125.00	5.31	515.00	100.00
9.00	0.00	37.50	0.00	150.00	19.24	615.00	100.00
11.00	0.00	45.00	0.00	180.00	48.75	735.00	100.00
13.00	0.00	52.50	0.08	215.00	80.35	875.00	100.00
15.50	0.00	62.50	0.19	255.00	95.68		

density distribution (log.)

x_m/µm	$q_3$lg	x_m/µm	$q_3$lg	x_m/µm	$q_3$lg	x_m/µm	$q_3$lg
1.50	0.00	16.93	0.00	68.47	0.02	278.88	0.56
4.97	0.00	19.94	0.00	82.16	0.04	333.65	0.00
5.98	0.00	23.18	0.00	97.21	0.13	398.47	0.00
6.98	0.00	27.39	0.00	114.56	0.49	473.31	0.00
8.22	0.00	33.54	0.00	136.93	1.76	562.78	0.00
9.95	0.00	41.08	0.00	164.32	3.73	672.33	0.00
11.96	0.00	48.61	0.01	196.72	4.09	801.95	0.00
14.20	0.00	57.28	0.01	234.15	2.07		

evaluation: WINDOX 5.7.1.0, *HRLD*		product: Alumina	
revalidation:		density:	4.22 g/cm³
reference measurement:	03-30 13:40:09	shape factor:	1.00
contamination:	0.00 %	C_{opt}= 8.60 %	

trigger condition: Test 2		dispersing method: 1 bar 50 % feeding rate	
time base: 1000.00 ms		cascade:	0
start:	c.opt >= 2%	pressure:	0.87 bar, vacuum: 0
valid:	always	revolution:	25.00 %
stop:	20s c.opt <= 1.9% or 99s real time	doser:	VIBRI, feed rate: 50.00 %

Appendix J: PSD analysis result of pure Coarse particles at segregated flow rate (Norcem)

Coarse 300 L/min		Coarse 350 L/min		Coarse 400 L/min		Coarse 450 L/min		Coarse 550 L/min		Coarse 700 L/min		Coarse 750 L/min	
Size (µm)	% Volume Under	Size (µm)	% Volume Under	Size (µm)	% Volume Under	Size (µm)	% Volume Under	Size (µm)	% Volume Under	Size (µm)	% Volume Under	Size (µm)	% Volume Under
0.1	0	0.1	0	0.1	0	0.1	0	0.1	0	0.1	0	0.1	0
0.11	0	0.11	0	0.11	0	0.11	0	0.11	0	0.11	0	0.11	0
0.12	0	0.12	0	0.12	0	0.12	0	0.12	0	0.12	0	0.12	0
0.132	0	0.132	0	0.13	0	0.13	0	0.13	0	0.13	0	0.13	0
0.145	0	0.145	0	0.15	0	0.15	0	0.15	0	0.15	0	0.15	0
0.158	0	0.158	0	0.16	0	0.16	0	0.16	0	0.16	0	0.16	0
0.174	0	0.174	0	0.17	0	0.17	0	0.17	0	0.17	0	0.17	0
0.191	0	0.191	0	0.19	0	0.19	0	0.19	0	0.19	0	0.19	0
0.209	0	0.209	0	0.21	0	0.21	0	0.21	0	0.21	0	0.21	0
0.229	0	0.229	0	0.23	0	0.23	0	0.23	0	0.23	0	0.23	0
0.251	0	0.251	0	0.25	0	0.25	0	0.25	0	0.25	0	0.25	0
0.275	0	0.275	0	0.28	0	0.28	0	0.28	0	0.28	0	0.28	0
0.302	0	0.302	0	0.3	0	0.3	0	0.3	0	0.3	0	0.3	0
0.331	0	0.331	0	0.33	0	0.33	0	0.33	0	0.33	0	0.33	0
0.363	0	0.363	0	0.36	0	0.36	0	0.36	0	0.36	0	0.36	0
0.398	0	0.398	0	0.4	0	0.4	0	0.4	0	0.4	0	0.4	0
0.437	0	0.437	0	0.44	0	0.44	0	0.44	0	0.44	0	0.44	0
0.479	0	0.479	0	0.48	0	0.48	0	0.48	0	0.48	0	0.48	0
0.525	0	0.525	0	0.53	0	0.53	0	0.53	0	0.53	0	0.53	0
0.575	0	0.575	0	0.58	0	0.58	0	0.58	0	0.58	0	0.58	0
0.631	0	0.631	0	0.63	0	0.63	0	0.63	0	0.63	0	0.63	0
0.692	0	0.692	0	0.69	0	0.69	0	0.69	0	0.69	0	0.69	0
0.759	0	0.759	0	0.76	0	0.76	0	0.76	0	0.76	0	0.76	0
0.832	0	0.832	0	0.83	0	0.83	0	0.83	0	0.83	0	0.83	0
0.912	0	0.912	0	0.91	0	0.91	0	0.91	0	0.91	0	0.91	0
1	0	1	0	1	0	1	0	1	0	1	0	1	0
1.1	0	1.1	0	1.1	0	1.1	0	1.1	0	1.1	0	1.1	0
1.2	0	1.2	0	1.2	0	1.2	0	1.2	0	1.2	0	1.2	0
1.32	0	1.32	0	1.32	0	1.32	0	1.32	0	1.32	0	1.32	0
1.45	0	1.45	0	1.45	0	1.45	0	1.45	0	1.45	0	1.45	0
1.58	0	1.58	0	1.58	0	1.58	0	1.58	0	1.58	0	1.58	0
1.74	0	1.74	0	1.74	0.03	1.74	0	1.74	0	1.74	0	1.74	0
1.91	0	1.91	0	1.91	0.07	1.91	0.01	1.91	0.01	1.91	0	1.91	0
2.09	0.02	2.09	0	2.09	0.12	2.09	0.06	2.09	0.05	2.09	0	2.09	0
2.29	0.06	2.29	0	2.29	0.17	2.29	0.1	2.29	0.1	2.29	0	2.29	0
2.51	0.1	2.51	0.01	2.51	0.22	2.51	0.15	2.51	0.15	2.51	0	2.51	0

2.75	0.15	2.75	0.04	2.75	0.27	2.75	0.2	2.75	0.19	2.75	0	2.75	0
3	0.19	3	0.07	3	0.32	3	0.25	3	0.24	3	0	3	0
3.31	0.24	3.31	0.1	3.31	0.38	3.31	0.3	3.31	0.29	3.31	0	3.31	0
3.63	0.29	3.63	0.14	3.63	0.44	3.63	0.35	3.63	0.33	3.63	0	3.63	0
3.98	0.33	3.98	0.18	3.98	0.5	3.98	0.4	3.98	0.38	3.98	0	3.98	0
4.37	0.38	4.37	0.23	4.37	0.57	4.37	0.45	4.37	0.43	4.37	0	4.37	0
4.79	0.44	4.79	0.27	4.79	0.63	4.79	0.5	4.79	0.47	4.79	0	4.79	0
5.25	0.49	5.25	0.32	5.25	0.7	5.25	0.56	5.25	0.52	5.25	0	5.25	0
5.75	0.56	5.75	0.37	5.75	0.78	5.75	0.62	5.75	0.57	5.75	0	5.75	0
6	0.58	6	0.39	6	0.81	6	0.65	6	0.59	6	0	6	0
6.92	0.69	6.92	0.48	6.92	0.93	6.92	0.75	6.92	0.67	6.92	0.01	6.92	0
7.59	0.76	7.59	0.53	7.59	1	7.59	0.81	7.59	0.71	7.59	0.02	7.59	0
8.32	0.83	8.32	0.58	8.32	1.08	8.32	0.88	8.32	0.76	8.32	0.07	8.32	0
9.12	0.9	9.12	0.64	9.12	1.15	9.12	0.95	9.12	0.82	9.12	0.13	9.12	0
10	0.97	10	0.69	10	1.23	10	1.02	10	0.87	10	0.19	10	0
11	1.03	11	0.73	11	1.3	11	1.09	11	0.94	11	0.26	11	0
12	1.1	12	0.78	12	1.37	12	1.17	12	1.01	12	0.34	12	0
13.2	1.16	13.2	0.83	13.2	1.45	13.2	1.25	13.2	1.09	13.2	0.43	13.2	0
15	1.24	15	0.9	15	1.57	15	1.37	15	1.22	15	0.56	15	0
16	1.29	16	0.95	16	1.64	16	1.44	16	1.29	16	0.63	16	0
17.4	1.36	17.4	1.02	17.4	1.74	17.4	1.54	17.4	1.39	17.4	0.71	17.4	0
19.1	1.45	19.1	1.11	19.1	1.87	19.1	1.66	19.1	1.51	19.1	0.79	19.1	0
20	1.51	20	1.17	20	1.96	20	1.73	20	1.58	20	0.83	20	0
22.9	1.71	22.9	1.38	22.9	2.22	22.9	1.95	22.9	1.76	22.9	0.92	22.9	0
24	1.78	24	1.45	24	2.32	24	2.03	24	1.82	24	0.94	24	0
27.5	2.06	27.5	1.73	27.5	2.65	27.5	2.28	27.5	1.97	27.5	0.94	27.5	0
30	2.26	30	1.92	30	2.86	30	2.44	30	2.04	30	0.94	30	0
32	2.42	32	2.06	32	3.03	32	2.55	32	2.07	32	0.94	32	0
36.3	2.72	36.3	2.32	36.3	3.34	36.3	2.76	36.3	2.07	36.3	0.94	36.3	0
39.8	2.92	39.8	2.49	39.8	3.56	39.8	2.88	39.8	2.07	39.8	0.94	39.8	0
45	3.12	45	2.65	45	3.82	45	2.99	45	2.07	45	0.94	45	0
47.9	3.18	47.9	2.69	47.9	3.96	47.9	3	47.9	2.07	47.9	0.94	47.9	0
52.5	3.24	52.5	2.73	52.5	4.18	52.5	3	52.5	2.07	52.5	0.94	52.5	0
57.5	3.24	57.5	2.73	57.5	4.48	57.5	3	57.5	2.07	57.5	0.94	57.5	0
64	3.24	64	2.73	64	5.02	64	3	64	2.07	64	0.94	64	0
69.2	3.27	69.2	2.75	69.2	5.6	69.2	3	69.2	2.07	69.2	0.94	69.2	0
75.9	3.35	75.9	2.8	75.9	6.51	75.9	3	75.9	2.07	75.9	0.94	75.9	0
83.2	3.69	83.2	3.1	83.2	8.03	83.2	3.01	83.2	2.07	83.2	0.94	83.2	0
91.2	4.36	91.2	3.73	91.2	10.07	91.2	3.09	91.2	2.07	91.2	0.94	91.2	0
100	5.41	100	4.79	100	12.68	100	3.33	100	2.08	100	0.94	100	0
110	7.16	110	6.63	110	16.13	110	3.96	110	2.15	110	0.94	110	0
120	9.87	120	9.59	120	20.56	120	5.39	120	2.54	120	0.96	120	0
132	13.42	132	13.5	132	25.72	132	7.62	132	3.46	132	1.12	132	0
145	17.86	145	18.43	145	31.59	145	10.77	145	5.05	145	1.5	145	0.01
158	23.73	158	24.95	158	38.44	158	15.66	158	8.4	158	2.89	158	0.16

174	30.51	174	32.43	174	45.75	174	21.8	174	13.36	174	5.71	174	0.86
191	38.02	191	40.64	191	53.36	191	29.02	191	19.85	191	10.12	191	2.38
209	46.23	209	49.5	209	61.14	209	37.4	209	28.17	209	16.76	209	5.35
229	54.79	229	58.5	229	68.66	229	46.62	229	38.24	229	26.21	229	11.09
251	63.24	251	67.21	251	75.74	251	55.99	251	48.92	251	37.09	251	18.93
275	71.43	275	75.44	275	82.28	275	65.3	275	59.92	275	49.06	275	28.79
302	78.78	302	82.53	302	87.74	302	73.91	302	70.38	302	61.29	302	40.95
331	85.08	331	88.36	331	92.15	331	81.42	331	79.48	331	72.33	331	53.64
363	90.43	363	93.12	363	95.68	363	87.87	363	87.22	363	81.93	363	66.03
398	94.7	398	96.7	398	98.27	398	93.09	398	93.32	398	89.64	398	77.51
437	97.42	437	98.72	437	99.5	437	96.52	437	97	437	94.36	437	86.21
479	99.15	479	99.73	479	100	479	98.79	479	99.13	479	97.55	479	92.9
525	99.99	525	100	525	100	525	99.99	525	100	525	99.4	525	97.58
575	100	575	100	575	100	575	100	575	100	575	99.9	575	99.59
631	100	631	100	631	100	631	100	631	100	631	100	631	99.99
692	100	692	100	692	100	692	100	692	100	692	100	692	100
759	100	759	100	759	100	759	100	759	100	759	100	759	100
832	100	832	100	832	100	832	100	832	100	832	100	832	100
912	100	912	100	912	100	912	100	912	100	912	100	912	100
1000	100	1000	100	1000	100	1000	100	1000	100	1000	100	1000	100

Appendix K: PSD of Pure fine particles before sieving (SINTEF)

Sympatec GmbH
System-Partikel-Technik

HELOS Particle Size Analysis
WINDOX 5

HELOS (H1223) & RODOS, R3: 0.5/0.9...175µm **2023-03-17, 14:27:52,709**
Alumina

x_{10} = 1.71 µm	x_{50} = 7.63 µm	x_{90} = 56.36 µm	SMD = 4.24 µm	VMD = 18.57 µm	
x_{16} = 2.55 µm	x_{84} = 35.46 µm	x_{99} = 122.59 µm	S_V = 1.42 m²/cm³	S_m = 3352.49 cm²/g	

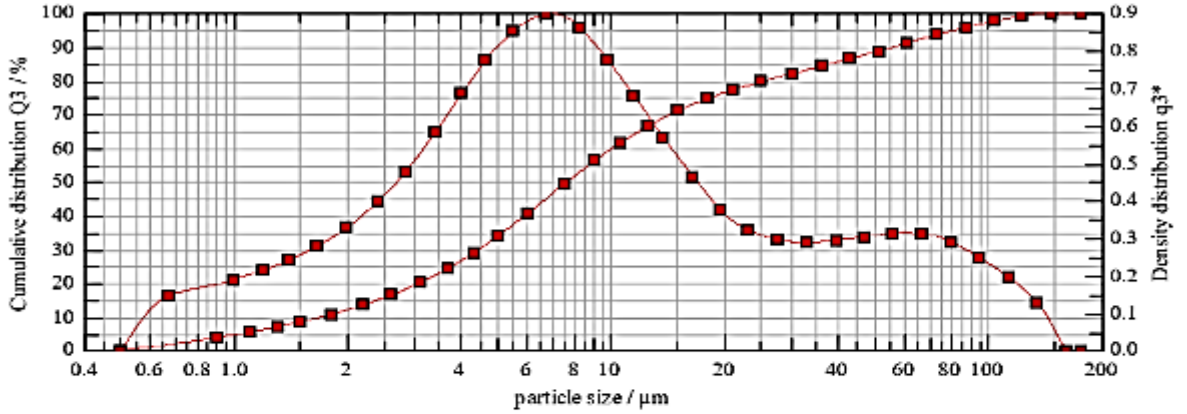

comment:

user parameters:
P1: P269
P2: Fine Particles1
P3: Nitish

cumulative distribution

x_0/µm	Q_3/%	x_0/µm	Q_3/%	x_0/µm	Q_3/%	x_0/µm	Q_3/%
0.90	3.75	3.70	24.45	15.00	71.02	61.00	91.12
1.10	5.39	4.30	28.92	18.00	74.67	73.00	93.54
1.30	6.94	5.00	34.00	21.00	77.16	87.00	95.73
1.50	8.44	6.00	40.74	25.00	79.59	103.00	97.52
1.80	10.62	7.50	49.42	30.00	81.92	123.00	99.03
2.20	13.49	9.00	56.23	36.00	84.20	147.00	100.00
2.60	16.36	10.50	61.41	43.00	86.46	175.00	100.00
3.10	20.00	12.50	66.54	51.00	88.70		

density distribution (log.)

x_m/µm	$q_3$lg	x_m/µm	$q_3$lg	x_m/µm	$q_3$lg	x_m/µm	$q_3$lg
0.67	0.15	3.39	0.58	13.69	0.57	55.78	0.31
0.99	0.19	3.99	0.68	16.43	0.46	66.73	0.31
1.20	0.21	4.64	0.78	19.44	0.37	79.69	0.29
1.40	0.24	5.48	0.85	22.91	0.32	94.66	0.24
1.64	0.28	6.71	0.90	27.39	0.29	112.56	0.20
1.99	0.33	8.22	0.86	32.86	0.29	134.47	0.13
2.39	0.40	9.72	0.77	39.34	0.29	160.39	0.00
2.84	0.48	11.46	0.68	46.83	0.30		

evaluation: WINDOX 5.7.1.0, *HRLD*
revalidation:
reference measurement: 03-17 14:20:50
contamination: 0.00 %

product: Alumina
density: 4.22 g/cm³
shape factor: 1.00
C_{opt}= 10.41 %

trigger condition: Test 2
time base: 1000.00 ms
start: c.opt >= 2%
valid: always
stop: 20s c.opt <= 1.9% or 99s real time

dispersing method: 1 bar 50 % feeding rate
cascade: 0
pressure: 0.85 bar, vacuum: 0
revolution: 25.00 %
doser: VIBRI, feed rate: 50.00 %

Appendix L: PSD of Pure fine particles after sieving (SINTEF)

Sympatec GmbH
System-Partikel-Technik

HELOS Particle Size Analysis
WINDOX 5

HELOS (H1223) & RODOS, R3: 0.5/0.9...175µm **2023-03-30, 15:12:45,650**
Alumina

x_{10} = 1.61 µm	x_{50} = 6.38 µm	x_{90} = 15.42 µm	SMD = 3.73 µm	VMD = 8.17 µm	
x_{16} = 2.37 µm	x_{84} = 12.91 µm	x_{99} = 30.14 µm	S_V = 1.61 m²/cm³	S_m = 3812.35 cm²/g	

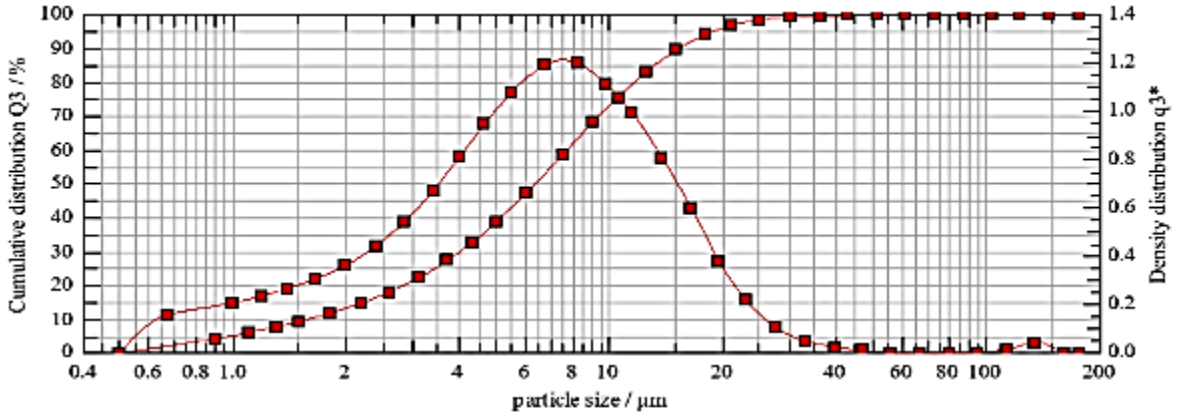

comment:	user parameters:
	P1: Alumina P2: fine particle 259 P3: Nitish

cumulative distribution

x_0/µm	Q_3/%	x_0/µm	Q_3/%	x_0/µm	Q_3/%	x_0/µm	Q_3/%
0.90	4.00	3.70	27.10	15.00	89.34	61.00	99.58
1.10	5.77	4.30	32.39	18.00	94.04	73.00	99.58
1.30	7.47	5.00	38.58	21.00	96.55	87.00	99.58
1.50	9.11	6.00	47.09	25.00	98.17	103.00	99.58
1.80	11.51	7.50	58.60	30.00	98.99	123.00	99.68
2.20	14.66	9.00	68.05	36.00	99.36	147.00	100.00
2.60	17.85	10.50	75.48	43.00	99.52	175.00	100.00
3.10	21.96	12.50	82.95	51.00	99.58		

density distribution (log.)

x_m/µm	$q_3$lg	x_m/µm	$q_3$lg	x_m/µm	$q_3$lg	x_m/µm	$q_3$lg
0.67	0.16	3.39	0.67	13.69	0.81	55.78	0.00
0.99	0.20	3.99	0.81	16.43	0.59	66.73	0.00
1.20	0.23	4.64	0.94	19.44	0.37	79.69	0.00
1.40	0.26	5.48	1.08	22.91	0.21	94.66	0.00
1.64	0.30	6.71	1.19	27.39	0.10	112.56	0.01
1.99	0.36	8.22	1.19	32.86	0.05	134.47	0.04
2.39	0.44	9.72	1.11	39.34	0.02	160.39	0.00
2.84	0.54	11.46	0.99	46.83	0.01		

evaluation: WINDOX 5.7.1.0, *HRLD*		product: Alumina	
revalidation:		density:	4.22 g/cm³
reference measurement:	03-30 15:10:59	shape factor:	1.00
contamination:	0.00 %	C_{opt}= 44.66 %	

trigger condition: Test 2		dispersing method: 1 bar 50 % feeding rate	
time base: 1000.00 ms		cascade:	0
start:	c.opt >= 2%	pressure:	0.89 bar, vacuum: 0
valid:	always	revolution:	25.00 %
stop:	20s c.opt <= 1.9% or 99s real time	doser:	VIBRI, feed rate: 50.00 %

Appendix M: PSD analysis result of Pure fine particles at segregated flow rate (Norcem)

Fine 200 L/min		Fine 250 L/min		Fine 300 L/min		Fine 350 L/min	
Size (µm)	% Volume Under	Size (µm)	% Volume Under	Size (µm)	% Volume Under	Size (µm)	% Volume Under
0.1	0	0.1	0	0.1	0	0.1	0
0.11	0	0.11	0	0.11	0	0.11	0
0.12	0	0.12	0	0.12	0	0.12	0
0.132	0	0.132	0	0.132	0	0.132	0
0.145	0	0.145	0	0.145	0	0.145	0
0.158	0	0.158	0	0.158	0	0.158	0
0.174	0	0.174	0	0.174	0	0.174	0
0.191	0	0.191	0	0.191	0	0.191	0
0.209	0	0.209	0	0.209	0	0.209	0
0.229	0	0.229	0	0.229	0	0.229	0
0.251	0	0.251	0	0.251	0	0.251	0
0.275	0	0.275	0	0.275	0	0.275	0
0.302	0	0.302	0	0.302	0	0.302	0
0.331	0	0.331	0	0.331	0	0.331	0
0.363	0	0.363	0	0.363	0	0.363	0
0.398	0	0.398	0	0.398	0	0.398	0
0.437	0	0.437	0	0.437	0	0.437	0
0.479	0	0.479	0	0.479	0	0.479	0
0.525	0	0.525	0	0.525	0	0.525	0
0.575	0.05	0.575	0	0.575	0.05	0.575	0.06
0.631	0.17	0.631	0.08	0.631	0.16	0.631	0.18
0.692	0.36	0.692	0.24	0.692	0.34	0.692	0.39
0.759	0.66	0.759	0.49	0.759	0.62	0.759	0.71
0.832	1.06	0.832	0.82	0.832	0.98	0.832	1.14
0.912	1.51	0.912	1.2	0.912	1.38	0.912	1.62
1	2	1	1.6	1	1.81	1	2.14
1.1	2.5	1.1	2.01	1.1	2.22	1.1	2.65
1.2	2.99	1.2	2.41	1.2	2.61	1.2	3.12
1.32	3.48	1.32	2.81	1.32	2.97	1.32	3.56
1.45	3.96	1.45	3.19	1.45	3.3	1.45	3.96
1.58	4.49	1.58	3.61	1.58	3.64	1.58	4.34
1.74	5.1	1.74	4.08	1.74	4.02	1.74	4.73
1.91	5.79	1.91	4.62	1.91	4.45	1.91	5.16
2.09	6.64	2.09	5.28	2.09	5	2.09	5.67

2.29	7.7	2.29	6.09	2.29	5.72	2.29	6.33
2.51	8.93	2.51	7.05	2.51	6.6	2.51	7.13
2.75	10.34	2.75	8.15	2.75	7.65	2.75	8.1
3	11.96	3	9.43	3	8.95	3	9.32
3.31	14.05	3.31	11.1	3.31	10.69	3.31	10.99
3.63	16.22	3.63	12.84	3.63	12.59	3.63	12.86
3.98	18.65	3.98	14.82	3.98	14.81	3.98	15.11
4.37	21.34	4.37	17.04	4.37	17.41	4.37	17.83
4.79	24.2	4.79	19.44	4.79	20.28	4.79	20.9
5.25	27.22	5.25	21.99	5.25	23.41	5.25	24.32
5.75	30.42	5.75	24.75	5.75	26.9	5.75	28.24
6	31.88	6	26.03	6	28.53	6	30.09
6.92	37.01	6.92	30.58	6.92	34.47	6.92	37.01
7.59	40.35	7.59	33.61	7.59	38.49	7.59	41.78
8.32	43.63	8.32	36.64	8.32	42.61	8.32	46.73
9.12	46.83	9.12	39.64	9.12	46.71	9.12	51.72
10	49.92	10	42.58	10	50.78	10	56.7
11	52.83	11	45.39	11	54.72	11	61.54
12	55.54	12	48.04	12	58.46	12	66.13
13.2	58.08	13.2	50.54	13.2	62.01	13.2	70.46
15	61.31	15	53.7	15	66.53	15	75.92
16	62.8	16	55.15	16	68.59	16	78.37
17.4	64.59	17.4	56.84	17.4	70.99	17.4	81.15
19.1	66.49	19.1	58.61	19.1	73.44	19.1	83.93
20	67.44	20	59.46	20	74.58	20	85.16
22.9	70.08	22.9	61.76	22.9	77.47	22.9	88.16
24	70.98	24	62.53	24	78.39	24	89.07
27.5	73.72	27.5	64.84	27.5	80.71	27.5	91.11
30	75.53	30	66.4	30	81.98	30	92.05
32	76.95	32	67.67	32	82.91	32	92.68
36.3	79.87	36.3	70.47	36.3	84.66	36.3	93.69
39.8	82.12	39.8	72.79	39.8	85.95	39.8	94.31
45	85.22	45	76.36	45	87.75	45	95.07
47.9	86.78	47.9	78.34	47.9	88.72	47.9	95.44
52.5	89.09	52.5	81.4	52.5	90.2	52.5	96.01
57.5	91.29	57.5	84.61	57.5	91.75	57.5	96.59
64	93.58	64	88.25	64	93.55	64	97.28
69.2	95.08	69.2	90.78	69.2	94.83	69.2	97.77
75.9	96.64	75.9	93.58	75.9	96.27	75.9	98.34
83.2	97.79	83.2	95.82	83.2	97.48	83.2	98.83
91.2	98.69	91.2	97.62	91.2	98.48	91.2	99.26
100	99.35	100	98.98	100	99.26	100	99.6
110	99.73	110	99.76	110	99.75	110	99.83

120	99.92	120	99.96	120	99.93	120	99.95
132	100	132	100	132	100	132	100
145	100	145	100	145	100	145	100
158	100	158	100	158	100	158	100
174	100	174	100	174	100	174	100
191	100	191	100	191	100	191	100
209	100	209	100	209	100	209	100
229	100	229	100	229	100	229	100
251	100	251	100	251	100	251	100
275	100	275	100	275	100	275	100
302	100	302	100	302	100	302	100
331	100	331	100	331	100	331	100
363	100	363	100	363	100	363	100
398	100	398	100	398	100	398	100
437	100	437	100	437	100	437	100
479	100	479	100	479	100	479	100
525	100	525	100	525	100	525	100
575	100	575	100	575	100	575	100
631	100	631	100	631	100	631	100
692	100	692	100	692	100	692	100
759	100	759	100	759	100	759	100
832	100	832	100	832	100	832	100
912	100	912	100	912	100	912	100
1000	100	1000	100	1000	100	1000	100

Appendix J PSD analysis result of Binary particles (Norcem)

Fine Pre-Binary Expt.		Coarse Pre-Binary Expt.		Fine post Binary Expt.		Coarse post Binary Expt.	
Size (µm)	% Volume Under	Size (µm)	% Volume Under	Size (µm)	% Volume Under	Size (µm)	% Volume Under
0.1	0	0.1	0	0.1	0	0.1	0
0.11	0	0.11	0	0.11	0	0.11	0
0.12	0	0.12	0	0.12	0	0.12	0
0.132	0	0.132	0	0.132	0	0.132	0
0.145	0	0.145	0	0.145	0	0.145	0
0.158	0	0.158	0	0.158	0	0.158	0
0.174	0	0.174	0	0.174	0	0.174	0
0.191	0	0.191	0	0.191	0	0.191	0
0.209	0	0.209	0	0.209	0	0.209	0
0.229	0	0.229	0	0.229	0	0.229	0
0.251	0	0.251	0	0.251	0	0.251	0
0.275	0	0.275	0	0.275	0	0.275	0
0.302	0	0.302	0	0.302	0	0.302	0
0.331	0	0.331	0	0.331	0	0.331	0
0.363	0	0.363	0	0.363	0	0.363	0
0.398	0	0.398	0	0.398	0	0.398	0
0.437	0	0.437	0	0.437	0	0.437	0
0.479	0	0.479	0	0.479	0	0.479	0
0.525	0	0.525	0	0.525	0	0.525	0
0.575	0.06	0.575	0.06	0.575	0.05	0.575	0
0.631	0.2	0.631	0.2	0.631	0.17	0.631	0
0.692	0.42	0.692	0.42	0.692	0.36	0.692	0
0.759	0.76	0.759	0.77	0.759	0.65	0.759	0
0.832	1.21	0.832	1.22	0.832	1.03	0.832	0
0.912	1.7	0.912	1.73	0.912	1.45	0.912	0
1	2.22	1	2.26	1	1.9	1	0
1.1	2.73	1.1	2.79	1.1	2.35	1.1	0
1.2	3.2	1.2	3.28	1.2	2.78	1.2	0
1.32	3.64	1.32	3.73	1.32	3.18	1.32	0
1.45	4.04	1.45	4.16	1.45	3.57	1.45	0
1.58	4.44	1.58	4.59	1.58	3.98	1.58	0
1.74	4.88	1.74	5.08	1.74	4.43	1.74	0
1.91	5.39	1.91	5.63	1.91	4.95	1.91	0
2.09	6.04	2.09	6.34	2.09	5.58	2.09	0
2.29	6.9	2.29	7.26	2.29	6.37	2.29	0

2.51	7.96	2.51	8.39	2.51	7.32	2.51	0
2.75	9.24	2.75	9.74	2.75	8.43	2.75	0
3	10.83	3	11.41	3	9.73	3	0
3.31	13.01	3.31	13.66	3.31	11.46	3.31	0
3.63	15.39	3.63	16.13	3.63	13.3	3.63	0
3.98	18.21	3.98	19.03	3.98	15.41	3.98	0
4.37	21.57	4.37	22.45	4.37	17.84	4.37	0
4.79	25.3	4.79	26.25	4.79	20.47	4.79	0
5.25	29.41	5.25	30.41	5.25	23.32	5.25	0
5.75	34.05	5.75	35.08	5.75	26.44	5.75	0
6	36.23	6	37.27	6	27.89	6	0
6.92	44.27	6.92	45.31	6.92	33.12	6.92	0
7.59	49.75	7.59	50.77	7.59	36.62	7.59	0
8.32	55.4	8.32	56.36	8.32	40.16	8.32	0
9.12	61.04	9.12	61.92	9.12	43.67	9.12	0
10	66.64	10	67.42	10	47.13	10	0
11	72.02	11	72.68	11	50.46	11	0
12	77.05	12	77.58	12	53.62	12	0
13.2	81.74	13.2	82.13	13.2	56.64	13.2	0
15	87.47	15	87.66	15	60.54	15	0
16	89.95	16	90.05	16	62.37	16	0
17.4	92.63	17.4	92.64	17.4	64.59	17.4	0
19.1	95.18	19.1	95.1	19.1	66.97	19.1	0
20	96.19	20	96.08	20	68.18	20	0
22.9	98.42	22.9	98.28	22.9	71.55	22.9	0
24	99.03	24	98.88	24	72.7	24	0
27.5	99.94	27.5	99.85	27.5	76.2	27.5	0
30	99.98	30	99.95	30	78.48	30	0
32	100	32	100	32	80.23	32	0
36.3	100	36.3	100	36.3	83.79	36.3	0
39.8	100	39.8	100	39.8	86.44	39.8	0
45	100	45	100	45	89.89	45	0
47.9	100	47.9	100	47.9	91.52	47.9	0
52.5	100	52.5	100	52.5	93.84	52.5	0
57.5	100	57.5	100	57.5	95.82	57.5	0
64	100	64	100	64	97.63	64	0
69.2	100	69.2	100	69.2	98.65	69.2	0
75.9	100	75.9	100	75.9	99.54	75.9	0
83.2	100	83.2	100	83.2	99.87	83.2	0
91.2	100	91.2	100	91.2	100	91.2	0.06
100	100	100	100	100	100	100	0.3
110	100	110	100	110	100	110	1.08
120	100	120	100	120	100	120	3.53

132	100	132	100	132	100	132	7.91
145	100	145	100	145	100	145	14.54
158	100	158	100	158	100	158	25.23
174	100	174	100	174	100	174	37.98
191	100	191	100	191	100	191	51.88
209	100	209	100	209	100	209	66.04
229	100	229	100	229	100	229	77.93
251	100	251	100	251	100	251	87.45
275	100	275	100	275	100	275	94.44
302	100	302	100	302	100	302	98
331	100	331	100	331	100	331	99.46
363	100	363	100	363	100	363	99.94
398	100	398	100	398	100	398	99.99
437	100	437	100	437	100	437	100
479	100	479	100	479	100	479	100
525	100	525	100	525	100	525	100
575	100	575	100	575	100	575	100
631	100	631	100	631	100	631	100
692	100	692	100	692	100	692	100
759	100	759	100	759	100	759	100
832	100	832	100	832	100	832	100
912	100	912	100	912	100	912	100
1000	100	1000	100	1000	100	1000	100